Improvement of Hybrid Codes for MIMO radar using multi-pulse waveforms and signal processing

Theoretical analysis and experimental evaluation

Max Ian Schöpe

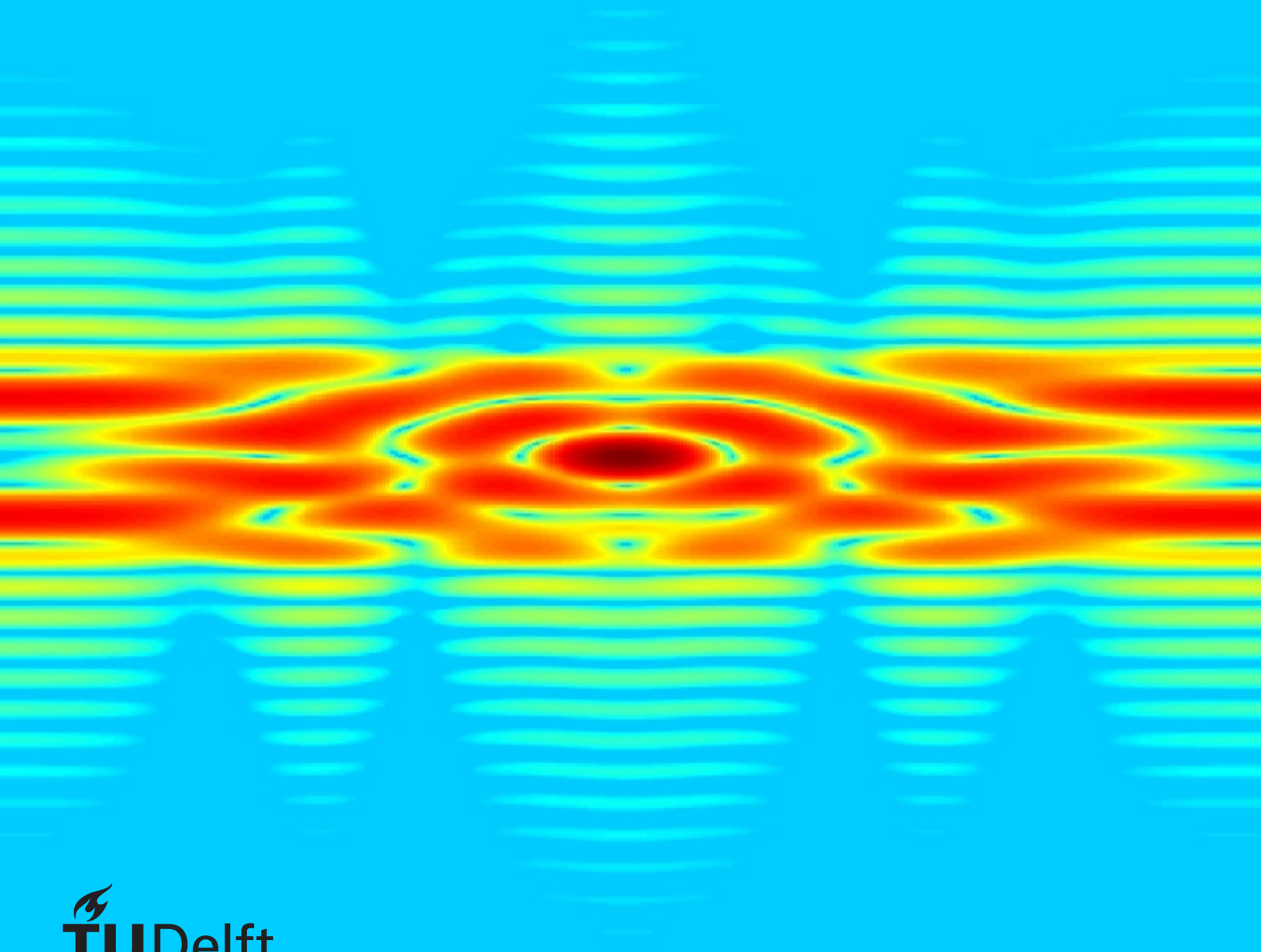

TU Delft

Improvement of Hybrid Codes for MIMO radar using multi-pulse waveforms and signal processing

Theoretical analysis and experimental evaluation

by

Max Ian Schöpe

to obtain the degree of Master of Science
at the Delft University of Technology (faculty EEMCS),
to be defended publicly on Friday October 20, 2017 at 11:00 AM.

Student number:	4500105	
Project duration:	January 1, 2017 – October 20, 2017	
Thesis committee:	Prof. dr. A. Yarovoy,	TU Delft, chairman of radar group
	Dr. ir. J. N. Driessen,	TU Delft, associate professor and supervisor
	Prof. dr. Marc Lesturgie,	International Affairs Director at ONERA and Professor at CentraleSupelec

TU Delft

Abstract

According to literature, MIMO radars often use orthogonal waveforms on their different channels to achieve a wide angular beam and so-called colored transmission. The generation of orthogonal signals is very difficult and true orthogonality cannot be achieved in practice. The Circulating Codes provide a simplified alternative to orthogonal signals, by transmitting the same waveform, but slightly shifted in time from channel to channel. By applying digital beamforming on transmit through signal processing on receive, a performance similar to orthogonal signals can be achieved. The Circulating Codes can also be used with a spatial code along the antenna elements, to improve the auto-correlation properties of the signal and thus the range resolution of the radar. These codes are called Hybrid or Delft Codes.

In this thesis, the Circulating Codes, as well as Hybrid Codes are revisited and analyzed again. An implementation for simulations has been created in Matlab to examine their behavior in more detail. To improve the range resolution of the Hybrid Codes, this thesis proposes the use of so-called Golay pairs as spatial codes. Each Golay pair consists of two codes, which have the property that the sum of their auto-correlation functions produces one strong peak and zero sidelobes. Since the application of these codes requires the transmission of two pulses, the phase shift due to the displacement of a moving target in between of the pulses has an impact on the result. This thesis focuses on the mitigation or correction of this phase shift, by the use of different methods and presents two possible solutions which perform well in simulations.

Finally, some of the techniques are applied in practical measurements with an available radar system. The results of these measurements show that the single-pulse techniques of the Circulating and Hybrid Codes perform well with the system, while the multi-pulse techniques with Golay pairs suffer from much higher sidelobes than expected from the simulations. First of all, this shows that the system has certain issues that need to be improved. Secondly, it shows that Hybrid Codes with Golay pairs are sensitive to disturbances and phase shifts. Therefore, very clean signals are required that might be difficult to generate in practice.

Preface

This thesis concludes my Master studies at TU Delft, after being a student for 8 years. It was a long journey, which started at the Technical University of Hamburg in October 2009. Not following a clear path in the beginning, I switched to the University of Applied Sciences of Hamburg and started working part-time for NXP Semiconductors Germany. While finishing my Bachelor degree in ”Electrical and Information Engineering”, I got a clearer idea of what I wanted to do during my Master studies. Therefore, I decided to broaden my horizon by moving to Delft and pursuing the Master track of ”Telecommunication and Sensing Systems” at TU Delft, to focus on electromagnetic waves and antennas.
My course choices and my interests soon led me to the field of radar and in the end of 2016, I started a small extra project in the ”Microwave Sensing, Signals and Systems” (MS3) group, which involved examining a radar system developed for MIMO radar purposes, the so-called ASTAP system. This topic then extended to my thesis project which is described in this document.

This thesis deals with the improvement of the MIMO radar technique of the so-called Hybrid Codes by the use of Golay code pairs, which theoretically produce a strong peak and no sidelobes. To examine the performance, both simulations and measurements were conducted.
The Hybrid Codes originate from the research of François Le Chevalier, who used to be a part-time professor in the radar group of TU Delft. To evaluate his theories experimentally, the ASTAP radar system had been built. Since this system has not been used until I started my thesis, the idea was to study it and the according theories, without having a clear research question in mind. The measurements that I previously conducted with it during my extra project, showed some effects that could not be easily explained. Hence, the first approach was to understand the behavior of the system, especially the waveform generator. It turned out that a complete analysis of the waveform generator would be very time consuming and not scientific enough for a thesis. I therefore started to focus on the theory. After spending a lot of time on understanding and analyzing the Hybrid Codes, I started to focus on the improvement of their range resolution. Finally, I also examined these new methods in practice with the ASTAP system.

It was a great experience to be able to spend a big amount of time on one topic and get to know it in detail. Understanding the underlying concepts was not always easy and I am very grateful for all the feedback I got. Thus, I would like express my gratitude to all the people that supported me during my studies and especially the thesis project.

First of all, I would like to thank my supervisor, dr. ir. Hans Driessen, for the many discussions we had on this topic and all the advice he gave me. He always managed to guide and support me, while still giving me the freedom to explore all of my ideas.

Secondly, I am very thankful to prof. dr. Alexander Yarovoy for the opportunity to work on such an interesting topic that involves many different aspects of radar systems.

I would also like to thank prof. dr. François Le Chevalier for helping me to understand the Circulating and Hybrid Codes. The discussions via email and in person were very valuable to me.

In addition to that, I would like to thank the technicians of the MS3 group for supporting me while I was conducting my measurements, the PhD students for all the useful advice and the relaxing discussions during lunch and Minke van der Put for the organizational support.

Last, but not least, I thank my family for supporting me morally and financially during my long study journey and Kalliopi Papangelopoulou for always listening to my complaints when I was having a bad day.

Max Ian Schöpe
Delft, October 2017

Contents

List of Figures

List of Tables

Nomenclature

Acronyms

ACF	Auto-correlation function
AF	Ambiguity function
ASTAP	Advanced space-time adaptive processing
AWG	Arbitrary waveform generator
BT product	Time-bandwidth product
CW	Continuous waveform
DBF	Digital beamforming
FFT	Fast fourier transform
FPGA	Field-programmable gate array
LFM	Linear frequency modulation
LOS	Line of sight
MIMO	Multiple-input and multiple-output
MTI	Moving target indicator
NLFM	Non-linear frequency modulation
PRF	Pulse repetition frequency
PRI	Pulse repetition interval
PRT	Pulse repetition time
RADAR	Radio detection and ranging
RCS	Radar cross section
RF	Radio frequency
SISO	Single-input and single-output
SNR	Signal-to-noise ratio

1 Introduction

The word radar is an acronym that stands for **Ra**dio **D**etection **A**nd **R**anging. This expression dates back to World War II, when the first working radar systems were being developed for military purposes [1, 2]. Modern radar systems are much more complex and include measurements and processing techniques that go far beyond the classical detection and ranging applications.

This introduction gives a short overview of general radar systems and concepts, as well as the modern approach including multiple-input and multiple-output (MIMO) radars. In addition to that, the scope of this thesis is defined and an outline of the chapters is given.

1.1. General radar background

Radar systems can usually be categorized by two characteristics: the antenna configuration and the transmitted signal.

Concerning the antennas, radar systems usually fall into the categories of mono-static or multi-static (mostly bi-static) radars (see figure 1.1). Mono-static means that the position of the transmit antenna is (almost) identical with the receive antenna. Therefore, only one single antenna is used for transmission and reception or both antennas are very close to each other. Bi-static or multi-static radar systems on the other hand, consist of several separate antennas that are placed in a considerable distance to each other [3].

Multi-static radars can also be used as so-called passive radars [4] that do not actively transmit a signal themselves, but receive the reflection coming from an unrelated transmitter, for instance a radio station. As in normal multi-static radar, the position of the transmitter needs to be known exactly. Since this type of radar is only receiving, it is completely invisible to electromagnetic detection systems and has a very low power consumption, because no signal has to be radiated.
Both, the mono-static and the multi-static concept, have their advantages and disadvantages, which will not be further addressed here.

The transmit signals of radar systems can be divided into two categories as well: continuous waveform (CW) and pulsed waveforms. Continuous waveform radars use the same signal (for example a linear frequency modulated (LFM) sweep) and constantly transmit it without interruption. Pulse radars transmit pulses of the signal with pauses in between, in which they listen for reflected signals [3].

In this thesis, only active mono-static pulse radars are being considered.

1.1.1. Basic single antenna radar

The basic radar uses a single antenna, physically rotating in azimuth, for both transmission and reception. It can only operate in the direction the antenna is pointing at the moment of the measurement. Most radar concepts can be explained with this simple example. For the following considerations, only

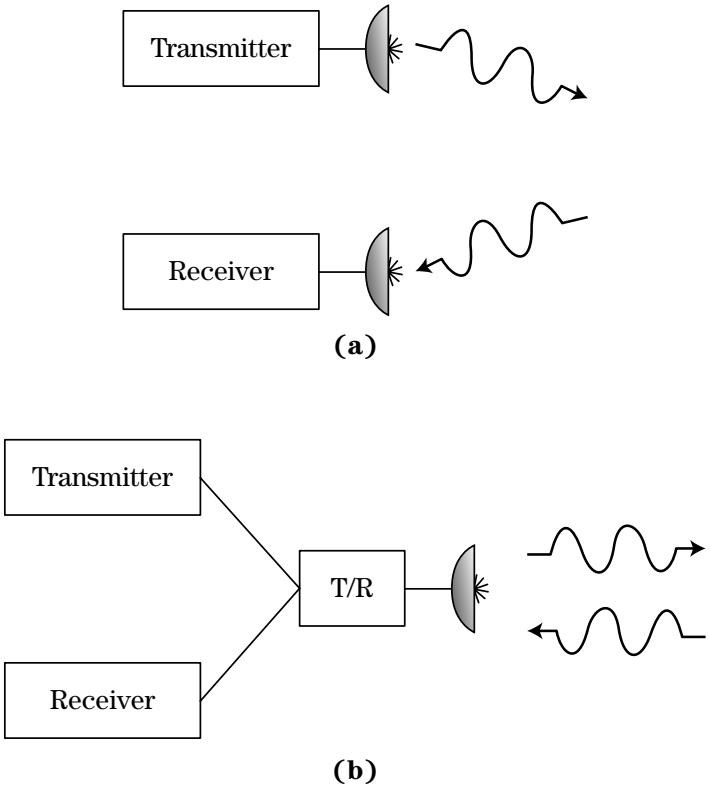

Figure 1.1: Difference between mono-static and bi-static radar systems. **(a)**: bi-static radar system with separated transmitter and receiver, **(b)**: mono-static radar system with the same antennas for transmit and receive (or very close to each other). Figure taken from [3].

the line of sight (LOS) between the radar antenna and the target is considered when distances are mentioned.

The radar equation

The basic equation for all radar systems is the so-called radar equation. It describes the relationship of signal power, signal frequency, antennas, the scattering of the wave due to the target and its distance to the antenna. In the following, it is briefly derived, following [3].

The power density Q_i in Watts per square meter at the target can be calculated by multiplying the transmit power by the gain in the direction of the target, divided by the surface of a sphere, because the wave spreads out spherically from the antenna. The power density is therefore given as

$$Q_i = \frac{P_t G_t}{4\pi R^2}\,, \tag{1.1}$$

where P_t is the transmit power, G_t the gain of the transmit antenna in the target direction and R the distance between transmit antenna and target.

The amount of reflected power is determined by the so-called radar cross section (RCS), which is the ratio of the scattered power back to the radar and the intercepted power density at the target. The RCS in square meters is therefore defined as

$$\sigma = \frac{P_{refl}}{Q_i}\,, \tag{1.2}$$

where P_{refl} is the reflected power from the target in the direction of the receive antenna.
The reflected power from the target is hence

$$P_{refl} = Q_i \cdot \sigma = \frac{P_t G_t \sigma}{4\pi R^2} \,. \tag{1.3}$$

The power density Q_r of the reflected signal back at the receive antenna can now be calculated by

$$Q_r = \frac{P_{refl}}{4\pi R^2} = \frac{P_t G_t \sigma}{(4\pi)^2 R^4} \,. \tag{1.4}$$

The received power is then given by the power density at the receive antenna multiplied with the effective area A_e of the antenna:

$$P_r = Q_r \cdot A_e = \frac{P_t G_t \sigma}{(4\pi)^2 R^4} \cdot A_e \,. \tag{1.5}$$

Since the gain is generally related to the effective area of the antenna and the wavelength of the signal as

$$G = \frac{4\pi A_e}{\lambda^2} \,, \tag{1.6}$$

where λ is the wavelength of the transmit signal carrier, the final equation for the received power is defined as

$$P_r = \frac{P_t G_t G_r \lambda^2 \sigma}{(4\pi)^3 R^4} \,, \tag{1.7}$$

as presented in [3] and [2], where G_r is the gain of the receive antenna. Thus, the received signal power can be calculated if the radar system, the target properties and its distance is known. All further concepts are based on the relationships described with this equation.

Range measurements

A pulse radar sends a pulse, which can consist of any kind of signal, depending on the purpose of the system. After transmitting a pulse, it listens for reflections to arrive at its antenna. Since the speed of light is known, the range of an object can be determined from the delay of the reflected signal. It has to be taken into account that the electromagnetic wave travels double the distance of the target [4]. The range of a target is then being calculated by

$$R = \frac{c \cdot \Delta t}{2} \,, \tag{1.8}$$

where c is the speed of light and Δt the delay of the signal with respect to the moment of transmission.

Pulses are sent with a so-called pulse repetition frequency (PRF). It defines the maximum unambiguous range of the radar system, when a single pulse is considered. The time between each pulse is called pulse repetition time (PRT), which is the inverse of the PRF. The smaller the PRF (or the longer the PRT), the longer the radar can wait for reflections. This means that the maximum delay of the target reflection has to be smaller than the time between two pulses. The principle is shown in figure 1.2. The maximum unambiguous range is thus defined as

$$R_{max} = \frac{c}{2 \cdot PRF} = \frac{c \cdot PRT}{2} \,. \tag{1.9}$$

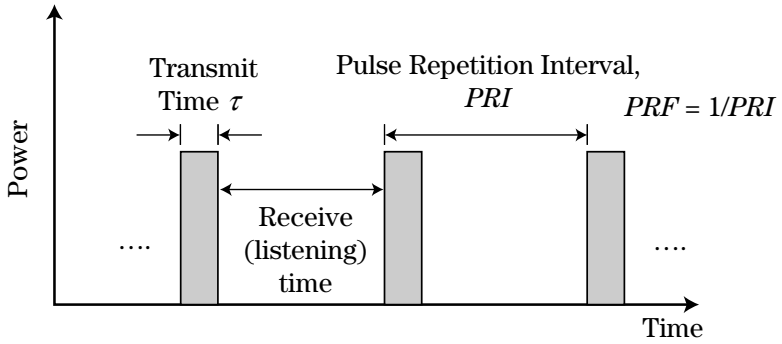

Figure 1.2: Basic priciple of a pulse radar. The radar transmits consecutive pulses with a distance of PRT (also called pulse repetition interval, PRI). In between the pulses, reflected signals can be received. Figure taken from [3].

Velocity measurements and Doppler effect

A pulse radar can also measure the velocity radial to the antenna, which means in the direction of propagation of the received signal, by making use of the Doppler effect. The faster a target moves, the more the frequency of the reflected signals differs from the original one, as shown in figure 1.3. By doing a Doppler analysis, the speed of the target can be determined from this frequency. This can be done by applying a frequency analysis with a Fast Fourier Transform (FFT), for instance. The sign of the measured velocity depends on the direction of the target with respect to the antenna.
By separating moving from static targets, a distinction can also be made between targets and unwanted detections, so-called clutter. A big part of available radar systems is only interested in detecting and tracking targets that are moving within certain velocity ranges, like airplanes or ships [3]. Clutter might cover real target detections and these systems thus remove a big part of the clutter by discarding static detections. This is called moving target indication (MTI).

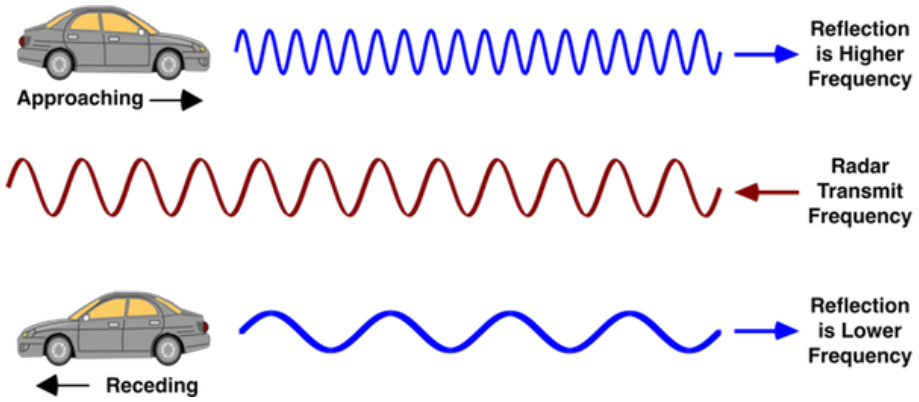

Figure 1.3: Simple explanation of the Doppler effect. The reflected signal from a moving target is shifted in frequency, because the movement in the propagation direction changes the wavelength of the signal. Figure taken from [5].

The PRF also defines the maximum unambiguous velocity (positive and negative), if a single pulse is used. This leads to the so-called Doppler dilemma: the lower the PRF, the higher the maximum unambiguous range, but the lower the maximum unambiguous velocity. Thus, a compromise between properly detectable range and properly detectable velocity without ambiguities has to be found. This compromise depends strongly on the purpose of the radar. If a long range of the radar is more important than the velocity measurements, the PRT will be set to a high value. But if a wide range of detectable velocities is needed, the PRT needs to be shorter. There is not one single solution for this Doppler dilemma.

If the direction of the target regarding the antenna and thus the sign of its velocity is unknown, the maximum unambiguous velocity for one transmit pulse is given by

$$v_{max} = \frac{\lambda \cdot PRF}{4} = \frac{c \cdot PRF}{4 \cdot f_{tx}} , \tag{1.10}$$

according to [2] and [4], where f_{tx} is the carrier frequency of the transmit signal.

If several pulses are transmitted (in so-called bursts), varying PRTs can be applied in between of the pulses. In the processing of the received signals, the different PRTs can be used to increase the maximum unambiguous Doppler velocity while keeping the range ambiguity at the desired level or vice versa. This is called range or Doppler unfolding and can for instance be applied by using so-called staggered PRTs or PRFs (see for example [3]). It is a possible technique to avoid the Doppler dilemma.

Range, Angle and Doppler resolution

The following equations hold for a standard radar with a focused pencil beam.

The range resolution of a simple non-modulated signal (e.g. a sine wave) is depending on the length of the transmit pulse. The shorter the pulse, the better the range resolution. In [2] and [3] the range resolution is described as

$$\Delta R = \frac{c\tau}{2} , \tag{1.11}$$

where τ is the length of the pulse. Thus, the radar can resolve two targets that are further away from each other than ΔR, because otherwise the reflected pulses overlap and both targets will appear as a single detection. This only applies for the LOS direction.

The angular resolution depends on the width (for azimuth) and height (for elevation) of the antenna. If this dimension is called L in the considered direction, the angular resolutions can be calculated with

$$\Delta\theta = \frac{c}{2L} , \tag{1.12}$$

as presented in [6].

The Doppler resolution depends on the observation time and the sampling frequency. The longer the target is observed, the higher the number of points in the FFT for the Doppler analysis. As a result, the steps between neighboring frequencies in the FFT plot are smaller. It can be described as

$$\Delta f_D = \frac{f_S}{N_S} , \tag{1.13}$$

where f_S is the sampling frequency and N_S is the number of samples recorded. Thus, the length of the pulse needs to be increased, or alternatively a bigger number of pulses needs to be transmitted.

LFM radar waveform

There are many waveforms that can be used for radar systems. From the simplest sine wave to complicated frequency or phase modulated signals. In this thesis, the focus lies on LFM waveforms. In baseband, this kind of signal can be described as

$$x(t) = A\cos\left(\pi\frac{B}{\tau}t^2\right) \quad -\frac{\tau}{2} \leq t \leq \frac{\tau}{2} , \tag{1.14}$$

following [3], where A is the amplitude, B is the bandwidth, τ is the pulse length and t is the time instant. When transmitted, the signal is centered at a certain radio frequency (RF) f_c. In [3] this is expressed as

$$x_{RF}(t) = A\cos\left(2\pi f_0 t + \pi\frac{B}{\tau}t^2\right) \quad -\frac{\tau}{2} \leq t \leq \frac{\tau}{2}\,. \tag{1.15}$$

In most systems, the received signal at RF will be mixed to baseband and a complex waveform is formed from the received signal, consisting of an in-phase (I) and quadrature (Q) part [3]. This complex signal is

$$x(t) = A\exp\left(j\pi\frac{B}{\tau}t^2\right) \quad -\frac{\tau}{2} \leq t \leq \frac{\tau}{2}\,. \tag{1.16}$$

A time domain representation of a typical LFM sweep as well as its instantaneous frequency are presented in figure 1.4.

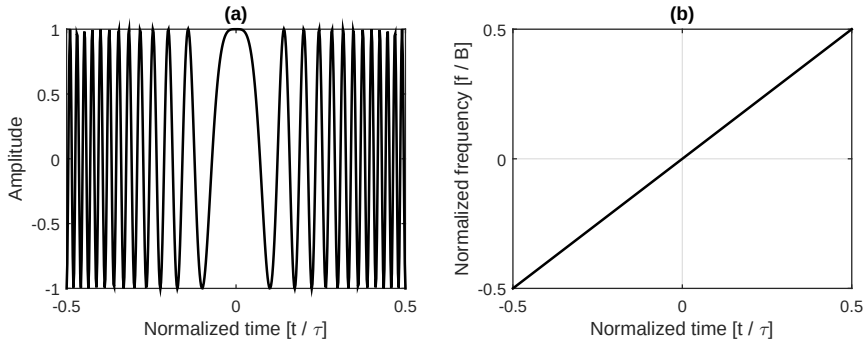

Figure 1.4: LFM baseband waveform in time and frequency domain. (a) time representation of an LFM signal, (b) instantaneous frequency of an LFM signal.

Pulse compression and matched filter

When using pulse compression, the signal inside the pulse is modulated, for example in phase or frequency. In combination with a matched filter, this technique makes the detection much easier, because the filter is matched to the transmit signal and thus gives the highest signal to noise ratio (SNR) when transmit and receive signal are exactly the same and aligned perfectly. The filtering operation can be represented as

$$y(t) = \int_{-\infty}^{\infty} x_{in}(u)h(t-u)du\,, \tag{1.17}$$

where $y(t)$ is the output of the matched filter at time t, x_{in} is the input signal and h is the filter as shown in for instance [1], [2], [3] and [7]. It turns out that the SNR is maximized when $h = x_{in}^*$ and this leads to

$$y(t) = \int_{-\infty}^{\infty} x_{in}(u)x_{in}^*(t-u)du\,, \tag{1.18}$$

which corresponds to the auto-correlation function.

If pulse compression is used, the equation for the range resolution is different to equation 1.11. The signal inside the pulse is modulated, which allows to use a long pulse with high energy but still achieve the resolution of a short pulse. Thus, even close reflections can be separated when applying a matched filter. In this case, the range resolution is defined by the bandwidth of the modulated signal, as explained in [3, 6]:

$$\Delta R = \frac{c}{2B}\,, \tag{1.19}$$

where B is the bandwidth of the pulse.

In modern pulse radar systems, pulse compression is commonly used and matched filtering is one of the most important processing steps. Figure 1.5 shows the concept of pulse compression for an LFM signal.

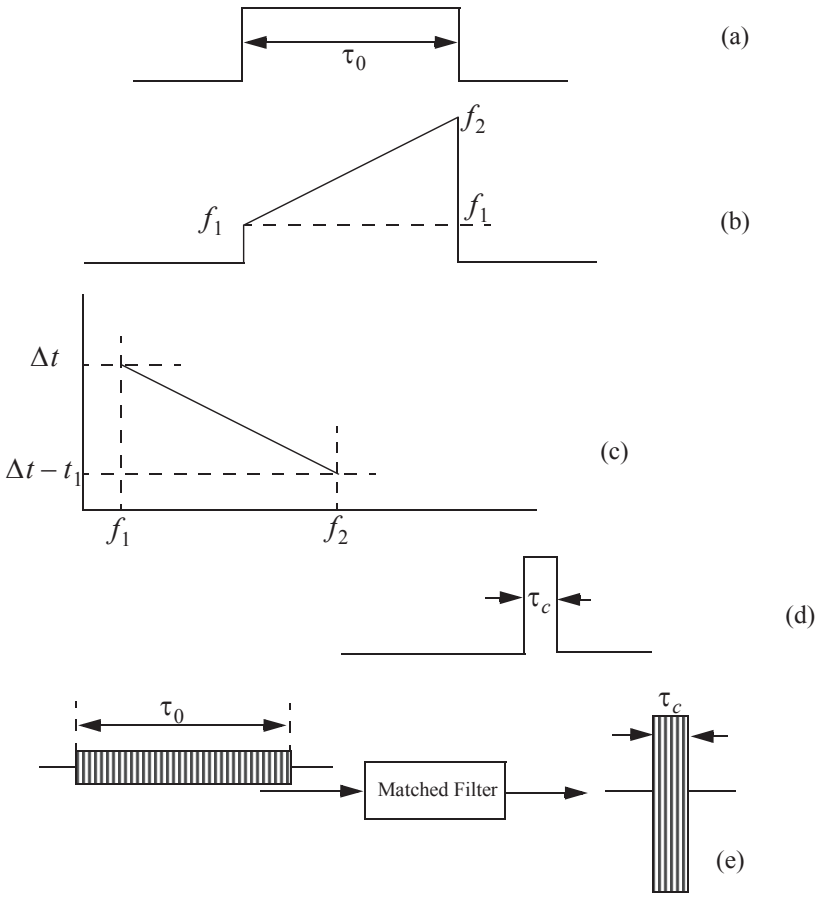

Figure 1.5: The basic principle of pulse compression. (a) the envelope of the transmit pulse of length τ_0, (b) modulation of the pulse (LFM), (c) matched filter time-delay characteristic, (d) the compressed pulse with new length τ_c, (e) the whole process is achieved by using a matched filter. Figure taken from [1].

1.1.2. Phased-array radar

To improve the performance of the basic radar, modern radars usually use antenna arrays made out of several antenna elements. These arrays mostly have a linear, planar or circular element pattern. By this means, the radiation pattern of the antenna can be adjusted to create the desired beampattern. For instance, this can be a narrow beam that can be steered electronically without moving the antenna. Such a beam is a combination of the wide element pattern and the array pattern resulting from the usage of several elements, as can be seen in figure 1.6.

The steering of the beam is done by using the same signal in all elements and then adding small phase shifts between the elements according to the desired angle. For a pencil beam, the correct phase shifts can be calculated by the use of equation 1.20 from [8]. Hereby, a linear antenna array can theoretically be steered from $-90°$ to $90°$.

$$\Phi = kd \cos\theta + \beta \,, \tag{1.20}$$

where $k = 2\pi/\lambda$ is the wavenumber, d is the distance between two elements in meters, θ is the steering angle and β is an additional phase shift (usually set to 0).

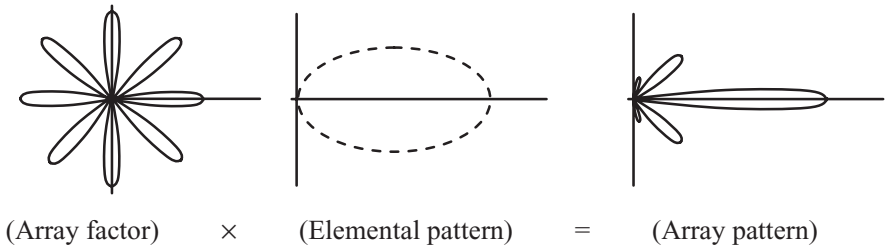

Figure 1.6: Explanation of the array pattern: the array factor (which is only depending on the number of elements) is multiplied by the element beam patterns and produces a narrow beam. With other array factors or element patterns, different array patterns can be achieved. Figure taken from [2].

1.1.3. MIMO radar

As mentioned above, when the same signal is used in every element of an antenna array, it interferes constructively and destructively and as a result, a narrow beam or other patterns can be steered in the desired directions. When arbitrary signals are used in each channel, a radar system is called a MIMO radar [9]. This concept is explained in figure 1.7. The different signals give this kind of radar an advantage over common phased array radars. In the following, it is assumed that each antenna element is connected to one channel of the radar system, which generates and transmits exactly one of the transmit signals.

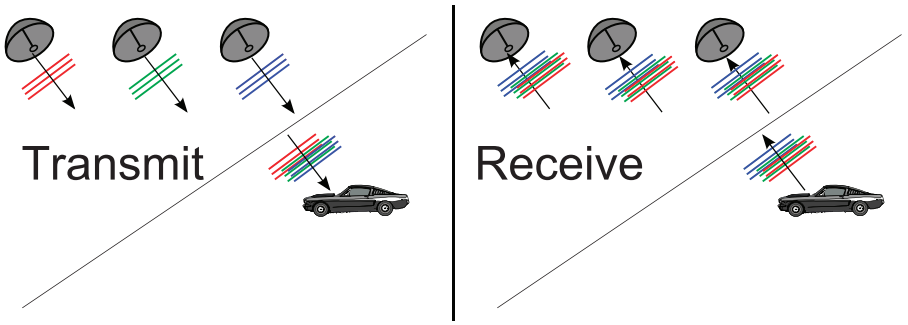

Figure 1.7: The basic concept of MIMO radar: different waveforms are transmitted in each channel of the MIMO radar. They are reflected by the target and are then received by the receiver channels. Since the transmitted signal looks different in every azimuth angle, the received signal can be associated with exactly one direction. Figure taken from [10].

Assuming a radar system with N_{tx} transmit and N_{rx} receive antennas that transmits narrowband signals in each channel, the overall transmit signal s_T to an assumed target can be described by the following equations 1.21 to 1.26 as derived in [9].

$$s_T(m) = \sum_{n=1}^{N_{tx}} e^{j2\pi f_0 \tau_m(\theta)} x_n(m) \triangleq \vec{a}^*(\theta)\vec{x}(m), \quad m = 1, \dots, M\ , \tag{1.21}$$

where f_0 is the carrier frequency of the radar, θ is the transmit angle, x_n is the signal in channel n, $\tau_m(\theta)$ is the time needed for the signal from the nth transmit antenna to reach the target, $\vec{a}$ are the complex amplitudes due to the phase shifts caused by the transmit antennas at angle θ, $(\cdot)^*$ is the conjugate transpose, $\vec{x}$ are the transmit signals in each channel and M is the number of samples of the transmit signal pulse in each channel.

The vector of the transmit signals in all channels is

$$\vec{x}(m) = \begin{bmatrix} x_1(m) & x_2(m) & \dots & x_{N_{tx}}(m) \end{bmatrix}^T \tag{1.22}$$

and its complex amplitude vector can be described as

$$\vec{a}(\theta) = \left[e^{j2\pi f_0 \tau_1(\theta)} \quad e^{j2\pi f_0 \tau_2(\theta)} \quad ... \quad e^{j2\pi f_0 \tau_{N_{tx}}(\theta)}\right]^T . \tag{1.23}$$

Let $y_n(m)$ now be the reflected signal from the target received by the nth receive antenna. The vector for all receive channels is

$$\vec{s}_R(m) = \left[\vec{s}_{R,1}(m) \quad \vec{s}_{R,2}(m) \quad ... \quad \vec{s}_{R,N_{rx}}(m)\right]^T \tag{1.24}$$

and the according complex amplitudes vector due to the receive antenna positions is

$$\vec{b}(\theta) = \left[e^{j2\pi f_0 \tilde{\tau}_1(\theta)} \quad e^{j2\pi f_0 \tilde{\tau}_2(\theta)} \quad ... \quad e^{j2\pi f_0 \tilde{\tau}_{Nrx}(\theta)}\right]^T , \tag{1.25}$$

where $\tilde{\tau}_n(\theta)$ is the time for the signal to be reflected from the target at θ and to reach the nth antenna. When a single point target is assumed, the received signal can be described by

$$\vec{s}_R(m) = \sum_{k=1}^{K} \beta_k \vec{b}^c(\theta_k) s_T(m) + \epsilon(m), \quad m = 1, ..., M , \tag{1.26}$$

where K is the number of targets, β_k are complex amplitudes related to the target reflection, ϵ is noise and interference and $(\cdot)^c$ is the complex conjugate.

Since all transmit signals are received by each receive antenna, the performance of such radar corresponds to a phased array radar with more elements than it actually uses. This concept is called antenna diversity and improves the performance, because the reflected signal is received at different positions and thus, each channel adds extra information to the measurement.
This bigger array is called a virtual array [10, 11] and leads to a better angular resolution. When N_{tx} orthogonal signals are transmitted through the same number of transmit antenna elements and the reflection from a target is then received with N_{rx} receive antenna elements, the resulting virtual array is longer than the physical one (see figure 1.8). It can even have a length of up to $N_{tx} \cdot N_{rx}$, if transmit and receive antenna are configured in a way that the virtual phase centers align without overlapping (see figure 1.9). This kind of array configuration is then called a Nyquist array [10, 11].

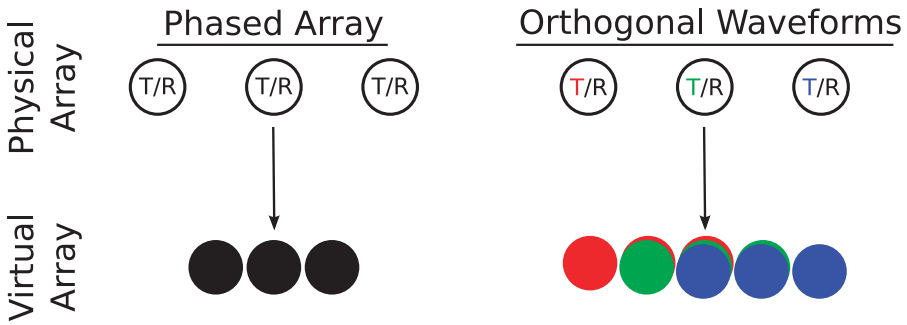

Figure 1.8: Physical arrays compared with their corresponding virtual arrays (filled colored circles). Left: A phased array radar with $N_{tx} = N_{rx} = 3$ leads to a virtual array of length 3. Right: A MIMO radar with $N_{tx} = N_{rx} = 3$ leads to a virtual array of length 5. Figure taken from [10].

In theory, one would prefer using orthogonal transmit signals, so that the transmit signals do not interfere constructively or destructively. Then, the different channels would be fully independent and the MIMO radar would radiate with a very wide beam. This means that its beam has the same strength in all directions simultaneously. Figure 1.10 shows this principle in comparison to a classical phased array radar. It is obvious that the MIMO radar transmits equally in all directions while the phased array radar produces beams that are very strong in some directions and very weak in others.

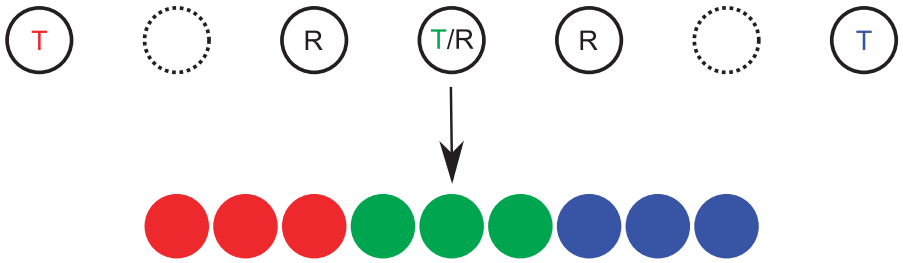

Figure 1.9: Nyquist array and its virtual array. When the transmit and receive elements are spaced properly, the virtual phase centers align without overlapping and the virtual array (filled colored circles) reaches its maximum length. Figure taken from [10].

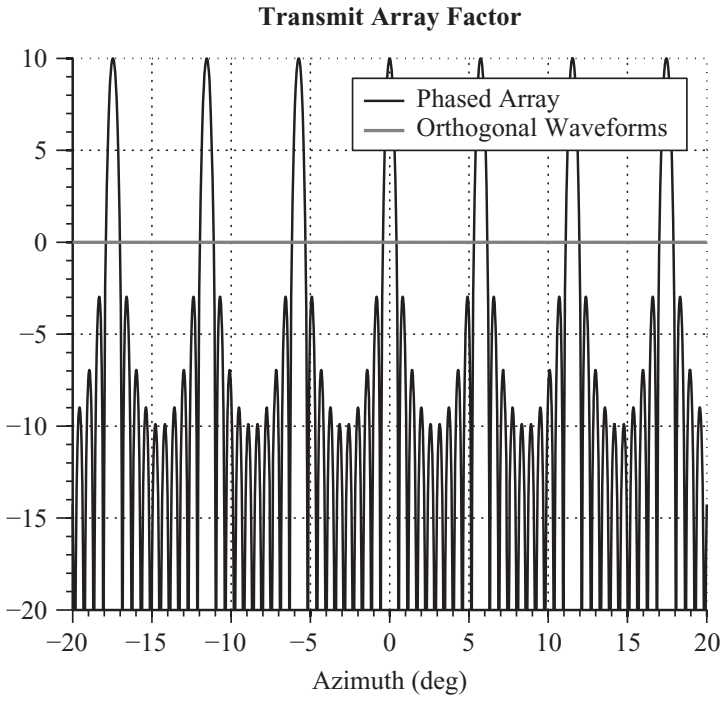

Figure 1.10: Transmit array factor for phased array radar and a MIMO radar using orthogonal waveforms. Figure taken from [11].

Therefore, MIMO radars radiate in all directions simultaneously, while transmitting a different signal in each azimuth direction, which makes it possible to sort out the transmitted signals from the received signals on the receiver side. More detailed examinations of the advantages of MIMO radar to phased-array radar have been conducted both in [9] and [11] and will not be discussed in this thesis. In chapter 2, the concept of colored space-time processing will be explained, which is based on general MIMO radar.

1.2. Thesis topic summary

The main advantage of MIMO radar over conventional single-input single-output (SISO) radar is the fact that it observes the whole space simultaneously. Since a SISO radar scans the different angles, small targets that only appear very briefly and are surrounded by strong clutter might be missed. This could be the periscope of a submarine for example, as suggested in [12]. MIMO radar could help detect this kind of targets and track many of them in parallel. In addition to that, MIMO radars could improve the Doppler resolution by providing a longer integration time. Because the radar is transmitting in all directions at the same time, a target will constantly be illuminated.

As already mentioned above, the optimal signals for a MIMO radar would be orthogonal to each other. In practice, orthogonality and perfect cross-correlation properties are very difficult to achieve or even impossible [13].
Firstly, there is only a limited number of signals that are theoretically orthogonal to each other. Not every kind of signal can thus be used for MIMO radar in general. Therefore, if all channel signals have to be orthogonal to each other, this restricts the choice of the used signal tremendously.
Secondly, it will never be possible to actually use orthogonal signals in practice because of the imperfections of a real system. There will always be noise and distortions, like clock leakages, which can lead to constant tone signals on top of the transmit signal. In addition to that, there is also always a certain amount cross-talk between the different channels. Finally, if an antenna array with a huge number of antenna elements N is being used, the effort for storing and generating these N signals might be challenging.

In order to tackle these problems, new techniques have been developed by Galina Babur et al. in [13] and [14]. These so-called Circulating Codes and their successors, the Hybrid Codes, also called Delft Codes, use only one waveform, which is transmitted in every channel, but with a small time delay. These techniques are described in detail in chapter 2.

1.2.1. Problem definition

This thesis is trying to improve these theories by using new waveforms with multi-pulse processing instead of single pulse processing as described in the original papers. The focus lies on the improvement of the range resolution.
In addition to the improvements, this thesis will also investigate how well these theories perform on a real system. The radar group of TU Delft has developed a radar system with 8 transmit and 1 receive channel to examine the theories mentioned in [13] and [14], which will be used for a series of measurements. Previous measurements showed that the system sufferes from constant tones, harmonics, cross-talk and some sort of unwanted frequency modulation that produces a ripple on the received signal. Despite these results, the systems performance was rated good enough to produce acceptable waveforms for the Circulating and Hybrid Codes.

1.3. Outline of this thesis

This chapter 1 gives an introduction and necessary background information. Chapter 2 describes the theories studied during literature review and the above mentioned codes in detail. In addition to that, the ASTAP radar system is briefly introduced. In chapter 3, the new approach for Hybrid Codes will be discussed and explained. Chapter 4 deals with the implementation of the new methods in Matlab and the analysis of the simulations and measurements. The last chapter 5 discusses the results mentioned in chapter 4 and draws conclusions. In addition, an outlook and recommendations are given for future work.

2

Theory in literature

This chapter explains already available theory that is the basis for this thesis. These concepts are all based on MIMO radar. All considerations are purely theoretical.

2.1. Digital beamforming (DBF)

Digital beamforming is a concept to form beams during signal processing, after the signal has been received. The idea is, to transmit the signal with a very wide beam (for example by only using one of the elements of an antenna array or by using an appropriate phase function between the elements) and then use all elements on receive. Since the same signal will be received in all receive antennas, but with a different phase, beams can be formed digitally in certain directions. The concept is explained in figure 2.1.

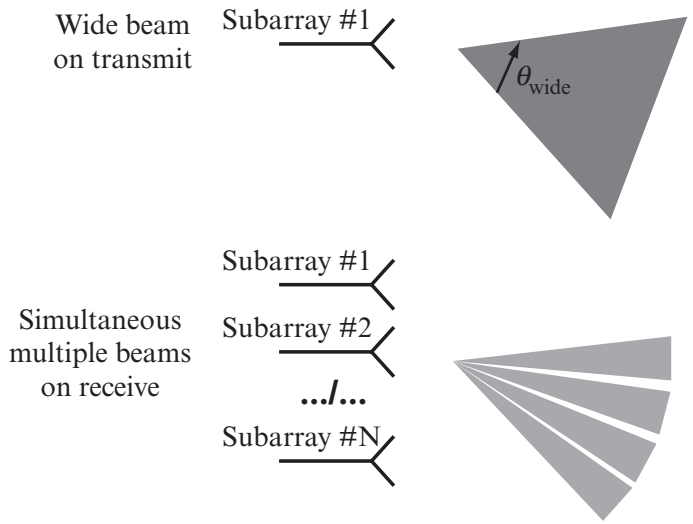

Figure 2.1: Digital beamforming: one signal is transmitted with a wide beam, by only using part of the existing antenna array. The reflected signal is then received in all channels. Since the different elements receive the signal with different phase shifts, beams can be formed digitally on receive in every direction after reception. Figure taken from [15].

The advantages of a widened beam on transmit are better visibility of short events, like so-called RCS flashes, when a target appears only for a very short moment and a higher Doppler resolution [15]. One disadvantage for airborne radars is that there is clutter spreading in Doppler because a bigger surface is illuminated. Ground objects will appear at various Doppler frequencies depending on their angle to

the antenna. For surface radars, a wide beam with the same transmit signal in every direction might be problematic, if clutter mostly appears at certain angles [15]. For instance, if one is interested in observing a certain part of airspace but not another, it would not be possible to easily suppress the reflections from that area. If an adjusted signal would be transmitted in that specific direction, clutter could be more easily suppressed. In general, DBF does not change the power budget with respect to a normal focused beam, because the lack in gain is compensated with a longer integration time [6, 15, 16].

To sum up, in certain situations it can be useful to transmit different signals in each direction. Therefore, in order to be able to use a wide beam but still be able to perform proper clutter rejection, the concept of colored transmission, also called colored space, has been introduced.

2.2. Colored Space-Time Processing

The idea of colored space-time processing is to transmit different transmit signals in each channel, preferably orthogonal, so that the different channels do not add up coherently and the overall transmit signal is different in every direction. This leads to a wide beam on transmit. But instead of only applying digital beamforming on receive, digital beamforming is also applied on transmit but by means of signal processing on receive [13]. This is done by taking into account the phase shifts due to the transmit antenna element positions and the known transmitted signal. The process is explained in figure 2.2 and equations 2.1 to 2.3. The result of this processing is a widened beam while still having a good clutter rejection.
In [6], François Le Chevalier summarizes the advantages of Colored Space-Time processing (also called Coherent Collocated MIMO processing) as a better target extraction of slow targets from clutter, noise and multipath, as well as a better identification due to longer observation times and larger bandwidths.

Digital beamforming on transmit by means of signal processing on receive is realized by forming ”beams” in all directions, on transmit as well as on receive. In order to do that, the transmitted signal, as well as the received signal in a certain direction θ are used as input signals for the matched filter. A sweep over the angles in all directions of the observed half-space is conducted. Therefore, 180° are being digitally scanned. The transmit signal can be described as

$$y_t(t) = \begin{bmatrix} e^{jk_0 \cdot x_{tx}^1 \cdot \sin(\theta)} & e^{jk_0 \cdot x_{tx}^2 \cdot \sin(\theta)} & \dots & e^{jk_0 \cdot x_{tx}^{N_{tx}} \cdot \sin(\theta)} \end{bmatrix} \cdot \begin{bmatrix} s_t^1(t) \\ s_t^2(t) \\ \vdots \\ s_t^{N_{tx}}(t) \end{bmatrix}, \tag{2.1}$$

while the received signal is

$$y_r(t) = \begin{bmatrix} e^{jk_0 \cdot x_{rx}^1 \cdot \sin(\theta)} & e^{jk_0 \cdot x_{rx}^2 \cdot \sin(\theta)} & \dots & e^{jk_0 \cdot x_{rx}^{N_{rx}} \cdot \sin(\theta)} \end{bmatrix} \cdot \begin{bmatrix} s_r^1(t) \\ s_r^2(t) \\ \vdots \\ s_r^{N_{rx}}(t) \end{bmatrix}, \tag{2.2}$$

where k_0 is the wavenumber of the carrier frequency, x_{tx}^n and x_{rx}^m are the positions of the nth transmit and mth receive antenna elements respectively, θ is the instantaneous transmit and receive angle, N_{tx} and N_{rx} are the numbers of transmit and receive antenna elements respectively, s_t^n is the signal transmitted on the nth transmit antenna element and s_r^m is the signal received on the mth receive antenna element.

Finally, the matched filter is applied on these transmit and receive signals. If the target is assumed to be stationary, this leads to the so called ambiguity function

$$\left|\chi(\tau)\right|^2 = \left| \int_{-\infty}^{\infty} y_t(t) y_r^*(t-\tau) dt \right|^2, \tag{2.3}$$

similar to the one presented in [7], where $\left|\chi(\tau)\right|^2$ is the ambiguity function when the received signal is displaced in time by τ. As shown in equation 2.3, the ambiguity function is mostly given as its magnitude squared [1, 2].

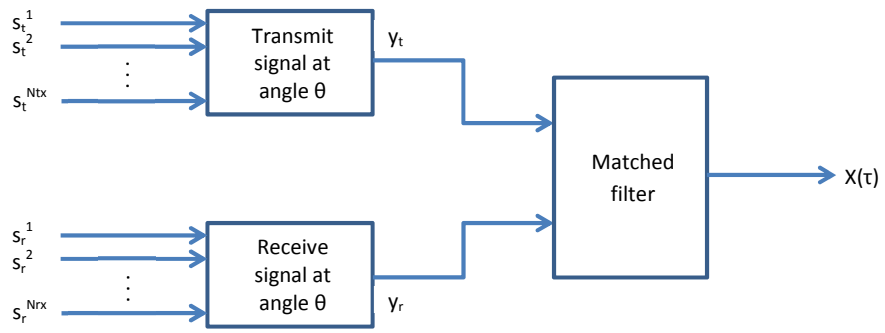

Figure 2.2: Simplified colored space-time processing. The beamforming is done by taking into account the antenna positions and the transmitted and received signal. Input for the matched filter are the transmitted and received signal in the assumed target direction θ.

The technique of colored space allows to monitor an unlimited number of beams [13] by applying the above signal processing on the received signal. This means that theoretically, an unlimited amount of targets can be detected and tracked simultaneously.

2.2.1. Circulating Codes

The usage of true orthogonal signals is impossible in reality, as has been stated above. This is why researchers at TU Delft developed an alternative that is more easily realizable and still gives the possibility to perform colored space-time signal processing. The concept is called Circulating Codes and is only based on one waveform.

The concept is very simple: there is only one waveform used, which is shifted in time between the different channels of the radar system. The signal in the nth channel can be described as

$$s^n(t) = a_n \cdot s(t - (n-1) \cdot \Delta t)\,, \tag{2.4}$$

according to [13], where a_n is the amplitude in the nth channel and Δt is the relative time shift between two channels. The overall concept is also shown in figure 2.3.

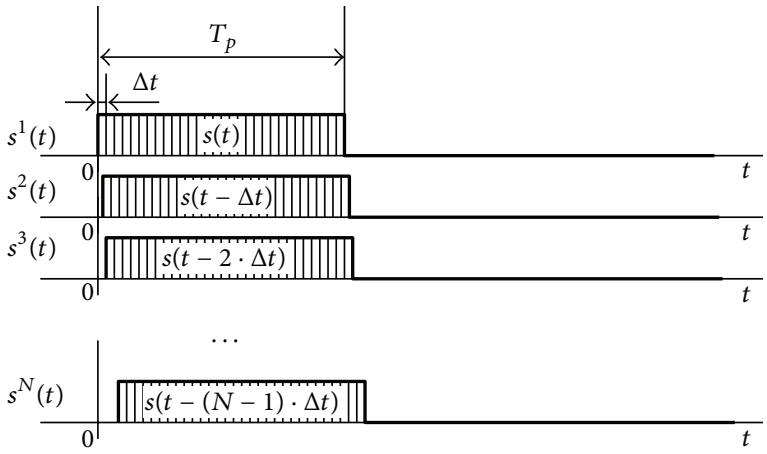

Figure 2.3: The concept of the Circulating Codes, as also described in equation 2.4. The signal $s^n(t)$ in each channel is shifted by another Δt in time. Figure taken from [13].

The Circulating Codes achieve a very wide beam when $\Delta t = 1/B$, according to [13]. This can be shown by looking at the phase between two neighboring channels. Under the assumption that the instantaneous frequencies f of two neighboring channels are identical at a given moment in time, the phase shift between them can be expressed as

$$\phi(f) = \phi_0 + 2\pi f \cdot \Delta t \,, \tag{2.5}$$

which is equivalent to the phase of a sine wave at frequency f. When the bandwidth is taken into account and we assume that $\phi_0 = 0$, the results are

$$\phi(f_1) = 2\pi \cdot (-\frac{B}{2}) \cdot \Delta t \tag{2.6}$$

and

$$\phi(f_2) = 2\pi \cdot (+\frac{B}{2}) \cdot \Delta t \,. \tag{2.7}$$

Since in theory, a wide beam of 180° is desired, the time shift is set to $\Delta t = 1/B$ because then the result of equations 2.6 and 2.7 is $-\pi$ and π, which is equivalent to the full angular coverage of 180° [13]. In other words, depending on the instantaneous frequency, the antenna array will illuminate the angles in between of -90° and 90°. Figure 2.4 shows how the beam direction changes within a Circulating Codes pulse. Obviously, the Circulating Codes do not constantly illuminate the whole 180° as is expected from a real MIMO system with orthogonal signals, but rather cover the whole angular area with a beam sweep during one pulse. Thus, if only part of the signal is used, the Circulating Codes could be used to only illuminate certain areas of the half-space.

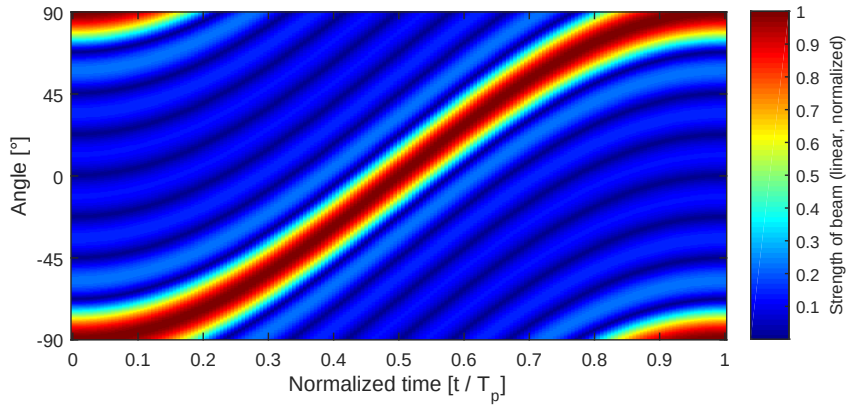

Figure 2.4: Change of the direction of the main beam during one Circulating Codes pulse with length T_p. It is obvious that the beam does not illuminate all directions at the same time but moves along the half-space.

The total transmit signal is the sum of the signals coming from each channel. It changes depending on the transmit angle. According to [13], when a certain target angle θ_0 is given, the total transmit signal in this direction can be described as

$$s_T(t, \theta_0) = \sum_{n=1}^{N_{tx}} e^{j\vec{k}(\theta_0)\cdot\vec{x}_{tx}(n)} \cdot s^n(t) \,, \tag{2.8}$$

where N_{tx} is the number of transmit antennas, $\vec{x}_{tx}$ is the vector of the transmit antennas positions and $\vec{k}$ is the wavenumber vector and $s^n(t)$ is the signal transmitted in channel n.
In [13], only one receive antenna is assumed because the authors wanted to focus on the DBF on transmit rather than on receive. Thus, the received signal can be written as

$$s_R^r(t,\theta_0) = e^{-j\vec{k}(\theta_0)\cdot\vec{x}_{rx}(r)} \cdot \dot{A} \cdot s_T(t-\tau_0,\theta_0) + e(t)\ , \tag{2.9}$$

where r is the number of the element of the antenna array used for reception, x_{rx} is the vector of the receive antenna positions, $\dot{A}$ is the complex scattering coefficient of the target, τ_0 is the time delay of the received signal due to the traveling of the wave and $e(t)$ is noise at time t.

Applying the matched filter leads to the multi-dimensional ambiguity function

$$\left|\chi(\tau,\theta',\theta_0)\right|^2 = \left|\int s_T(t-\tau,\theta') \cdot (s_R^r(t,\theta_0))^* dt\right|^2\ , \tag{2.10}$$

where τ is the displacement between s_T and s_R^r and θ' is the hypothesis about the target direction. In the end, the final simplified result of the matched filter output found by Babur et al. in [13] is

$$\left|\chi(\tau',\theta',\theta_0)\right|^2 = \begin{cases} \left|ACF_{rect}(\tau') \cdot \sum_{n=1}^{N_{tx}} \sum_{n'=1}^{N_{tx}} e^{j(\vec{k}(\theta')\cdot\vec{x}(n)-\vec{k}(\theta_0)\cdot\vec{x}(n'))}\right|^2 & for\ |\tau'| \le \frac{N_{tx}\cdot\Delta t}{2}, \\ 0 & for\ elsewhere\ \tau'. \end{cases}\ , \tag{2.11}$$

where $\tau' = (\tau_0 - \tau)$, ACF_{rect} is the auto-correlation function of a rectangular pulse, n is the index of the transmitted signal and n' is the index of the replica or received signal. The conclusion drawn from this result is that the peak resulting from the Circulating Codes method is N_{tx} times wider than for a phased array system. Thus, this simple MIMO technique comes with the disadvantage of less range resolution.

In their simulations in [13], Babur et al. showed that LFM sweeps show the best properties and results for this kind of processing. Some of the according simulation results are shown in figure 2.5. As a consequence, only LFM sweeps are considered in this thesis. It should be noted that the performance will improve when more than one receive antenna elements are used. In addition to that, there is also the possibility to add weighting in time and over the antennas to improve the results, especially in angle.

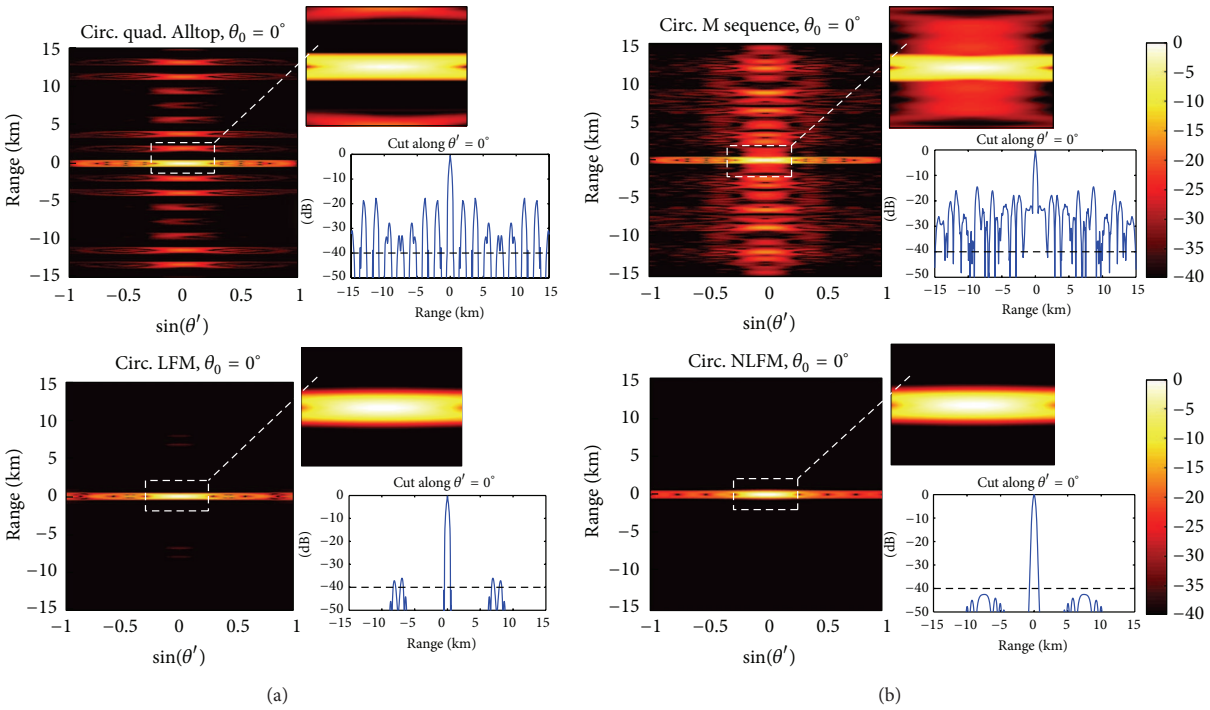

Figure 2.5: Simulation results for Circulating Codes by Babur et al. For each waveform, the range-angle ambiguity function is shown, including a zoom into the center, as well as the range cut at hypothesis angle $\theta' = 0°$. The different waveforms are quadratic Alltop (top left), M-sequence (top right) LFM (bottom left) and non-linear frequency modulation (NLFM, bottom right). LFM signals were found to produce the best results in range. Figure taken from [13].

2.2.2. Hybrid Codes

To improve the performance, a variation of the Circulating Codes has been proposed, the so-called Hybrid Codes [14]. The idea is to add a spatial code over the transmit antenna elements to influence the auto-correlation function. In contrast to the Circulating Codes, all transmit antenna elements are also used on receive in the equations, thus $N = N_{rx} = N_{tx}$ and $\vec{x} = \vec{x}_{rx} = \vec{x}_{tx}$.

The basic signal can therefore be written as in equation 2.12 from [14]:

$$s_T^n(t) = c_n \cdot s^n(t - (n-1) \cdot \Delta t) \,, \tag{2.12}$$

where c_n is the spatial code along the antenna elements.

The proof of the illumination of the whole angular domain is the same, as for the Circulating Codes. But since an extra spatial code is used that multiplies the channels signals with +1 or -1, the beampattern during one pulse looks different. In fact, the difference between +1 and -1 corresponds to a phase shift of 180° which produces more than one beam at a time. Figure 2.6 shows the beampattern over one pulse for a length 7 spatial Barker code. Several moving beams are visible. Still, the Hybrid Codes manage to illuminate the whole 180° area during one pulse.

Naturally, it is also possible to use code elements different to -1 and +1. To be able to decrease the side-lobes around the peak, it was proposed to apply a so-called mismatched filtering instead of matched filtering [17]. The basic principle is to select a new mismatched phase code for the reception of Hybrid Codes, which is longer than the original spatial code, usually by factor 3. The replica stays the same. Since this processing method has been analyzed in detail (see [17–20]), this thesis does not focus further on mismatched filtering. Thus, no corresponding simulations or measurements will be presented.

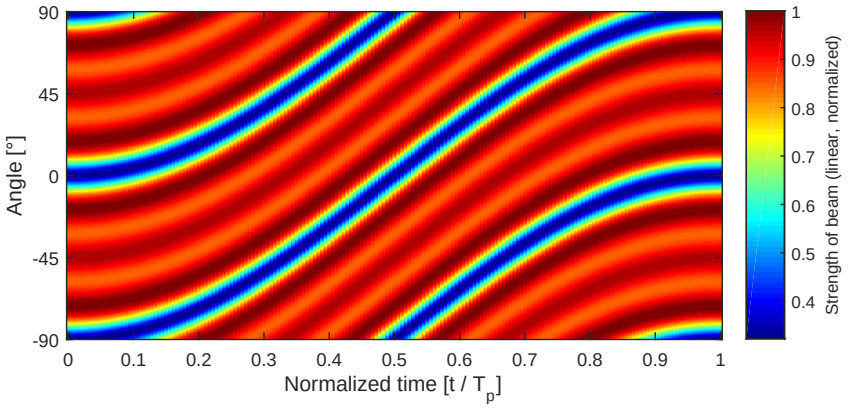

Figure 2.6: Change of the direction of the main beam during one Hybrid Codes pulse. Similar to the Circulating Codes, the beam pattern changes over time.

A matched filter can now be applied similar to equation 2.10. The result according to [14] is

$$\left|\chi(\tau,\theta',\theta_0)\right|^2 = \left|\int \left(\sum_{n=1}^{N} e^{j\cdot\vec{k}(\theta')\cdot\vec{x}(n)}\cdot c^n\cdot s(t+\tau-n\cdot\Delta t+\Delta t)\right)\cdot\left(\sum_{m=1}^{N} e^{j\cdot\vec{k}(\theta_0)\cdot\vec{x}(m)}\cdot c^m\cdot s(t-m\cdot\Delta t+\Delta t)\right)^{*} dt\right|^2, \tag{2.13}$$

where θ' is again the hypothesis about the target direction and θ_0 is the direction of the digital beamforming on receive. When the ambiguity function is only considered in the direction of the receive beamforming, the exponential factors can be omitted and the equation simplifies to

$$\left|\chi_{\theta'=\theta_0}(i)\right|^2 = \left|\sum_{n=1}^{N}\sum_{m=1}^{N} c_n\cdot c_m^{*}\cdot ACF_S(i-n+m)\right|^2, \tag{2.14}$$

according to [14]. By assuming that the signal $s(t)$ has a very large time-bandwidth (BT) product (>100), the discrete ACF of the signal can be replaced by a Dirac delta function [14] which leads to the following equations:

$$\left|\chi_{\theta'=\theta_0}(i)\right|^2 \cong \begin{cases} \left|\sum_{n=1}^{N} c_n\cdot\sum_{m=1}^{N} c_m^{*}\cdot\delta(i-n+m)\right|^2 & for\ |i|<N \\ 0 & for\ elsewhere\ i \end{cases} \tag{2.15}$$

$$\cong \begin{cases} \left|\sum_{n=1}^{N} c_n\cdot c_{i-n}\right|^2 & for\ |i|<N \\ 0 & for\ elsewhere\ i \end{cases} \tag{2.16}$$

$$\cong \begin{cases} \left|ACF_C(i)\right|^2 & for\ |i|<N \\ 0 & for\ elsewhere\ i \end{cases}. \tag{2.17}$$

This means that the main ”corridor” of width $2N-1$ in the ambiguity function is defined by the spatial code. So, if a code with a good ACF is chosen, the resulting peak should be as narrow as for a phased array signal with single waveform [14].

The problem is that this spatial code only defines the narrow peak, but the sidelobes around can still be quite high. Figure 2.7 shows some of the simulation results from the paper. Barker codes have excellent auto-correlation properties, since the produced sidelobes are minimized. As a result, they were used by Babur et al. as spatial codes in their simulations. As already mentioned above, the performance of the Hybrid Codes can be improved by using more receive antennas and weightings.

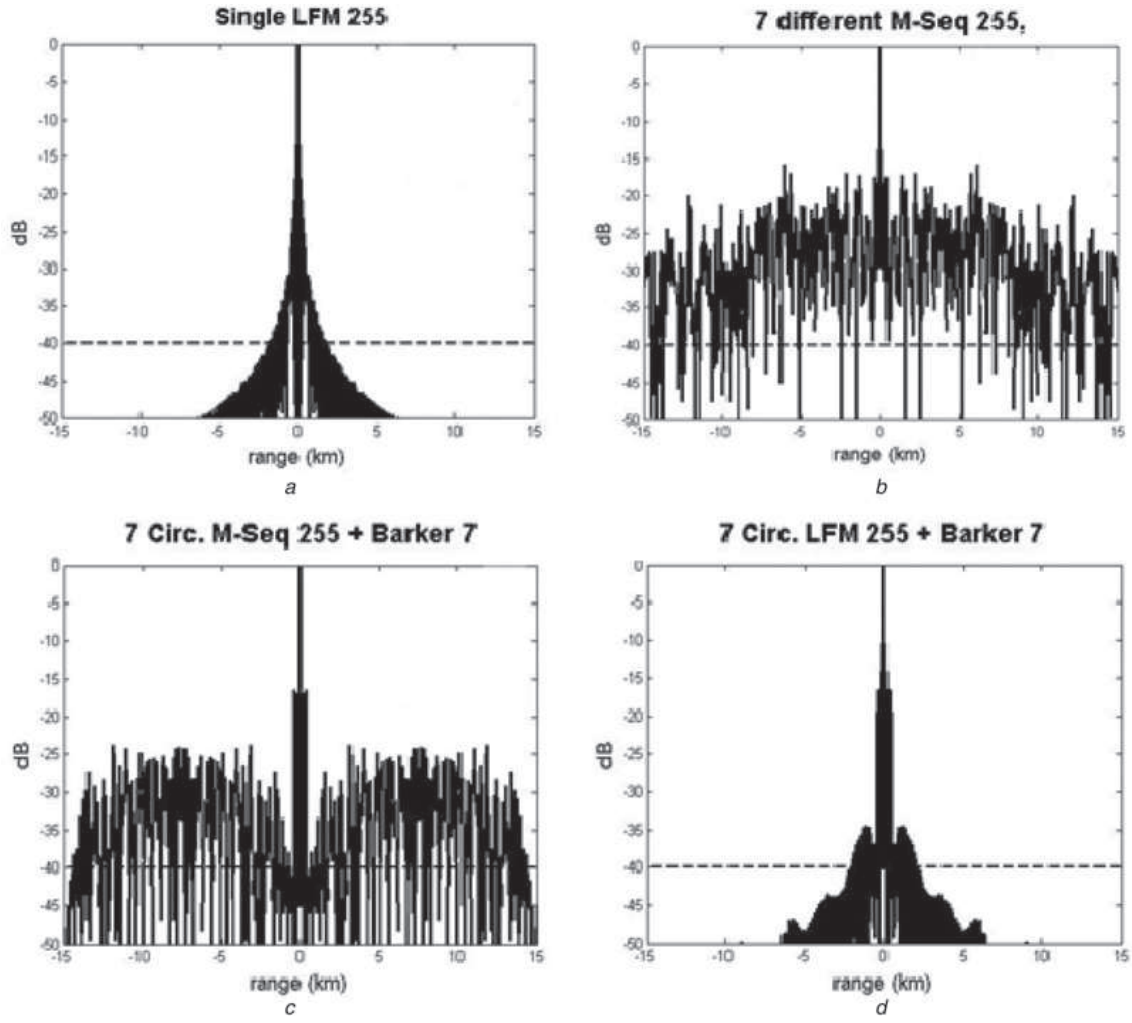

Figure 2.7: Simulation results for Hybrid Codes by Babur et al. Like for the Circulating Codes, different waveforms have been examined (see figure 2.5). For each case, the range cut at $\theta = 0°$ is shown. Figure taken from [14].

2.3. The ASTAP system

In order to apply the theories in practice and do measurements, the radar group of TU Delft built a small radar system, the so-called ASTAP (Advanced Space-Time Adaptive Processing). It consists of an arbitrary waveform generator (AWG) with 8 independent transmit channels and one receive channel, as well as an up- and down-converter for X-band with the same amount of channels.

The AWG consists of a National Instruments FlexRIO field-programmable gate array (FPGA) module with a Timing and Synchronization module and 4 Analog Output Adapter Modules with 2 output channels each. Each output channel consists of a positive and negative output, so that the system can be used in single-ended or balanced mode. The system is controlled by a LabVIEW interface on a computer. The waveform is being generated in Matlab or similar software and then imported as a text file. After it has been downloaded onto the FPGA, the trigger can be started and the transmission of the signal starts periodically. The AWG outputs the signals with a carrier frequency of 300MHz. With an

oscilloscope, the output of the AWG, as well as the received signal from the RF stage can be examined. At the time of this thesis, an antenna was not yet available. A block diagram of the system is shown in figure 2.8 while a photo of it can be found in figure 2.9.

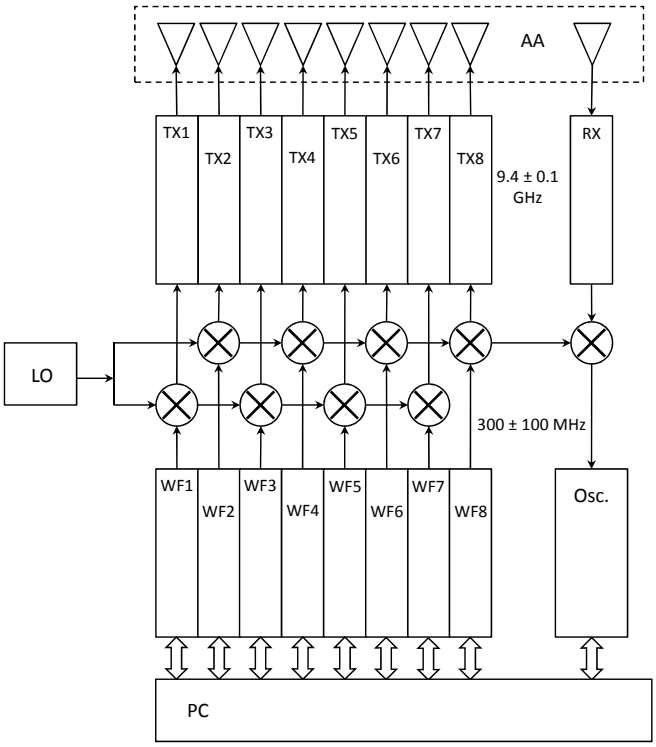

Figure 2.8: Block scheme of the ASTAP system.

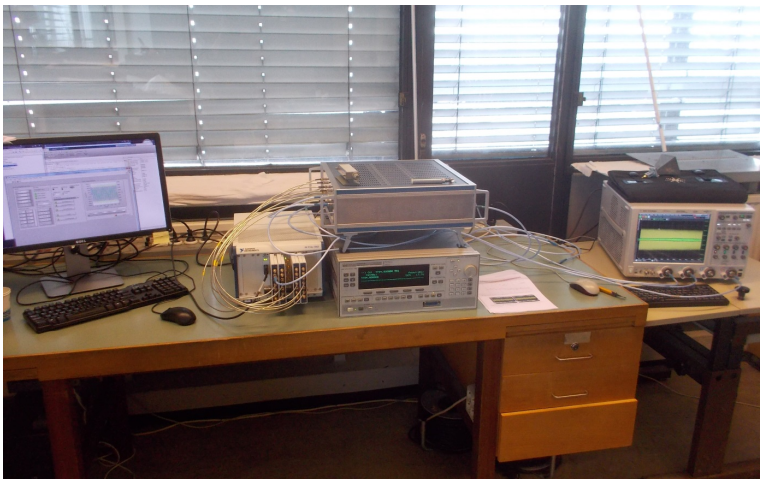

Figure 2.9: The ASTAP system with all of its parts. On the screen on the left, the LabVIEW interface is visible. The three devices in the middle are the AWG (left), the RF stage (top right) and an extra signal generator for synchronization (bottom right). The output of the AWG and the output of the receiver channel are connected to the oscilloscope on the right of the photo.

As already mentioned, previous measurements showed that the system has some issues like constant tones, harmonics and cross-talk between the channels, as well as some kind of unwanted frequency modulation. This thesis investigates how suited the system is for Circulating Codes and Hybrid Codes. In addition to that, measurements with the new improved techniques are being performed.

3

New techniques for Hybrid Codes

The beam pattern of an antenna array is mostly depending on its structure and the radiation pattern of the elements used. The more antenna elements are available in a certain dimension, the narrower the beam in this dimension. On the other hand, a lot of elements in the antenna lead to a very wide peak in range when Circulating Codes are used, as can be seen from equation 2.11. This equation explains the relation of the number of antenna elements to the width of the peak in range.
The used signal has only a very small impact on the beampattern in angle. Thus, improving the Circulating or Hybrid Codes in angle is not useful and is not examined in this thesis. This work focuses on improving the range resolution. First steps have already been taken, like using a spatial coding in the Hybrid Codes or applying mismatched filtering (see section 2.2.2). The new method involves using complementary sequences, also called Golay sequences.

3.1. Complementary Golay sequences

The Golay sequences were first introduced by Marcel Golay in 1961 in [21] and have the property that the sum of the auto-correlation functions of a pair add up constructively and cancel out the sidelobes. Taking a Golay pair a_i and b_i which both have length n, their auto-correlation functions are given as

$$c_{a,j} = \sum_{i=1}^{n-j} a_i a_{i+j} \tag{3.1}$$

and

$$c_{b,j} = \sum_{i=1}^{n-j} b_i b_{i+j} \ , \tag{3.2}$$

as stated in [21], where i is the lag or shift of the codes to each other and j is the index of the output function. If these two auto-correlation functions are added up, the result is

$$c_{a,j} + c_{b,j} = \begin{cases} 0 & for\ j \neq 0 \\ 2n & for\ j = 0 \end{cases} \ . \tag{3.3}$$

Thus, the result of this calculation is 0 for all indexes that are unequal 0. Obviously, this code pair has excellent properties for a radar application, because in theory, the code produces no sidelobes at all. Figure 3.1 shows an example calculation with a Golay pair. In this chapter it is examined, how Golay pairs can be used in combination with Hybrid Codes to improve the resolution of the resulting peak in range.

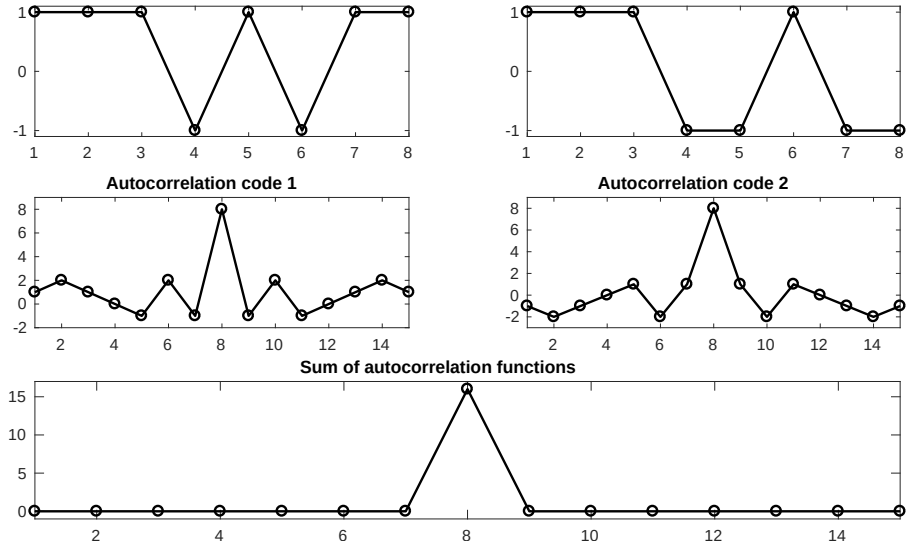

Figure 3.1: Golay principle with pair of length 8. The x-axis is samples in time, while the y-axis is amplitude.

3.2. Transmitting Golay sequences consecutively and processing them individually

The easiest way to make use of Golay pairs in Hybrid Codes, is to send two consecutive pulses, each containing one of the two codes. A matched filter is applied to the received reflected signal from each pulse individually. This means that the first pulse has to be received before the second one will be sent, so the PRT has to be adjusted accordingly. Afterwards, the results from both matched filter operations are coherently added up to remove the sidelobes. The use of this technique with moving targets is difficult since both the Doppler effect, as well as the phase shift due to the displacement influence the signals if the pulses are transmitted at different times.

3.2.1. Stationary targets

At first, the simple case of static targets is examined. Since the target has no speed, no Doppler effect can be observed. Also there is no phase difference between the two pulses due to a displacement, so the processing operation can be described as

$$y(\tau) = \int_{-\infty}^{\infty} x_1(t)\tilde{x}_1^*(t-\tau)dt + \int_{-\infty}^{\infty} x_2(t)\tilde{x}_2^*(t-\tau)dt\ , \tag{3.4}$$

where y is the processed matched filter output of the Golay pair, τ is the displacement of the received signal in time, x_1 and x_2 are the originally transmitted signals with Golay code 1 and 2 respectively and $\tilde{x}_1$ and $\tilde{x}_2$ are the received waveforms. Since the object is not moving, the result is the same, no matter how much time is between the two pulses.

3.2.2. Moving targets

Since many applications involve the observation of moving targets, the influence of their movement on the measurements is going to be analyzed now. The problem is that the Doppler effect, as well as the phase shift due to the displacement of the object during the PRT, influence the processing result. For the following considerations, it is assumed that the target is not changing its velocity during the transmission and reception of one Golay pulse pair.

Doppler effect

The general Doppler effect has already been explained in chapter 1. The movement of a target leads to a reflected signal that is slightly shifted in frequency. Since LFM pulses are used in this study, this means that the whole LFM pulse is shifted in frequency, which corresponds to a shift in time of the same. Thus, after applying a matched filter, the target appears to be slightly closer or further than it actually is, according to the moving direction of the target.
If an X-band radar is assumed, one can expect maximum frequency shifts of a few tens of kilohertz when fast air targets are assumed. Since the bandwidth of the used LFM sweep is most likely in the order of several megahertz, its frequency slope is not very steep and a frequency shift of the mentioned extend is only leading to a relatively small offset in the delay. Therefore, the main focus here lies on the phase shift. The Doppler effect is included in the equations, but usually has a very small impact on the result.

Phase shift

Since the Golay pair has to be transmitted in two pulses at different times, the target is going to move in the meantime. This leads to a phase shift, because the signals have different travelling distances to the target and back. This phase shift influences the signal and the result of the matched filter. Thus, the results can not simply be added up coherently. In [3], it is emphasized that it is very important to consider the phase shift when doing coherent signal processing since a change in range of a fourth of the wavelength $(\lambda/4)$ will shift the phase by π, because the phase shift can be written as

$$\Delta\phi = \frac{-4\pi R_0}{\lambda_c}\,, \tag{3.5}$$

where $\Delta\phi$ is the phase shift, R_0 is the target distance and λ_c is the wavelength of the carrier signal. When equation 3.5 and the Doppler frequency shift are included into equation 3.4 and a constant target velocity is assumed, this leads to

$$y(\tau) = \int_{-\infty}^{\infty} x_1(t)\cdot e^{-j4\pi R_0/\lambda_c}\cdot \tilde{x}_1^*(t-\tau)e^{j2\pi f_d t}dt \;+\; \int_{-\infty}^{\infty} x_2(t)\cdot e^{-j4\pi R_1/\lambda_c}\cdot \tilde{x}_2^*(t-\tau)e^{j2\pi f_d t}dt \tag{3.6}$$

$$= e^{-j4\pi R_0/\lambda_c}\cdot \int_{-\infty}^{\infty} x_1(t)\tilde{x}_1^*(t-\tau)e^{j2\pi f_d t}dt \;+\; e^{-j4\pi R_1/\lambda_c}\cdot \int_{-\infty}^{\infty} x_2(t)\tilde{x}_2^*(t-\tau)e^{j2\pi f_d t}dt, \tag{3.7}$$

where R_0 and R_1 are the distances of the target, when it is illuminated by Golay pulse 1 and 2 respectively and f_d is the Doppler frequency shift.

For these considerations, it is not important to look at the overall phase shift due to the target distance. It will thus be focused on the phase difference between the received reflection of the two Golay pulses. As a result, R_0 can be set to 0 and R_1 will be exchanged with the change in distance due to the speed within the PRT. The resulting equation is

$$y(\tau) = \int_{-\infty}^{\infty} x_1(t)\tilde{x}_1^*(t-\tau)e^{j2\pi f_d t}dt \;+\; e^{-j4\pi(v\cdot PRT)/\lambda_c}\cdot \int_{-\infty}^{\infty} x_2(t)\tilde{x}_2^*(t-\tau)e^{j2\pi f_d t}dt\,, \tag{3.8}$$

where v is the velocity of the target and PRT is the time between the two Golay pulses. If the velocity of the target is known precisely, the phase shift can be removed by multiplying the processed matched filter result of the second pulse by the factor $e^{j4\pi(v\cdot PRT)/\lambda_c}$. When the phase shift is removed, a clear peak is found at the target velocity. If the velocity of the target is not known exactly, the phase shift compensation can be done for a limited number of assumed velocities. Since there is a limited unambiguous velocity interval (see chapter 1), there can also be peaks found at other velocities than the actual one. This is explained in figure 3.2. As a result, the velocity of the target must be roughly known, in order for the radar to correctly detect it. Changing the PRT between the Golay pulses, changes the sidelobes due to the velocity ambiguity, as can be seen from equation 1.10.

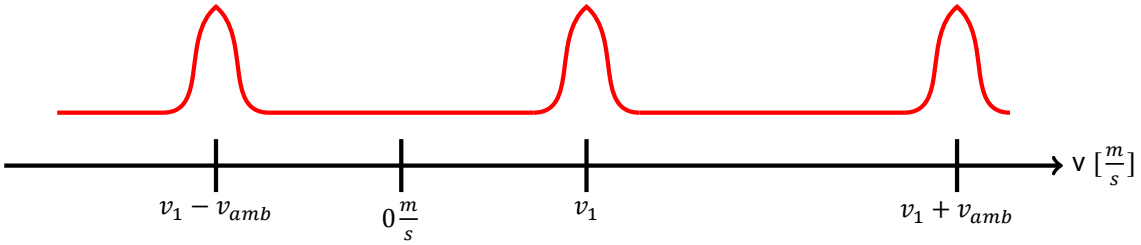

Figure 3.2: When the phase shift is compensated for a limited number of velocities, peaks appear at the actual velocity and at the actual velocity plus minus multiples of the maximum unambiguous velocity, so: $v = v_1$ and $v = v_1 \pm n \cdot v_{max}$ with $n = 1, 2, 3, ...$ The velocity measurement is only unambiguous up to a certain maximum velocity, as has been explained in chapter 1.

3.3. Transmitting more than one Golay pair consecutively and process them individually

The Golay code pair is only useful at the correctly compensated velocity. There are still sidelobes at other velocities that are a result of the phase shift. By transmitting several consecutive Golay pulse pairs and adding up the processing results, these sidelobes can be reduced. The reason for this is that for every new Golay pair, the target will be at a new position and the phase of the reflected signal will thus be different. Due to these different phases of the received signal, the correction will lead to sidelobes that are positioned at slightly different velocities for each Golay pair while the main peak at the correctly compensated velocity stays the same for all of them. Thus, the main peak gets stronger with every Golay pair while the sidelobes do not grow much, because they spread over all velocities. The sidelobes due to the velocity ambiguity still exist and need to be taken into account.

3.4. Transmitting Golay pair in parallel on different elements

Another concept examined in this thesis, is the transmission of both Golay codes at the same time through different elements of the antenna array. If both codes were transmitted at the same moment in time and within the same pulse, there would not be any phase shift and the resulting peak would be as narrow as for stationary targets. Since the Golay pair is transmitted at the same moment, the double amount of transmit antenna elements needs to be used.
The problem with this technique is that since we are transmitting simultaneously, we have to use separate elements that will also be separated physically to a certain extend. Unfortunately, this leads again to the introduction of a phase shift due to slightly different distances from the different elements to the target and might ruin the expected narrow peak produced by the Golay pair.

There are different ways to implement this. One possibility is to change the spatial code to a code of the double length which consists of both Golay codes. This corresponds to equation 2.13. Another possibility is to transmit two Hybrid Codes in parallel on different elements. This means that two channels always transmit exactly in parallel (without the time shift Δt between them). This can be described with a signal x that consists of two sub-signals x_1 and x_2, which leads to the matched filter result

$$y(\tau) = \int_{-\infty}^{\infty} (x_1(t) + x_2(t)) \, (\tilde{x}_1(t-\tau) + \tilde{x}_2(t-\tau))^* \, dt \, . \tag{3.9}$$

3.5. Transmitting Golay pair in parallel at different frequencies

The idea to submit the signals simultaneously but at different carrier frequencies, could also solve the problem of the phase shift due to displacement. For example, the first Golay code can be transmitted by using an LFM sweep with a center frequency below the carrier frequency while the other one has a center frequency above the carrier frequency. But the same problem occurs, since the two codes are being transmitted at different frequencies, also their wavelengths differ and thus the phases due to

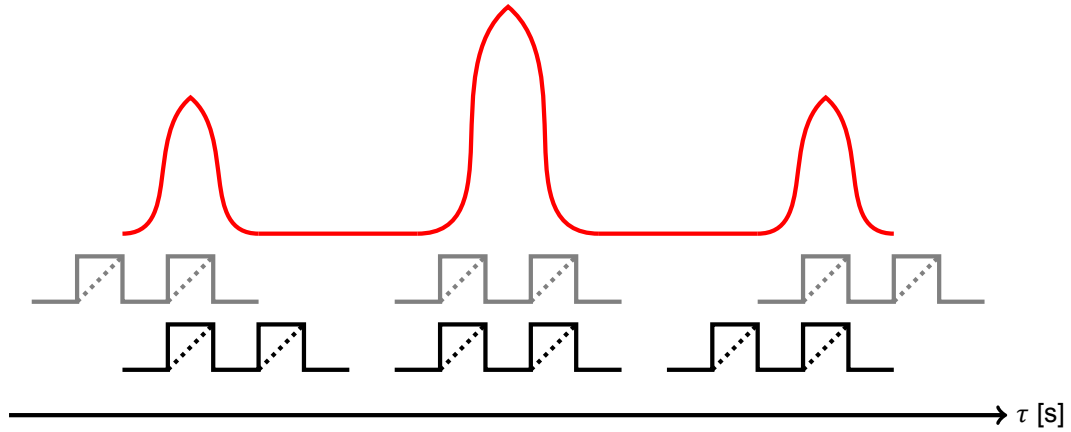

Figure 3.3: Matched filter output for two close Golay pulses consisting of two consecutive up-chirps. When the replica and received signal are aligned perfectly, the auto-correlation function shows one big peak. But when the left pulse aligns with the right one and vice versa, there are additional strong sidelobes in the auto-correlation function.

the distance to the target do not match. This might also negatively influence the results. In this case, equation 3.9 also holds.

3.6. Transmitting Golay pair very closely in time

Alternatively, the two Golay pulses could also be transmitted right after each other, with no or only a very short pause in between. Like this, there will still be a phase shift, but its effect will be minimized. This technique is actually very similar to the technique described in section 3.2, but in this case, the matched filter is not applied on each pulse individually, but as a whole on both pulses. The question is, how high the sidelobes are, since two similar signals are used close to each other which will lead to one strong peak and two strong sidelobes as shown in figure 3.3. Most likely, this effect can be reduced by using an LFM up-chirp in combination with an LFM down-chirp.

4

Analysis

This chapter deals with the implementation of the aforementioned methods in Matlab, in order to run simulations. In addition to that, the measurements done with the ASTAP system are being presented.

4.1. Implementation of techniques

It was decided to create three different Matlab scripts (see appendix C). The first one is generating a circulating LFM signal (*generate_lfm.m*) that can be used in the second script, which does the processing of the received signal (*af_normalized.m*). These two scripts are mainly used to verify the already existing theories of circulating and Hybrid Codes, since only one single pulse can be generated and processed. The third script runs the signals generation and the processing for a defined number of Golay pairs for a possibly moving target (*af_normalized_golay.m*) to verify the new methods as described in sections 3.2 and 3.3. The purpose of the mentioned Matlab scripts is explained hereafter.

4.1.1. generate_lfm.m

The purpose of this script is to generate a complex LFM sweep that can be used in further scripts. It has the following adjustable input parameters:

- Number of antenna elements (N)
- Sampling frequency (Fs)
- Carrier frequency (Fc)
- Bandwidth (B)
- Pulse length (T)
- Spatial code along the antennas (code)

The output of the script is a matrix that contains the signals of each channel. Note that the signal is generated in baseband with a center frequency of 0Hz. The carrier frequency input parameter is used to add the phase shifts introduced by the antenna and possibly the Doppler effect.

4.1.2. af_normalized.m

This script can be run consecutively to *generate_lfm.m*. It takes the LFM signal and uses it for a simulation of the processing result for a defined static target by adding the according phase shifts due to the antenna positions, performing digital beamforming and then applying the matched filter. It has the following input parameters:

- Range (r) and angle (ra) of the target
- Transmit antenna positions (x_tx)
- Receive antenna positions (x_rx)

The output of the script is a 2-dimensional ambiguity function (range and angle) that is the basis for several figures.

4.1.3. af_normalized_golay.m

This script is basically a combination of the two above mentioned scripts. It both generates the circulating LFM signal and applies the processing for a defined number of Golay pairs. It has the following input parameters:

- Number of antenna elements (N)
- Sampling frequency (Fs)
- Carrier frequency (Fc)
- Bandwidth (B)
- Pulse length (T)
- Spatial code along the antennas (code)
- Number of Golay pulses (np_max)
- Range (r) and angle (ra) of the target
- Doppler frequency caused by the target movement (fD)
- Assumed Doppler frequencies (fD_assumed)
- Pulse repetition time within a Golay pair (PRT)
- Golay pair repetition time (GRT)
- Transmit antenna positions (x_tx)
- Receive antenna positions (x_rx)

The assumed Doppler frequencies vector defines the Doppler area for which the phase shift due to displacement is corrected (see chapter 3). For a correctly corrected phase shift, the matched filter produces a strong and narrow peak. The number of Golay pulses should be a multiple of two, since one Golay pair consists of two Golay pulses. The output of the script is a 3-dimensional ambiguity function which is the sum of the processing results of every pulse. Its three dimensions are angle, range and Doppler. This script is the basis for several figures.

4.2. Simulation results

Several simulations have been conducted to verify the theoretical approaches mentioned in chapter 3. First, the well-known Circulating and Hybrid Codes, as well as the phased array case have been examined again, before implementing the new methods.

The general simulation setup is an assumed radar antenna that uses its elements for transmit, as well as receive. One single point target is assumed to reflect the transmit signal, which is then received again by the radar antenna and processed. Since this is a purely mathematical examination of the techniques, no noise or losses are included in the simulations. In addition to that, it is assumed that the target reflects the whole transmit signal. Therefore, the amplitudes of the transmitted and received signal are the same. If not mentioned otherwise, the simulations are conducted for static targets.

The simulation parameters for each simulation are summarized in each subsection. In general, the parameters are based on the ones that were used in [13] and [14], to make the simulation results comparable to the existing studies. The target is situated at 0m and 0° in azimuth. The elements of the antenna are spaced $\lambda_c/2$ from each other where λ_c is the wavelength of the carrier signal. For receiving, only one element is used in the figures discussed here, which matches with the simulations done in the papers. Finally, it is assumed that all antenna elements have an isotropic radiation pattern and the targets are single point objects that reflect the incoming wave entirely. To show the potential of these techniques, figures can be found in the appendix that were generated with the use of all antenna elements on receive, in combination with a hamming weighting in time and a 30dB Taylor weighting over the antenna elements to decrease sidelobes.

4.2.1. Phased array

As stated in section 2.2.1, the Circulating Codes produce a peak in range that is N times wider than for a phased array. In section 2.2.2, it is shown that the Hybrid Codes manage to recover the range resolution of a phased array with a single waveform. To verify this, the ambiguity function in range and angle of a phased array has been simulated. It is used for comparison in the following sections. The simulation parameters are summarized in table 4.1 and the result is shown in figure 4.1. The highest sidelobes in range can be found at -13.5dB, while the sidelobes in angle are at about -12.8dB. The peak in range has a width of about 120m.

Table 4.1: Parameters used for phased array simulation.

Parameter	**Value**
Number of antennas (N):	8
Sampling frequency (Fs)	1.25GHz
Carrier frequency (Fc)	10GHz
Bandwidth (B)	2.55MHz
Length of each LFM sweep (T)	100μs

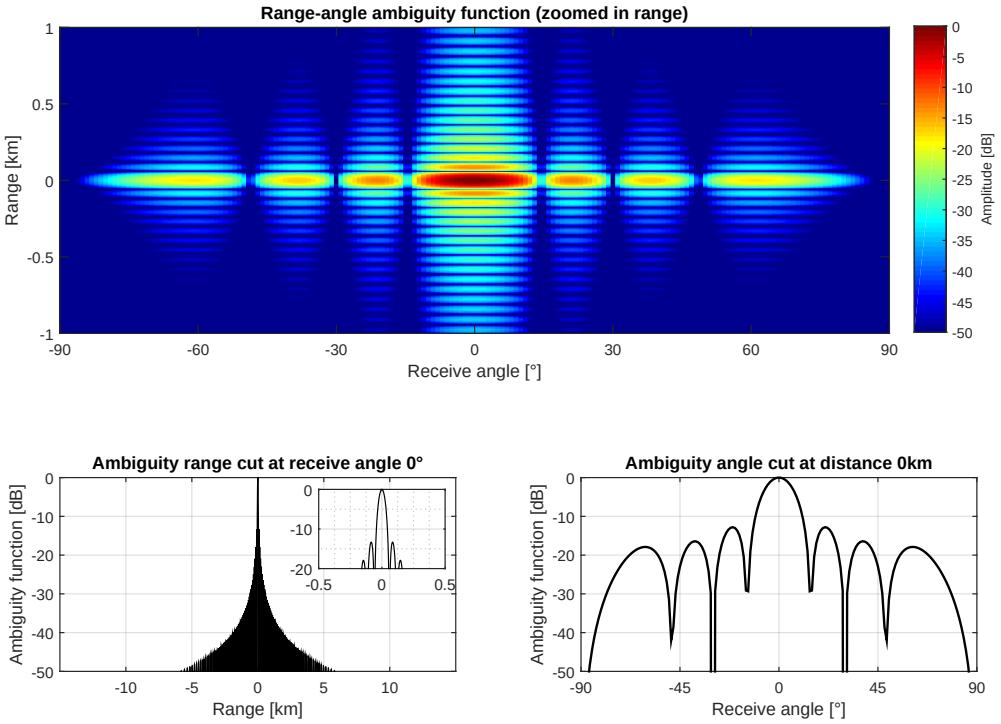

Figure 4.1: Simulation results for one phased array pulse with single waveform in Matlab. The parameters used in this simulation are shown in table 4.1. Top: two-dimensional ambiguity function in range and angle. Bottom left: range cut at angle 0°. Bottom right: angle cut at range 0km.

4.2.2. Circulating Codes

As can be seen from figure 4.2, the figures from the Matlab simulation match the results from [13] as shown in chapter 2. A peak is visible at 0° and 0m, which has a width of about 950m. This corresponds to the results of Babur et al., since it is about N times wider in range than the phased array peak in figure 4.1. Also, the sidelobe level of about -35dB is the same. The angle cut looks like the one presented in the paper, with the highest sidelobes at about -12.8dB. Interestingly, the results of the paper and the simulation slighty differ in the shape of the range sidelobes at -7.5km and 7.5km. The reason might be a different way of generating the LFM pulse.
In the appendix, additional figures of Circulating Codes simulations can be found. An angle-angle cut of the ambiguity function that has also been presented in [13] can be found in figure A.1, while the results for different target angles are shown in figures A.2 and A.3.
By adding weightings and the usage of all elements on receive, the performance of the Circulating Codes can be drastically improved, as can be seen in figure A.4 in the appendix, where the highest range sidelobes are found at about -39.3dB and and the highest angle sidelobes at -36.2dB. The parameters used for this simulation are summarized in table 4.2.

Table 4.2: Parameters used for Circulating Codes simulation.

Parameter	Value
Number of antennas (N):	8
Sampling frequency (Fs)	1.25GHz
Carrier frequency (Fc)	10GHz
Bandwidth (B)	2.55MHz
Length of each LFM sweep (T)	100µs

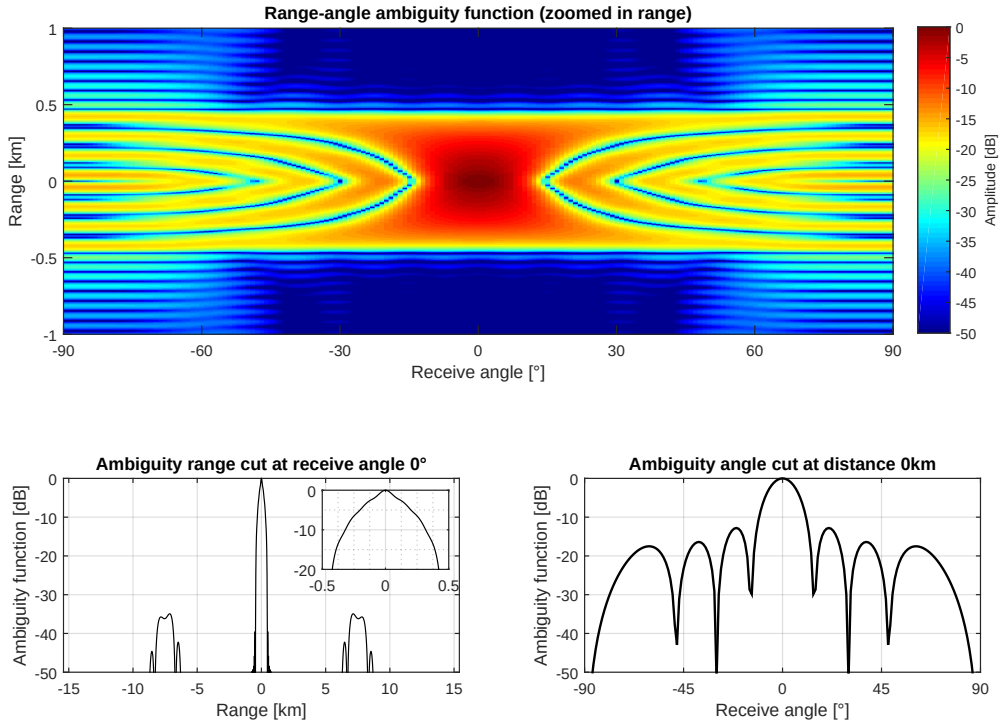

Figure 4.2: Simulation results for one Circulating Codes pulse in Matlab. The parameters used in this simulation are shown in table 4.2. Top: two-dimensional ambiguity function in range and angle. Bottom left: range cut at angle 0°. Bottom right: angle cut at range 0km.

4.2.3. Hybrid Codes

As already mentioned in chapter 2, Barker codes have optimal auto-correlation properties. They are thus used as spatial codes in these simulations. Figure 4.3 shows the Matlab simulation results for Hybrid Codes with Barker 7 code. These match the results from [14], which were also briefly presented in chapter 2. A narrow peak is visible at 0° and 0m, surrounded by a sidelobe plateau with sidelobes between -16.5db and -10.4dB. The peak has the same width in range as the one for a phased array in figure 4.1. The sidelobe pattern in angle looks almost the same as for the Circulating Codes, with a slightly wider main lobe. The highest sidelobes in angle are at about -12.7dB. The results generally match the ones Babur et al. presented in their work.
By adding weightings and the usage of all elements on receive, the performance can be drastically improved, as can be seen in figure A.5 in the appendix. In that simulation, the sidelobes plateau in range is below -16.4dB, while the other sidelobes are even below -47dB. In angle, the sidelobes are as low as -41dB, but only at exactly 0km. The parameters used are summarized in table 4.3.

Table 4.3: Parameters used for Hybrid Codes simulation.

Parameter	Value
Number of antennas (N):	7
Spatial code:	Barker 7
Sampling frequency (Fs)	1.25GHz
Carrier frequency (Fc)	10GHz
Bandwidth (B)	2.55MHz
Length of each LFM sweep (T)	100μs

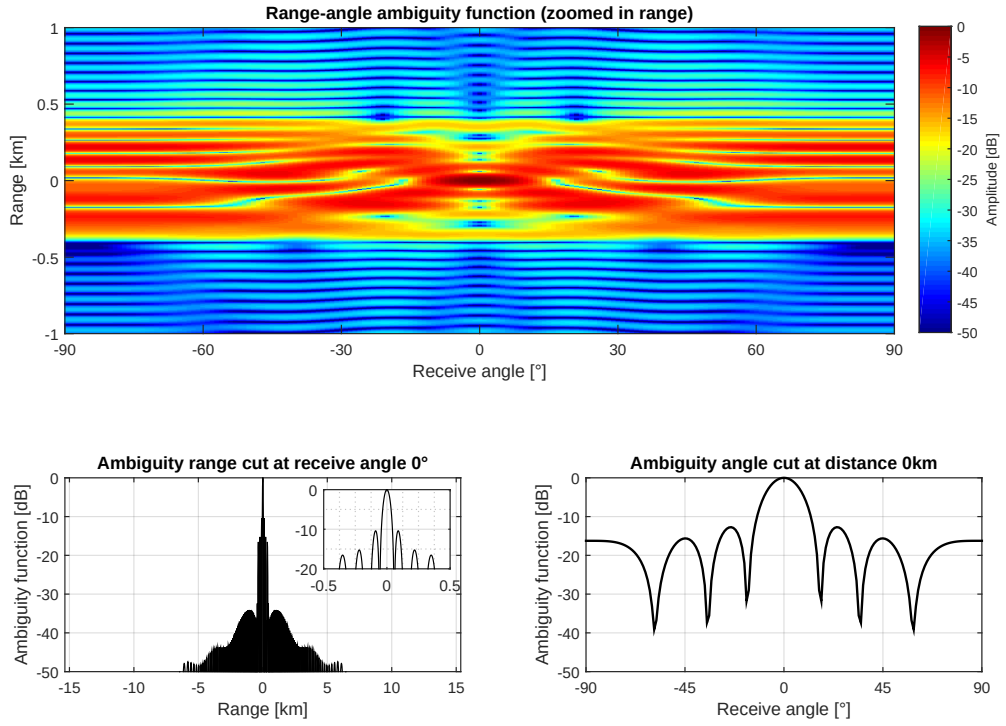

Figure 4.3: Simulation results for one Hybrid Codes pulse with Barker 7 code in Matlab. The parameters used in this simulation are shown in table 4.3. Top: two-dimensional ambiguity function in range and angle. Bottom left: range cut at angle 0°. Bottom right: angle cut at range 0km.

4.2.4. Hybrid Codes with Golay sequences

In this section, the new ideas for improvement of Hybrid Codes by the use of Golay pairs are examined in Matlab simulations. The same basic settings are used as for the simulations of the Circulating Codes and the Hybrid Codes above. The antennas are placed at the same positions and again only one receive antenna is used.

Transmitting Golay sequences consecutively and processing them individually

In this simulation, two Hybrid Code pulses are assumed to be transmitted, each one with one Golay code of a pair as spatial code. As can be observed in figure 4.4, a very narrow peak in range is formed at $0°$, corresponding to the phased array result in figure 4.1. Generally, the resulting range cut looks almost identical to the phased array simulation result. The sidelobes in range are at about -13.3dB, which is lower than in the Hybrid Code case. In addition to that, there is a smaller number of sidelobes in range. It is obvious that the sidelobe corridor in azimuth, has a width of about 0.5 kilometers. This is half as for the Circulating or Hybrid Codes. The angular pattern is still very similar, due to the usage of the same antenna configuration. The highest angular sidelobes are at -11.8dB.
Figure 4.5 shows the impact of the Doppler frequency shift and especially the phase shift due to the displacement of the object. It shows the range cut, when the phase shift is corrected for different assumed velocities of the object. Only when the phase shift is properly corrected according to the target velocity, the sidelobes are removed and the result corresponds to the one for a static target, as presented in figure 4.4.
By adding weightings and the usage of all elements on receive, the performance can again be drastically improved, as can be seen in figure A.6 in the appendix. The range sidelobes there are located at -35.7dB, while the sidelobes in angle have a magnitude of -20.4dB. The used parameters are summarized in table 4.4.

Table 4.4: Parameters used for Hybrid Codes pulses with Golay sequences simulation.

Parameter	**Value**
Number of antennas (N):	8
Spatial code:	Golay pair
Sampling frequency (Fs)	1.25GHz
Carrier frequency (Fc)	10GHz
Bandwidth (B)	2.55MHz
Length of each LFM sweep (T)	100μs
Time between pulses (PRT)	200μs
Corrected Doppler frequencies	-4kHz to +4kHz
Corrected velocities	-60 $\frac{m}{s}$ to +60 $\frac{m}{s}$
Doppler frequency of target	1kHz
Velocity of target	15 $\frac{m}{s}$

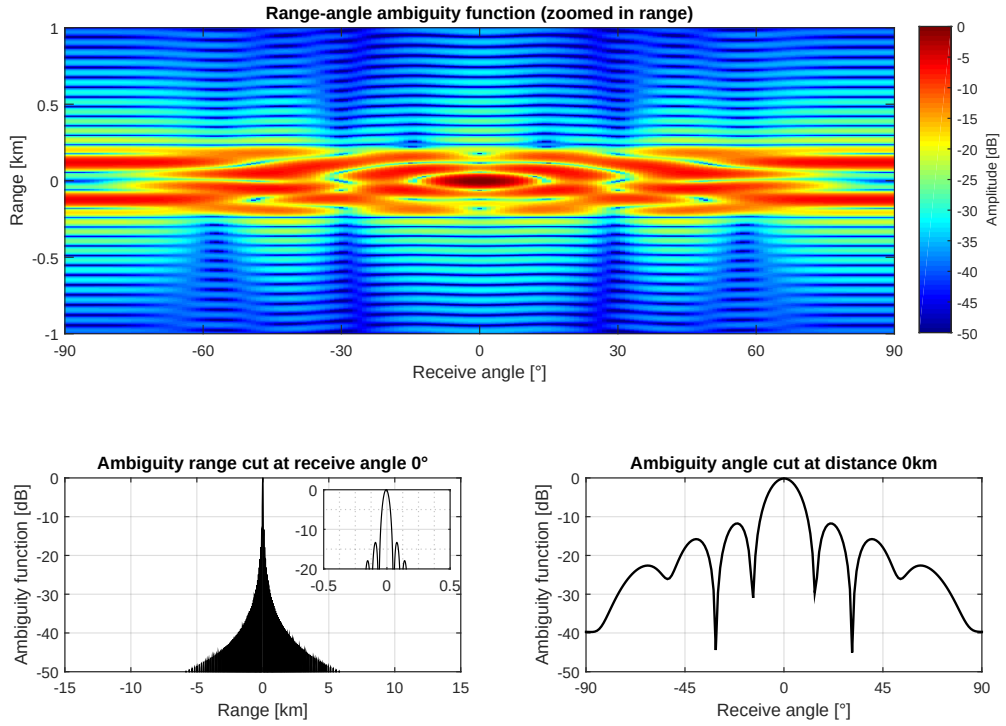

Figure 4.4: Simulation results for individually processed Hybrid Codes pulses with Golay sequences in Matlab. The parameters used in this simulation are shown in table 4.4. Top: two-dimensional ambiguity function in range and angle. Bottom left: range cut at angle 0°. Bottom right: angle cut at range 0km.

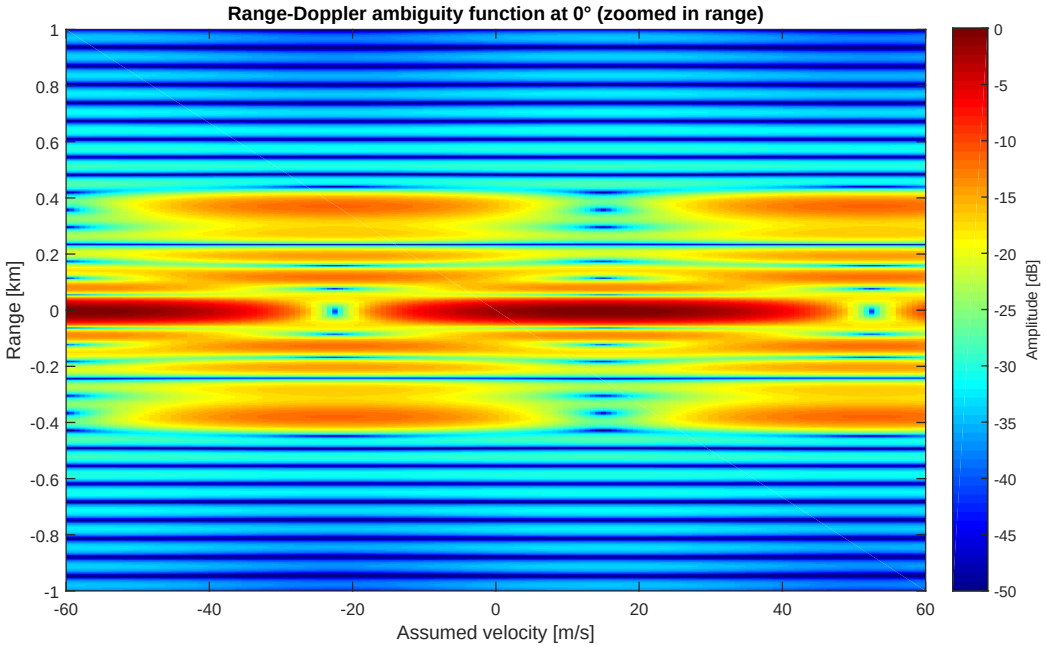

Figure 4.5: Simulation results for individually processed Hybrid Codes pulses with Golay sequences in Matlab involving a moving target. The parameters used in this simulation are shown in table 4.4. The figure shows the range cut at angle 0° for different corrected Doppler frequencies. At the Doppler frequency of the target, a narrow peak in range can be observed.

Transmitting more than one Golay pair consecutively and process them individually

To improve the sidelobe levels in Doppler, several Golay pairs are transmitted after each other and each pulse is processed individually in this simulation. Since the phase shift due to displacement of the target is slightly different for each Golay pulse, this extra information can now be used to reduce the sidelobes as explained in section 3.3. This can be observed in figure 4.6. It is obvious that the peak at range 0m is very narrow, but that there are still a lot of very high sidelobes (up to -11dB) at other Doppler frequencies. The strongest of these sidelobes are located exactly in the middle of the main peak and its ambiguity. They are caused by the fact that each identical pulse is repeated after a time that is equivalent to the sum of PRT and GRT. Therefore, these sidelobes are ambiguities produced by both pulses, but related to a PRT of 0.4ms, instead of 0.2ms. Transmitting more pulses is narrowing these sidelobes further, but not removing them entirely. The used simulation parameters are summarized in table 4.5.

Table 4.5: Parameters used for simulation of several individually processed Hybrid Codes pulses with Golay sequences.

Parameter	**Value**
Number of antennas (N):	8
Spatial code:	Golay pair
Number of Golay pairs:	8
Sampling frequency (Fs)	1.25GHz
Carrier frequency (Fc)	10GHz
Bandwidth (B)	2.55MHz
Length of each LFM sweep (T)	100μs
Time between pulses (PRT)	200μs
Time between Golay pairs (GRT)	200μs
Corrected Doppler frequencies	-4kHz to +4kHz
Corrected velocities	-60 $\frac{m}{s}$ to +60 $\frac{m}{s}$
Doppler frequency of target	1kHz
Velocity of target	15 $\frac{m}{s}$

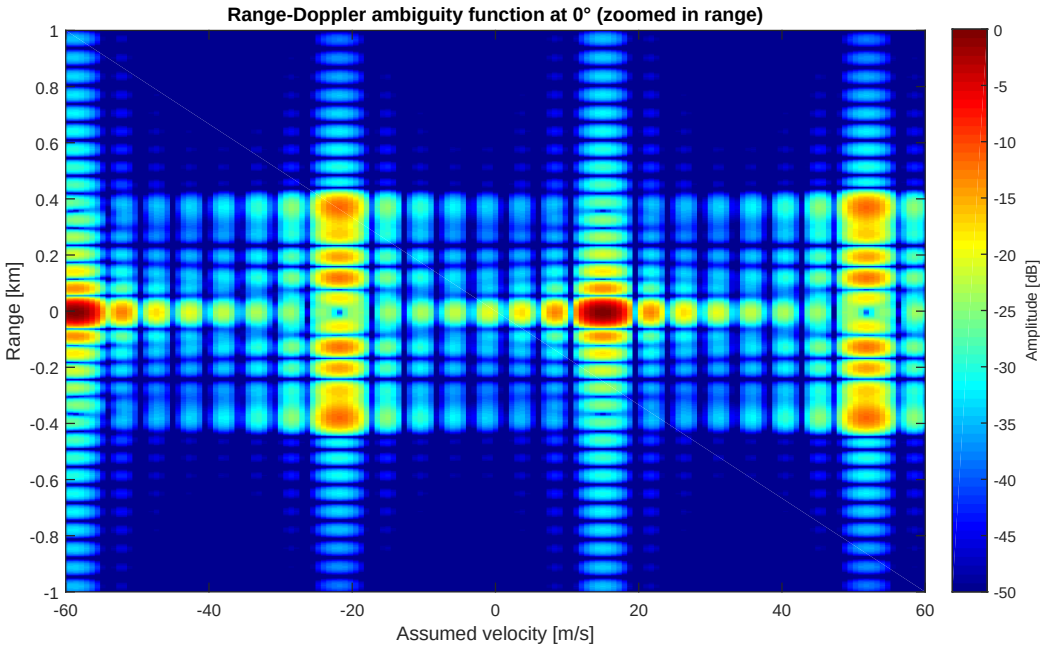

Figure 4.6: Simulation results for several individually processed Hybrid Codes pulses with Golay sequences in Matlab. The figure shows the range cut at angle $0°$ for different corrected Doppler frequencies. At the Doppler frequency of the target, a narrow peak in range can be observed. The parameter for this simulation are shown in 4.5.

Transmitting Golay pair in parallel on different elements

In order to avoid the effect of the phase shift due to the displacement of the target, which leads to the effects shown in figures 4.5 and 4.6, it was tried to combine both parts of a Golay pair in one pulse. This was done in this simulation by transmitting them on different antenna elements. A typical example is shown in figure 4.7, where 16 elements are used. The first 8 elements are transmitting Golay Code 1, while the second 8 elements are transmitting Golay Code 2. Each element starts at another time according to the time shift for Circulating and Hybrid Codes. It is thus one Hybrid Code pulse with 16 elements. Although the main peak recovers the range resolution of a phased array, a lot of sidelobes are visible at -12.3dB and the resulting sidelobe plateau is very wide. The parameters used for this simulation are summarized in table 4.6.

Table 4.6: Parameters used for Hybrid Codes pulses with Golay sequences simulation on different antenna elements.

Parameter	Value
Number of antennas (N):	16
Spatial code:	Golay pair
Sampling frequency (Fs)	1.25GHz
Carrier frequency (Fc)	10GHz
Bandwidth (B)	2.55MHz
Length of each LFM sweep (T)	100μs

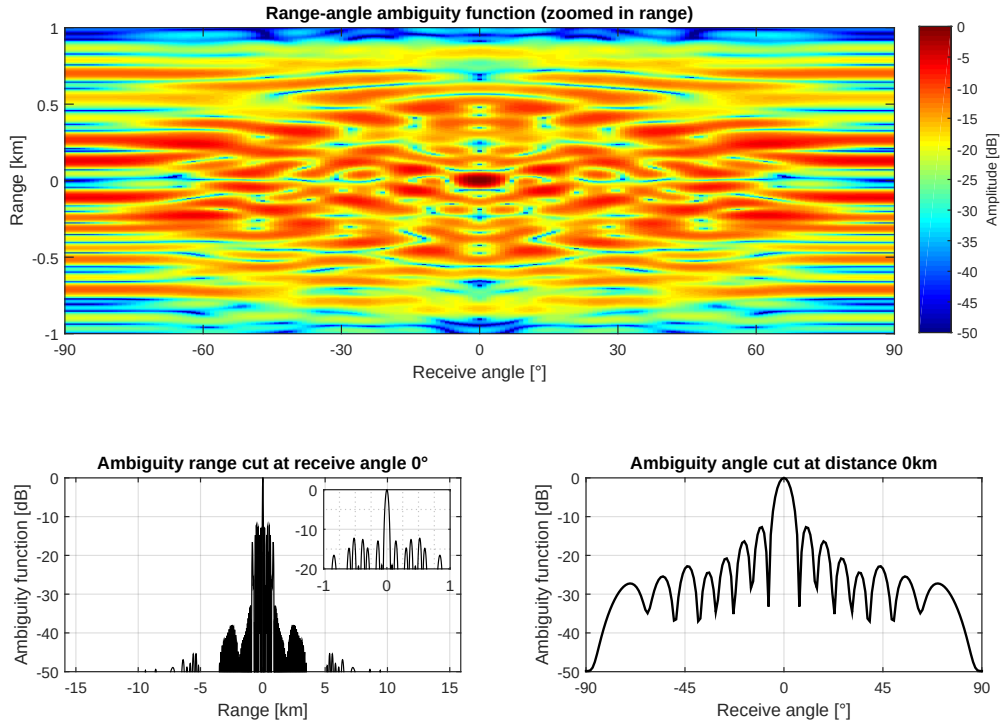

Figure 4.7: Simulation results for Hybrid Codes pulses with Golay sequences on different antenna elements in Matlab. The parameters used in this simulation are shown in table 4.6. Top: two-dimensional ambiguity function in range and angle. Bottom left: range cut at angle 0°. Bottom right: angle cut at range 0km.

Transmitting Golay pair in parallel at different frequencies

To combine the whole Golay pair in one pulse, it was also investigated if they can be transmitted in parallel at different frequencies. The result of the corresponding simulation is shown in figure 4.8. In this case, the two codes are transmitted on 9.99GHz and 10.01GHz respectively. It can be observed that there is a very narrow peak at range 0 kilometers. There is also a sidelobe plateau similar to the processing results of the Hybrid Codes including Barker code with a magnitude of up to -11.4dB. In general, the sidelobes are similar to the Hybrid Codes with Barker 7 spatial code. Different carrier frequencies of the two signals deliver similar results. The parameters used for the simulation is shown in table 4.7.

Table 4.7: Parameters used for Hybrid Codes pulses with Golay sequences simulation at different frequencies.

Parameter	Value
Number of antennas (N):	8
Spatial code:	Golay pair
Sampling frequency (Fs)	1.25GHz
Carrier frequency (Fc)	9.99GHz and 10.01GHz
Bandwidth (B)	2.55MHz
Length of each LFM sweep (T)	100μs

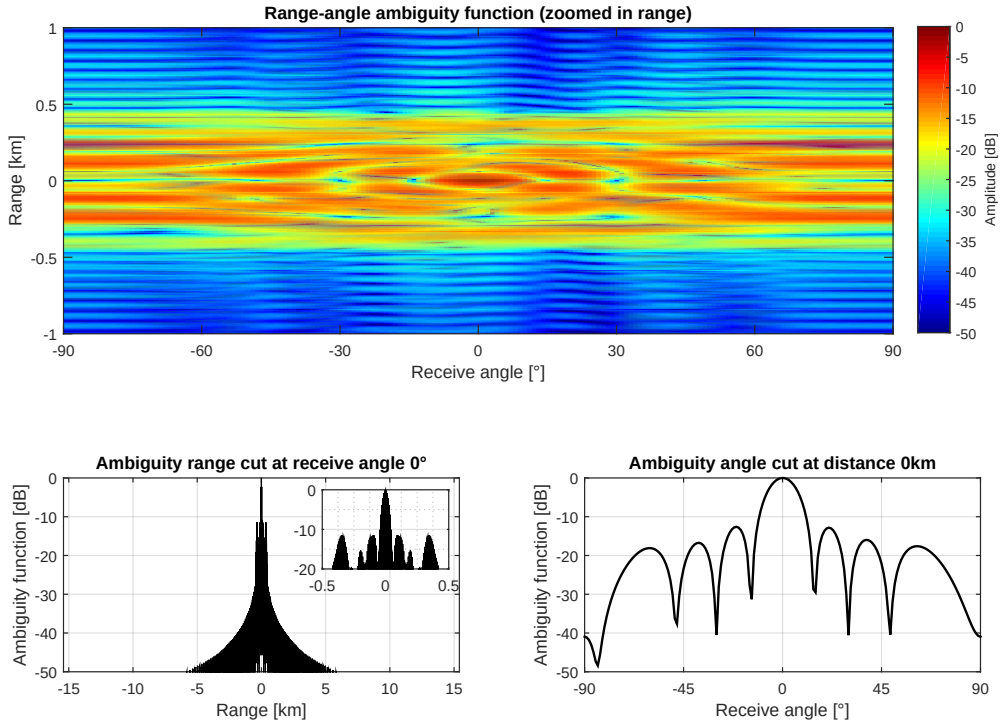

Figure 4.8: Simulation results for Hybrid Codes pulses with Golay sequences at different frequencies in Matlab. The parameters used in this simulation are shown in table 4.7. Top: two-dimensional ambiguity function in range and angle. Bottom left: range cut at angle 0°. Bottom right: angle cut at range 0km.

Transmitting Golay pair very closely in time

Another idea in order to remove, or at least decrease the effect of the phase shift due to the displacement of the target, is to transmit the two Golay Codes right after each other with only a small delay. Figure 4.9 shows the result when two consecutive up-chirp LFM signals are used. This simulation does not involve a moving target, because its performance for static targets is the most important aspect. The influence of the Doppler effect and the according phase shift due to displacement are assumed to be almost negligible in this case.
The sidelobe corridor is almost identical to the one in figure 4.4. One strong peak at range 0m is visible, but also two strong -13.8dB sidelobes at about -16km and +16km. This corresponds to the expectations explained in section 3.6. By using both an up- and down-chirp LFM signal, the sidelobes can be decreased, as can be seen in figure 4.10. The highest sidelobes in range are then at -13.3dB, which corresponds to the result in figure 4.4. The angular sidelobes can be found at -12.7dB.
The parameters for the simulation are shown in table 4.8. By adding weightings and the usage of all elements on receive, the performance can be slightly improved, as can be seen in figure A.7 in the appendix.

Table 4.8: Parameters used for Hybrid Codes pulses with Golay sequences simulation when both codes are transmitted very closely in time to each other.

Parameter	Value
Number of antennas (N):	8
Spatial code:	Golay pair
Sampling frequency (Fs)	1.25GHz
Carrier frequency (Fc)	10GHz
Bandwidth (B)	2.55MHz
Length of each LFM sweep (T)	100μs
Distance of Golay Code pulses	1000 samples (0.8μs)

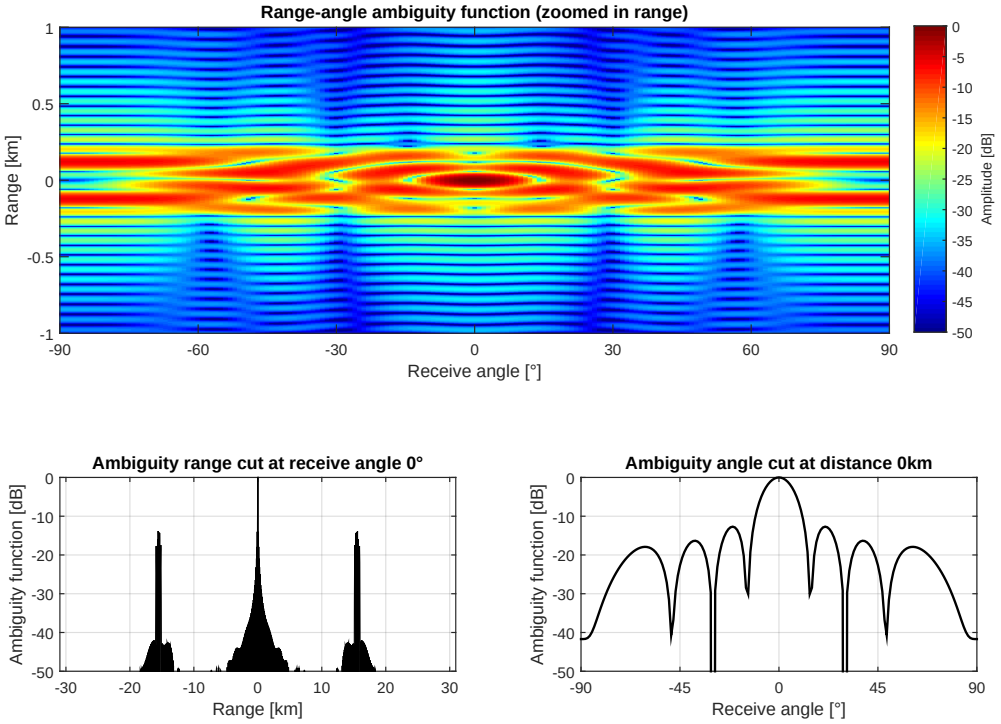

Figure 4.9: Simulation results for Hybrid Codes pulses with Golay sequences transmitted very close in time in Matlab with two LFM up-chirps. The parameters used in this simulation are shown in table 4.8. Top: two-dimensional ambiguity function in range and angle. Bottom left: range cut at angle $0°$. Bottom right: angle cut at range 0km.

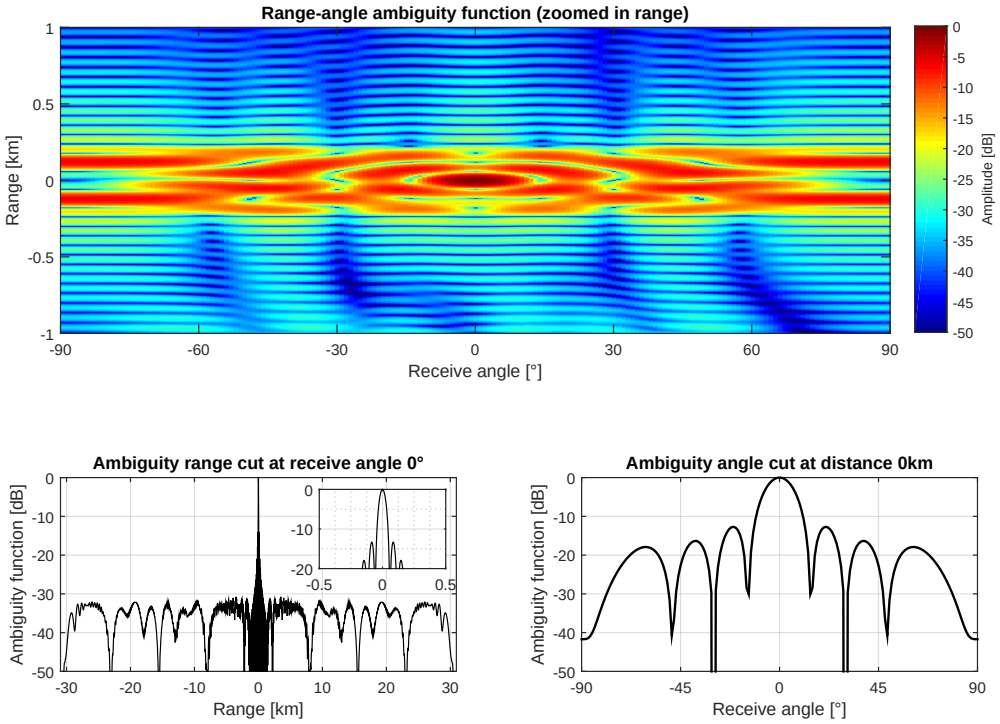

Figure 4.10: Simulation results for Hybrid Codes pulse with Golay sequences transmitted very close in time in Matlab with one LFM up- and one LFM down-chirp. The parameters used in this simulation are shown in table 4.8. Top: two-dimensional ambiguity function in range and angle. Bottom left: range cut at angle 0°. Bottom right: angle cut at range 0km.

4.3. Measurement results

The measurements have been conducted with the same parameters as the simulations that have been presented in the last section. Since the system consists of several parts, as can be seen in figures 2.8 and 2.9, the focus here lies on the AWG. Conducting proper measurements with the whole system was too time consuming and would have exceeded the extent of this thesis. In addition to that, no antenna or combiner for X-band was available at that time.

The signals have not been generated in baseband like in the simulations, but at a carrier frequency of 300MHz. To properly examine the capabilities of the AWG, the outputs of all of its 8 channels were combined with an 8-channel combiner. Its datasheet can be found in figure B.1 in the appendix. Although this combiner is not designed for frequencies around 300MHz, a measurement of the transmission losses showed that its behavior is almost linear in the frequency area of interest. The results are very close to the results obtained without combiner, when the channels are measured individually and summed in Matlab. These results can be found in figures B.3 to B.6 in the appendix.
Simply adding the signals up corresponds to a transmit direction of 0°. In addition to that, only static targets are assumed in the measurements, because the antenna of the ASTAP system was not yet available. Hence, the same results as in the simulations are expected.

4.3.1. Circulating Codes

The measurement of the Circulating Codes has been conducted with the same signal as in the simulation. The parameters can be found in table 4.2. Figure 4.11 shows a result that is very close to the simulation (see figure 4.2). The peak has the same width and position as in the simulations. There are range sidelobes at -7.5km and 7.5km with a magnitude of up to -32.4dB. The sidelobes in angle are at about -11.8dB. Both the angle cut, as well as the range cut, are not symmetrical anymore.
When no combiner is used and the channels of the system are added up in Matlab, the result looks very similar (see figure B.3).

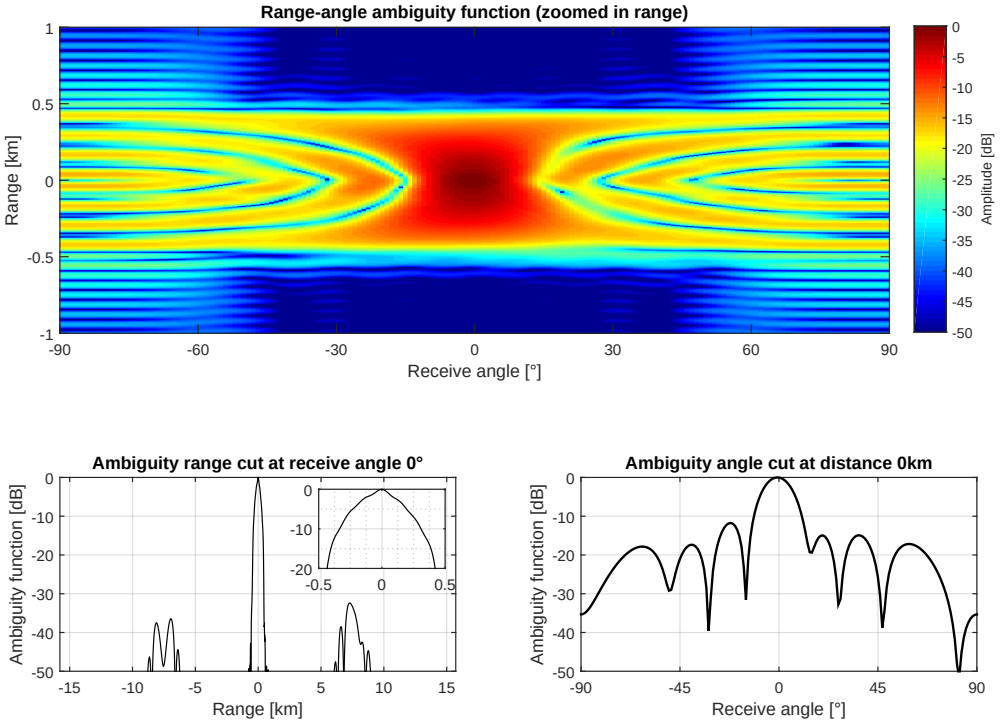

Figure 4.11: Measurement results for one Circulating Codes pulse. The parameters used in this simulation are the same as for the corresponding simulation and shown in table 4.2. Top: two-dimensional ambiguity function in range and angle. Bottom left: range cut at angle 0°. Bottom right: angle cut at range 0km.

4.3.2. Hybrid Codes

The signal used in the measurement is the same as in the simulation (see table 4.3). As for the Circulating Codes, the result for the Hybrid Codes in figure 4.12 is very similar to the simulation result (see figure 4.3). Both the range cut, as well as the angle cut, are not symmetrical. The sidelobes in range are at about -7.1dB and there are additional ones at 12 to 15 kilometers with a magnitude of less than -45dB. The highest sidelobes in angle are at about -11.7dB. When no combiner is used and the channels of the system are added up in Matlab, the result looks very similar (see figure B.4).

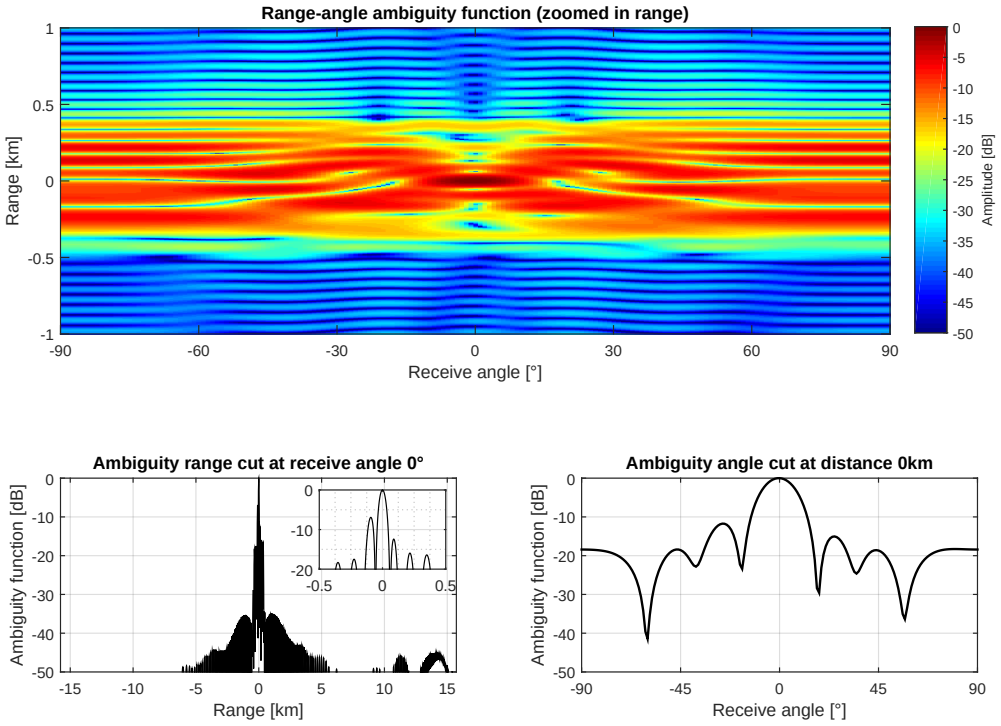

Figure 4.12: Measurement results for one Hybrid Codes pulse with Barker 7 code. The parameters used in this simulation are shown in table 4.3. Top: two-dimensional ambiguity function in range and angle. Bottom left: range cut at angle 0°. Bottom right: angle cut at range 0km.

4.3.3. Hybrid Codes with Golay sequences

This measurement examines, if the output of the AWG can be used in combination with Hybrid Codes and a Golay pair. Two separately processed and summed Hybrid Code pulses with Golay sequences and two pulses transmitted very closely in time to each other are examined (see sections 3.2 and 3.6). As before, the same parameters are used as in the simulations (see table 4.4), although the AWG will generate signals at a carrier frequency of 300MHz. The results are shown in figures 4.13 and 4.14. The results look very different from each other, although the corresponding simulations are almost the same. Again, the angle cut and the range cut of the ambiguity function are not symmetrical for both figures.
For the individually processed pulses, the sidelobes in range are at about -8.5dB and there is an additional sidelobe of less than -40dB at 15km. The sidelobes in angle are at -12.3dB.
For the pulses transmitted closely in time, the figure shows very high sidelobes in the whole corridor in azimuth. The range sidelobes can be found at -5.2dB, while the highest sidelobes in angle are even at -3.1dB. Apart from that, for ranges of less than -0.5km or more than 0.5km, the sidelobe level is always below -23dB. When no combiner is used and the channels of the system are added up in Matlab, the result improves slightly for both cases (see figures B.5 and B.6).

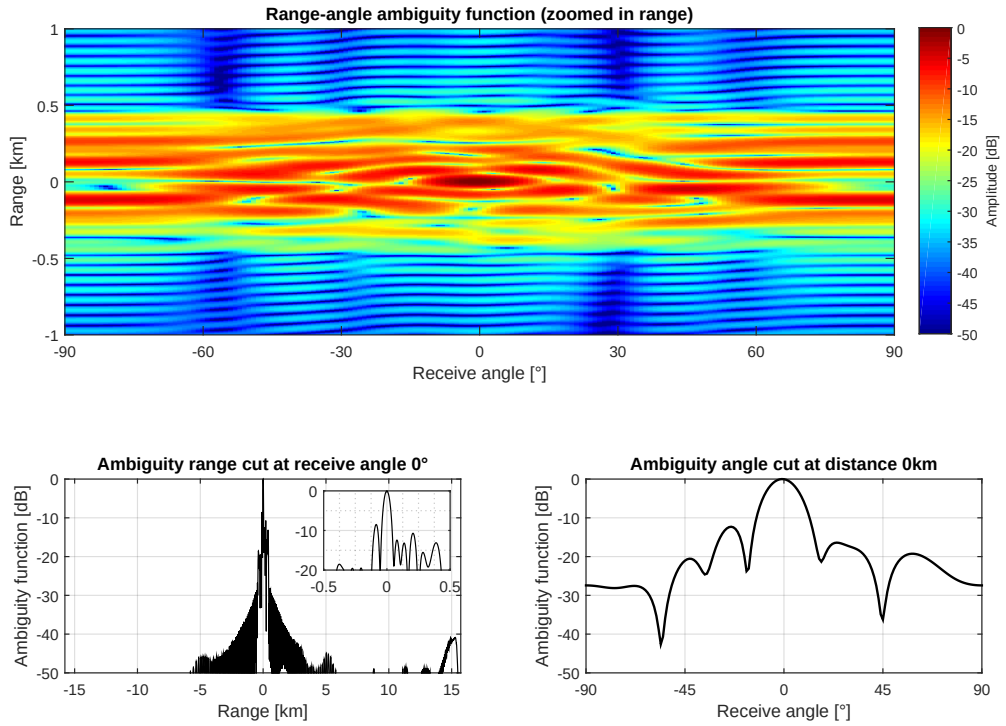

Figure 4.13: Measurement results for individually processed Hybrid Codes pulses with Golay sequences. The parameters used in this simulation are shown in table 4.4. Top: two-dimensional ambiguity function in range and angle. Bottom left: range cut at angle $0°$. Bottom right: angle cut at range 0km.

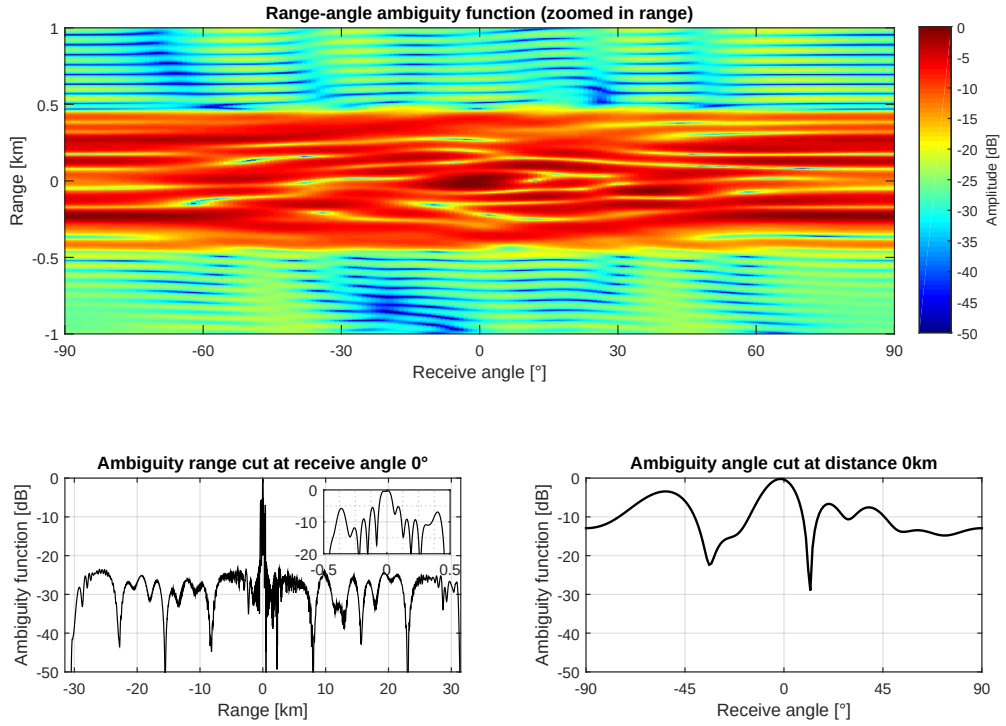

Figure 4.14: Measurement results for Hybrid Codes pulses with Golay sequences with its pulses transmitted closely in time. The parameters used in this simulation are shown in table 4.8. Top: two-dimensional ambiguity function in range and angle. Bottom left: range cut at angle $0°$. Bottom right: angle cut at range 0km.

5

Discussion

This last chapter deals with the discussion of the simulation and measurement results. It tries to make a statement about the applicability of the examined waveforms and give advice for future work.

5.1. Discussion of simulation and measurement results

The Matlab simulation of the waveforms, discussed in chapters 2 and 3, is the most powerful tool to verify their theoretical performance. Since it is not considering any losses or distortions (like interfering signals from within the radar system or from the environment), the simulation can only give an indication, if the examined waveforms can deliver reasonable results in practice.

To rate its performance, each simulation result can be compared with the simulation results for a standard phased array radar. This has been done in chapter 4, as well as in [13] and [14]. From the techniques mentioned in chapter 3, only the ones that are able to deliver a comparable performance to a phased array radar are considered for further investigation and measurements. Since the ASTAP system is not completely operational, the measurements could only be conducted with the AWG. The radar system consists of additional parts, as can be seen from figure 2.8. Therefore, these measurements can only give an indication and verify, if the generated signals are clean enough, to be used in such a radar system. The up-conversion to X-band, the transmission through antennas, the scattering of the waves due to targets and the environment, as well as the down-conversion will introduce more effects that cannot be discussed within this thesis.

5.1.1. Circulating Codes

The simulation results from the new implementation of the Circulating Codes shown in figure 4.2 match the results that were presented in [13]. The shape of the sidelobes are different, but the position, as well as the height are the same. The reason for this might be a differently generated transmit signal in combination with a different sampling frequency. Note that the figure shows the processing result for the use with a single receive antenna. Only the case of one target at a range of 0m and 0° from the radar antenna was assumed in these simulations. Further simulation results that also include different target angles, can be found in appendix A.
The measurement result, presented in figure 4.11, is very close to the simulation results. The highest sidelobes in range are only about 2.6dB higher than in the simulations, while the sidelobes in angle are only 1dB higher. What strikes, is the fact that both the range, as well as the angle cut, are by far not as symmetrical as in the simulation results. The result without combiner in figure B.3 matches the theory as well.

To put it in a nutshell, the simulation confirms the results presented by Babur et al., except for the shape of the sidelobes. The measurement results look very similar to the simulations, with slightly higher sidelobes. In addition, it strikes that both the range and angle cuts are not symmetrical anymore.

5.1.2. Hybrid Codes

The simulation results from the new implementation of the Hybrid Codes in combination with a Barker 7 code in figure 4.3 match the results that were presented in [14]. Just like for the Circulating Codes, both figures show the processing result for the use with a single receive antenna. Again, only the case of one target at a range of 0m and 0° from the radar antenna was assumed in this simulations. Further simulation results can be found in appendix A.
The measurement result, presented in figure 4.12, is also very close to the simulation results, but the system produces higher sidelobes with Hybrid Codes. The highest sidelobes in range are about 3.3dB higher, while the sidelobes in angle are about 1dB higher than in the simulations. The result without combiner, in figure B.4, is very similar.

Like for the Circulating Codes, the simulations confirm the results in the paper by Babur et al. Also the measurement result looks as expected, with slightly higher sidelobes. Apart from that, there is no clear symmetry anymore in range or angle.

5.1.3. Hybrid Codes with Golay sequences

The five techniques using Hybrid Codes with Golay pairs led to different results, which are discussed individually in the following paragraphs. Like for the Circulating and Hybrid Codes before, one target at 0km and 0° is assumed, as well as one receive antenna.

Transmitting Golay sequences consecutively and processing them individually

As can be seen from the simulation result in figure 4.4, this technique shows an extremely good range performance for static targets. At least in the range cut at 0 degrees, this technique seems to recover the performance of standard phased array radar. The sidelobes in range are about 2.9dB lower than for the single-pulse Hybrid Codes with Barker 7 code. The angular performance is similar, but the main lobe is a few degrees more narrow and the sidelobes at higher angles are much lower. The main reason for the changed angular pattern is that 7 antenna elements are used for the Hybrid Codes with Barker 7 code, while 8 antenna elements are used for the Hybrid Codes with Golay sequences, which leads to a narrower main lobe. The angular performance can easily be improved by adding weightings in time and space and by using more antennas for reception (see figure A.6 in appendix A).
Figure 4.5 shows the results of the simulation involving the phase shift due to the displacement. The phase shift of the ambiguity function is corrected for a range of values. It is obvious that this technique only delivers good results, when the phase shift is properly corrected. When this is done, the result is as good as for static targets, otherwise there are sidelobes of up to -11dB. In addition to that, the target peak is very wide in Doppler.

A problem of this combination of processing and waveform is that it only works properly for one target or several targets with the same velocity. If several targets with different velocities are observed, only one target displacement phase shift can be corrected at a time. The other targets still have high sidelobes and can also cover other targets. Generally, not knowing the exact velocity of the target, means a big effort for the processing and a huge amount of data, because a 3-dimensional matrix (range, angle, velocity) needs to be filled. If the velocity interval of the targets is well known, this amount of data can be considerably reduced. Still, the processing is costly.

The measurement with the AWG of the ASTAP system for an assumed static target does look similar, but the sidelobes are considerably higher. In range, they are about 4.8dB higher, while in angle only 1dB higher than in the simulations. In general, the sidelobe corridor in azimuth is wider than expected. In the simulations, this corridor is about 0.5km wide, but the measurements it has a width of almost 1km, which is comparable to the Circulating or Hybrid Codes. When no combiner is used, the overall result looks a little bit different, which is shown in figure B.5 in the appendix. There, the sidelobes in range are 5.1dB higher than in the simulations and the angle sidelobes are now about 3.6dB higher. The width of the sidelobe corridor is smaller than with combiner. A reason might be that the different channels of the combiner are not completely isolated from each other and a manual summing produces cleaner results.

Transmitting more than one Golay pair consecutively and process them individually

As explained in chapter 3, the sidelobes in Doppler can be reduced by processing more than one Golay pair and adding up the results coherently. Figure 4.6 shows that this technique is indeed a big improvement. The target peak is now very narrow in Doppler, which facilitates the detection. There are still sidelobes at other Doppler frequencies with a magnitude of -11dB, but they become more narrow, the more Golay pairs are being used, although they cannot be completely removed. The reason for these sidelobes has been explained in section 4.2.4 and is related to the fact that due to the use of PRT and GRT, a second PRT is formed, which is the sum of PRT and GRT. This new PRT is responsible for new ambiguities, which become visible in the sidelobes.
A difficulty is that several consecutive Golay pulse pairs need to be transmitted and received. This means that the target will be illuminated for a long time and the target might move quite much in that time. Depending on the application, this could again lead to a decreased range resolution, because the target peak would widen in range. No measurements have been conducted for this technique.

Transmitting Golay pair in parallel on different elements

As can be seen from figure 4.7, this technique delivers no good results. Several variants of different antenna setups have been examined, but the results were all similar. Although the target peak is very narrow and the sidelobes in range are comparable to the ones from the individual processing of the pulses, the sidelobe corridor is much wider in range than for the other techniques. In addition to that, the double amount of antenna elements is necessary, which makes this technique more expensive.
Since the simulation results of this technique were not satisfying, no measurements have been conducted.

Transmitting Golay pair in parallel at different frequencies

This technique does not deliver good results either. Figure 4.8 shows a typical result. Although the peak is again very narrow and the sidelobes at about -11.4dB, there is no big improvement visible from Hybrid Codes with Barker 7 code. Therefore, no measurements have been conducted with this technique.

Transmitting Golay pair very closely in time

Here, only an up- and down-chirp is considered as transmit signal, because it achieves the best performance. The result of this technique is quite similar to processing each pulse individually. But since the pulses are transmitted very close to each other in time, the effect of the phase shift due to the displacement of the target would be very small. The simulation result (which does not include any moving target) is shown in figure 4.10. The sidelobes corridor in azimuth around 0m is almost identical to the one that is shown in figure 4.4, the magnitude of the highest sidelobes is the same. The difference between both techniques is the sidelobe level at ranges further away from the target. While the individually processed pulses achieve sidelobe levels of less than -40dB at a range of $\pm$1.5km and more, transmitting the pulses close to each other in time leads to a general sidelobe level of slightly under -30dB for all ranges of more than $\pm$1.5km. In angle, the sidelobes generated by this technique are even about 1dB lower.
The measurement presented in figure 4.14 shows that the sidelobes are generally much higher over the whole azimuth sidelobe corridor than in the simulations. In range, they are about 8.1dB higher, while in angle even 9.6dB. The result without combiner looks similar.

5.2. Summary and conclusions

This thesis studied the MIMO radar techniques of the Circulating Codes and the Hybrid Codes. After a general radar introduction in chapter 1 and an introduction to the mentioned techniques in chapter 2, a new method has been presented to improve the performance of the Hybrid Codes. This method involves the usage of Golay sequences as spatial codes. Since the sum of the auto-correlation functions of a so-called Golay pair theoretically produces one narrow peak and zero sidelobes, they have perfect

properties for use in combination with radar.
In chapter 4, the implementation of the Matlab simulations is explained. In addition to that, the results of the simulations and measurements are presented. The simulations of the Circulating and Hybrid Codes confirm the results of Babur et al. presented in [13] and [14]. Hence, the implementation in Matlab is correct.

The simulations of the Hybrid Codes in combination with Golay pairs showed a very narrow peak in range for static targets, as expected from the theory. Since this technique is adding the processing results for two pulses coherently, small phase shifts have a big influence on the final result.
A moving target introduces a phase shift due to its displacement in between of the two pulses. Therefore, the biggest challenge is to deal with this phase shift. Several ways of avoiding or at least minimizing this phase shift have been presented in chapter 3 and examined in chapter 4. The most promising techniques are firstly, transmitting, receiving and processing two or more pulses individually and then correcting the phase shift due to a range of assumed velocities, before adding up the ambiguity functions and secondly, transmitting the two Golay pulses very closely in time to each other and applying one matched filter on the reflected signal.
Both these techniques deliver good results in the simulations. Processing the pulses individually gives the lowest sidelobes in range, but the velocity of the targets needs to be roughly known already. Furthermore, the detection of several targets with different velocities is difficult, because the sidelobes due to an incorrectly removed phase shift can lead to false alarms or cover other targets. Often, these sidelobes will only disturb the measurements for a short time, but it might also be possible to reduce these problems by applying some kind of multi-target processing. In addition to that, a 3-dimensional ambiguity function (range, angle, Doppler) is produced with this technique, which makes it computationally expensive. Transmitting the pulses very close to each other still involves a phase shift, but for most targets, it will be small enough to omit it. The average level of sidelobes in range is higher than for the individual processing.
To conclude, the usage of Hybrid Codes with Golay pairs for detecting moving targets is complicated. This thesis showed that it is theoretically possible to remove or avoid the phase shift effect due to the displacement of the target.

The measurements with the ASTAP system show that already the AWG introduces a lot of extra sidelobes in the processing results. For single pulse applications like Circulating or Hybrid Codes, its performance seems to be sufficiently good, since the differences between the measurement and simulation results are not very big, as has been discussed in sections 5.1.1 and 5.1.2. But it is questionable, if this system can produce signals that are clean enough for a multi-pulse waveform processing approach. As has already been discussed in section 5.1.3, the results produced with the ASTAP system have much more sidelobes than expected and the symmetry of the figures gets lost.
Firstly, this means that the techniques applied in this thesis are more sensitive to distortions and phase shifts than the Circulating or Hybrid Codes. Secondly, the results show that the ASTAP system might not be reliable enough for these kinds of multi-pulse waveforms. The measurements did not produce the expected outcome. Especially the measurement involving two Hybrid Code pulses with Golay sequences transmitted closely in time shows that the results provided by the system are very different from the expectations.

5.3. Possible applications

Here, two techniques are considered for possible applications: the Hybrid Codes with Golay sequences that are individually transmitted and processed and the ones that are transmitted closely in time and then processed jointly. In the first case, the biggest problem is the PRT. Since two individually processed pulses are used to produce the narrow peak, the PRT plays an important role here and the Doppler dilemma (see chapter 1) comes into play.
To avoid a bad Doppler performance when the targets are at a big distance from the antenna, this technique should be used for comparatively slow or static targets, or targets that usually have velocities within a well known interval, for example ships, cars or even pedestrians. For fast moving targets or targets with fast changing velocities, this technique does not seem suited, because of the necessary phase shift compensation that can only be done for a limited amount of velocities. In addition to that, the

technique should only be used, if all targets have a similar velocity (like cars on a highway, for instance) or if only one or very few targets are observed. Since the phase shift can only be compensated for one velocity at a time, targets with different velocities create high sidelobes.
For example, when both the PRT and the GRT are 300µs, this leads to a maximally observable distance of 45km and a maximal unambiguous velocity of 25m/s according to equations 1.9 and 1.10 with a carrier frequency of 10GHz. Therefore, this radar could detect targets with velocities of -25m/s and +25m/s. Alternatively, any other velocity interval of width $2 \cdot 25m/s = 50m/s$ can be observed, if one can be certain that the target velocities stay in this area.
For the second case of the pulses being processed jointly, neither the phase shift due to displacement, nor the PRT play a role in theory. Since the signal is transmitted as one piece, it can be used for almost all known radar application and the phase shift due to the displacement of the target should be negligible. As the measurements delivered bad results for this technique, it has to be examined more carefully before making propositions about possible applications.

5.4. Outlook and recommendations

This thesis showed that it is theoretically possible to decrease the range sidelobes of Hybrid Codes by doing multi-pulse processing in combination with Golay pairs. Future work should focus on the phase shift, when applying multi-pulse processing on moving targets. If the effect of this phase shift on the final ambiguity function of Hybrid Codes with Golay sequences is understood better, the processing could be improved.

In addition to that, the whole ASTAP system should be examined experimentally. In a first try, the same measurements, as presented in chapter 4, could be conducted, while using all parts of the ASTAP system as shown in figure 2.8, in combination with a combiner for X-band instead of the antenna. In a next step, the measurements could be repeated with an antenna in an open field environment. In general, it might be useful to examine the local oscillator of the AWG and closely compare the outputs of each channel. If the ASTAP system does not fulfill the expectations, it might be necessary to improve the AWG or replace it with more stable equipment.

Appendices

A

Simulations

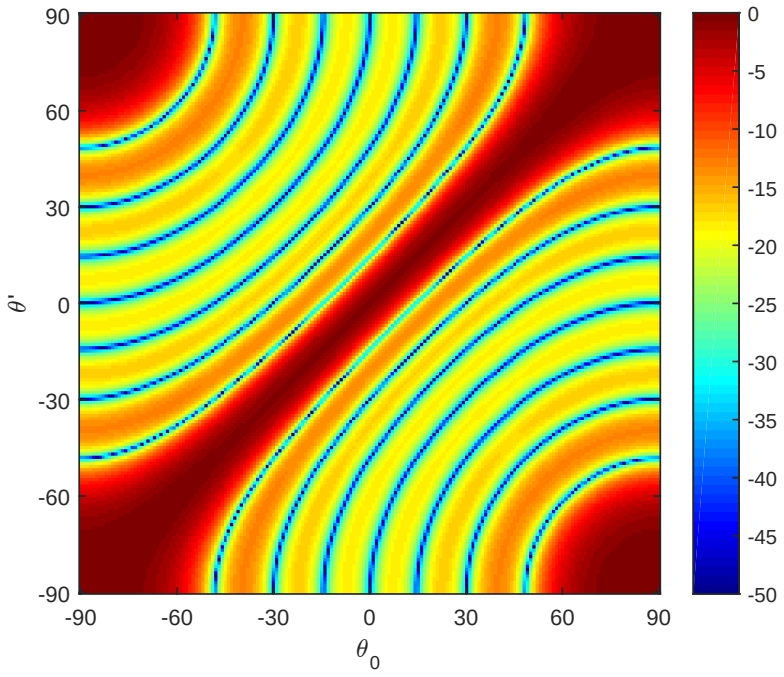

Figure A.1: Angle-angle cuts of ambiguity function for Circulating Codes. θ' is the beamforming angle, while θ_0 is the direction of the target from the antenna. The parameters used in this simulation are shown in table 4.2.

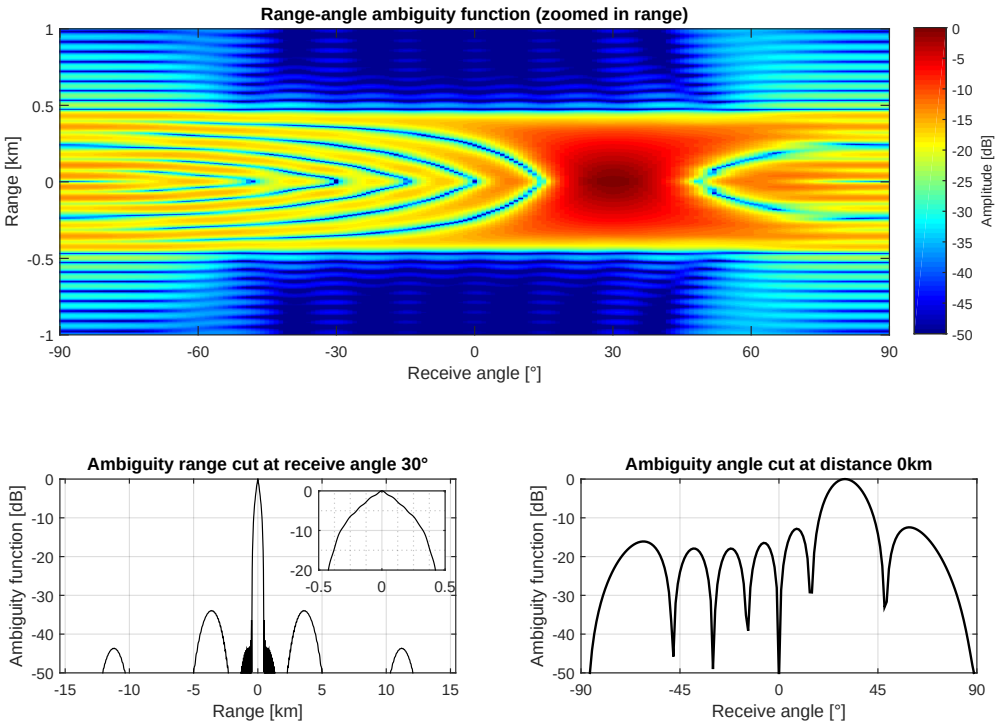

Figure A.2: Simulation results for one Circulating Codes pulse with an assumed target at 30°. The parameters used in this simulation are shown in table 4.2. Top: two-dimensional ambiguity function in range and angle. Bottom left: range cut at angle 0°. Bottom right: angle cut at range 0km.

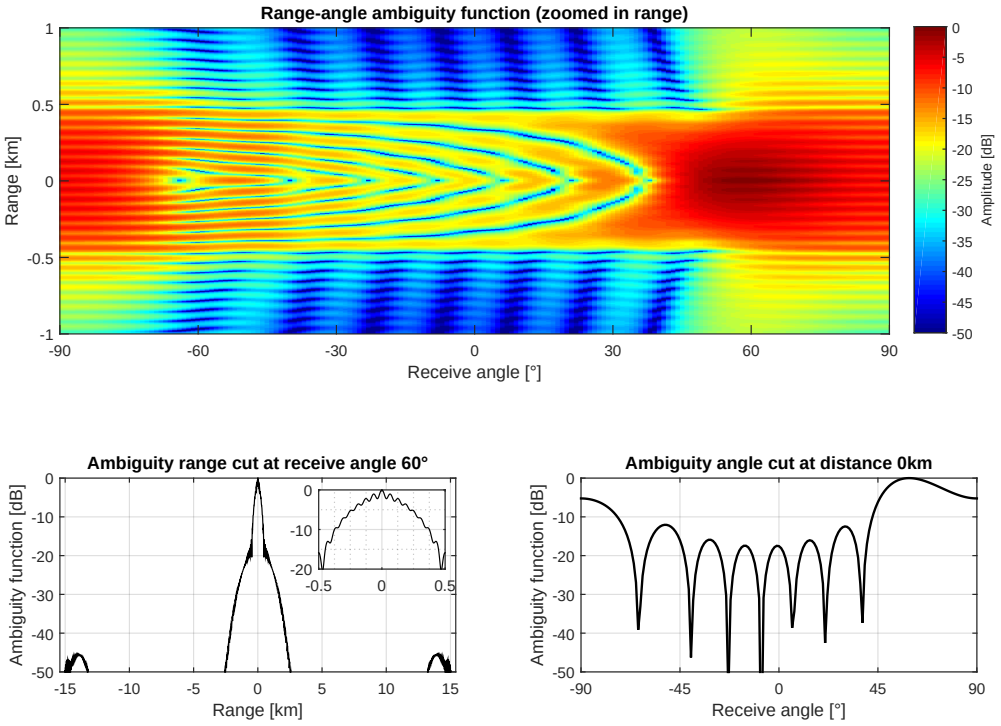

Figure A.3: Simulation results for one Circulating Codes pulse with an assumed target at 60°. The parameters used in this simulation are shown in table 4.2. Top: two-dimensional ambiguity function in range and angle. Bottom left: range cut at angle 0°. Bottom right: angle cut at range 0km.

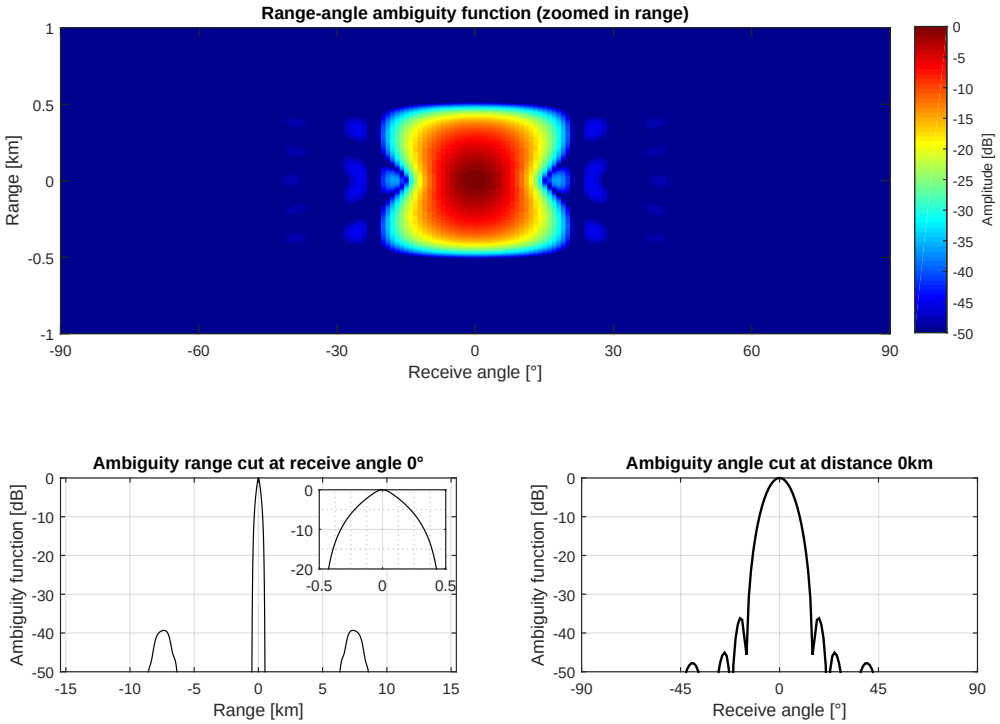

Figure A.4: Simulation results for one Circulating Codes pulse with improved processing. All antenna elements are used for receiving the reflected signal. In addition to that, hamming weights are applied on the replica in time and 30dB Taylors weightings are applied in space over the antenna elements. The parameters used in this simulation are shown in table 4.2. Top: two-dimensional ambiguity function in range and angle. Bottom left: range cut at angle 0°. Bottom right: angle cut at range 0km.

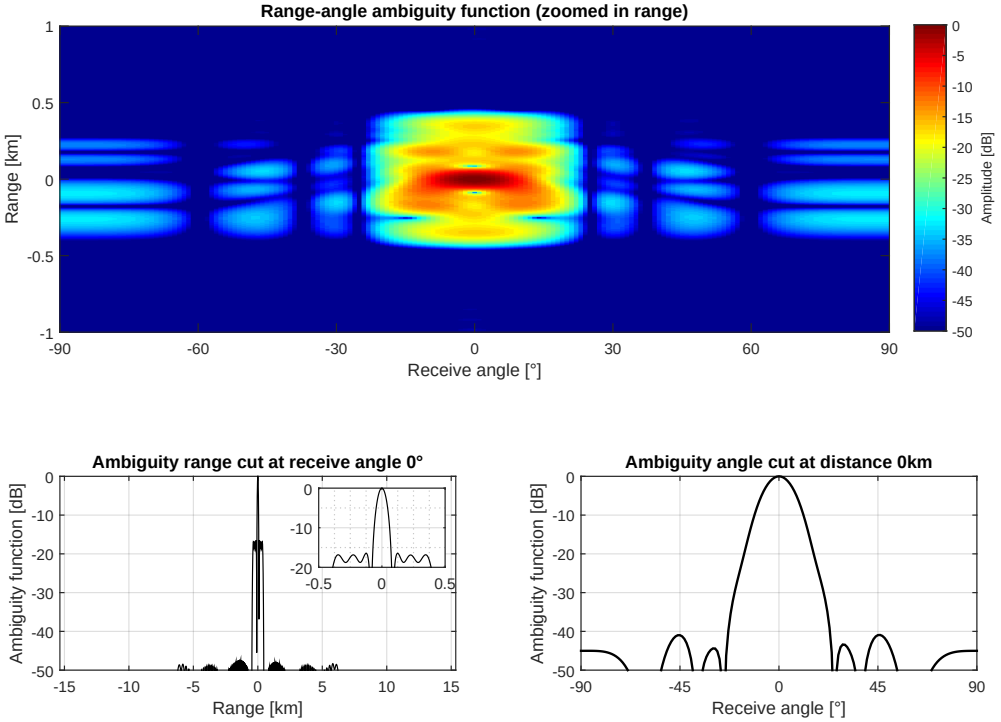

Figure A.5: Simulation results for one Hybrid Codes pulse with Barker 7 code with improved processing. All antenna elements are used for receiving the reflected signal. In addition to that, hamming weights are applied on the replica in time and 30dB Taylors weightings are applied in space over the antenna elements. The parameters used in this simulation are shown in table 4.3. Top: two-dimensional ambiguity function in range and angle. Bottom left: range cut at angle $0°$. Bottom right: angle cut at range 0km.

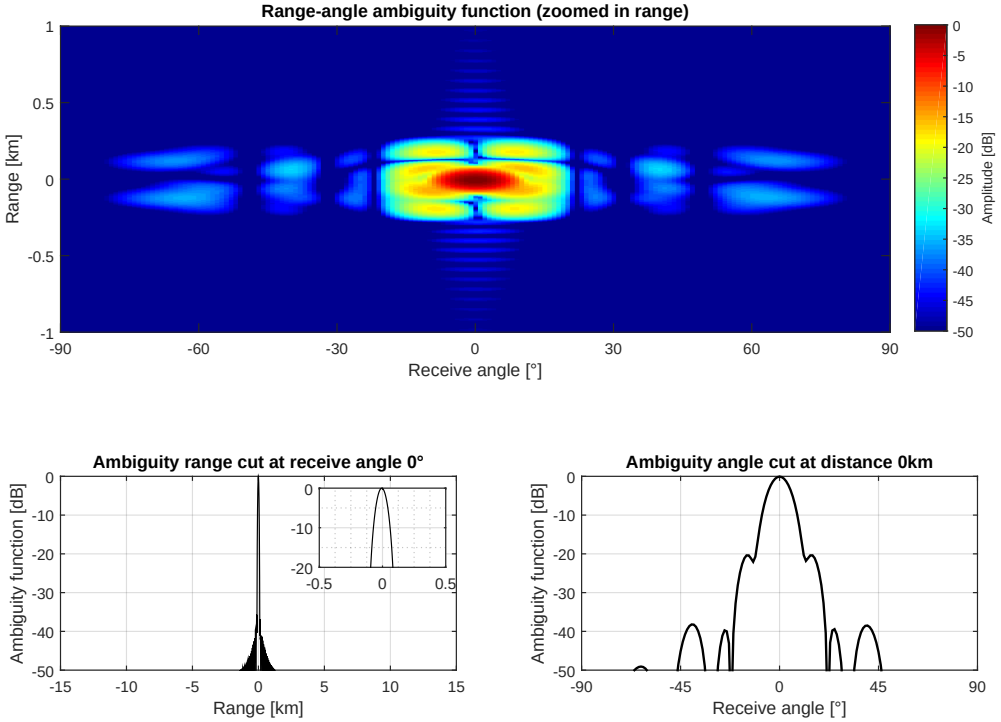

Figure A.6: Simulation results for individually processed Hybrid Codes pulses with Golay sequences with improved processing. All antenna elements are used for receiving the reflected signal. In addition to that, hamming weights are applied on the replica in time and 30dB Taylors weightings are applied in space over the antenna elements. The parameters used in this simulation are shown in table 4.4. Top: two-dimensional ambiguity function in range and angle. Bottom left: range cut at angle $0°$. Bottom right: angle cut at range 0km.

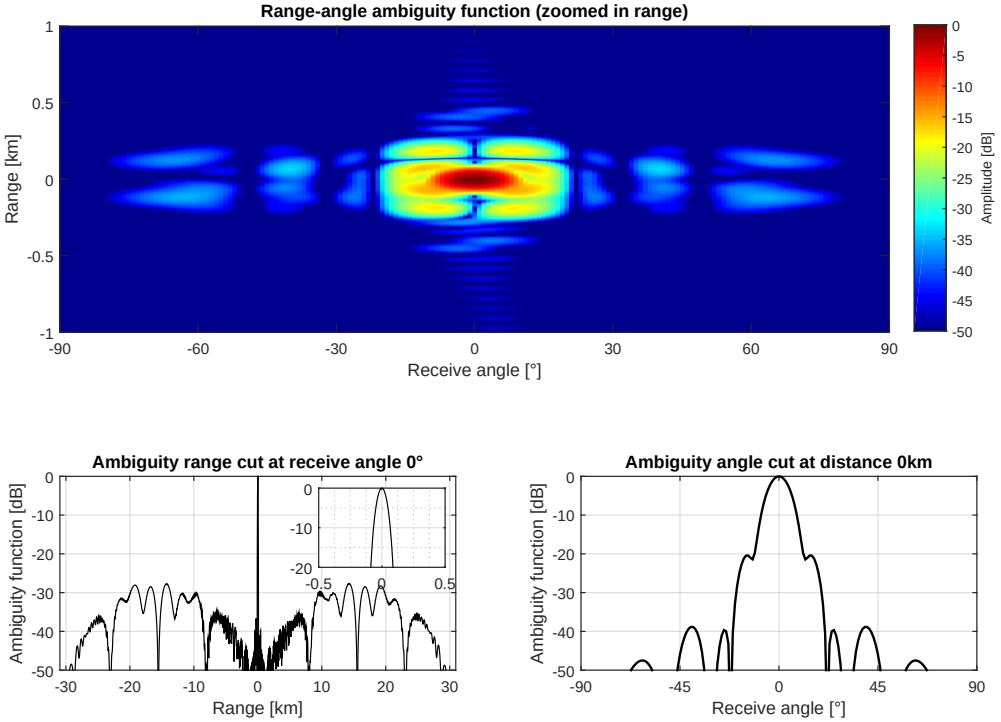

Figure A.7: Simulation results for Hybrid Codes pulses with Golay sequences transmitted very closely in time in Matlab with one LFM up- and one LFM down-chirp with improved processing. All antenna elements are used for receiving the reflected signal. In addition to that, hamming weights are applied on the replica in time and 30dB Taylors weightings are applied in space over the antenna elements. The parameters used in this simulation are shown in table 4.8. Top: two-dimensional ambiguity function in range and angle. Bottom left: range cut at angle $0°$. Bottom right: angle cut at range 0km.

B

Measurements

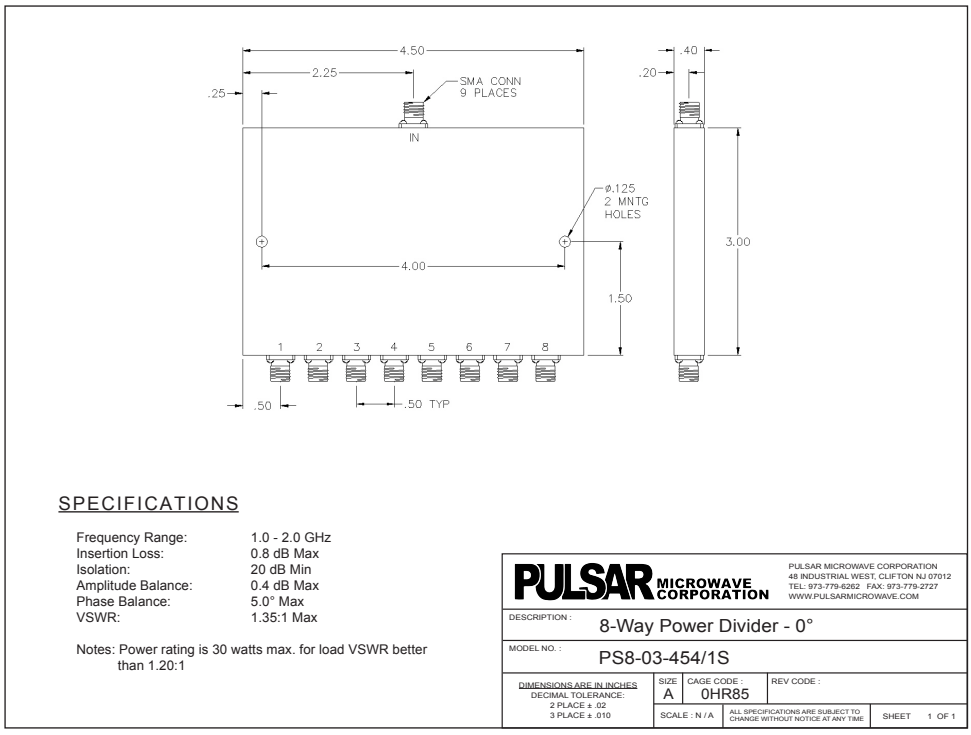

Figure B.1: Datasheet of the 8-way combiner that was used for the measurements. Figure taken from [22].

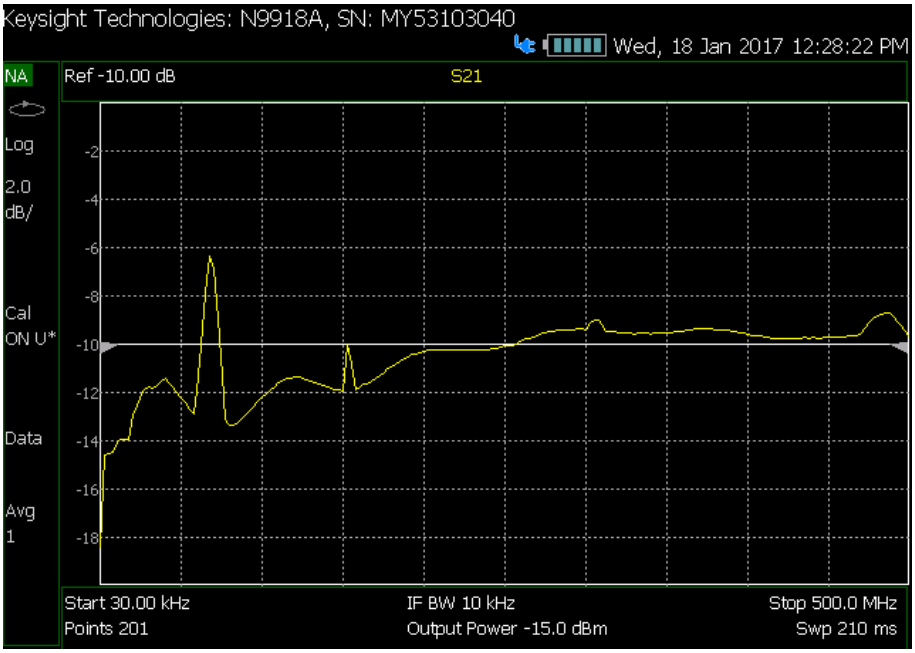

Figure B.2: Measurement result of the loss between one input and the output for the combiner. Around 300MHz, the loss is linear enough for the measurements.

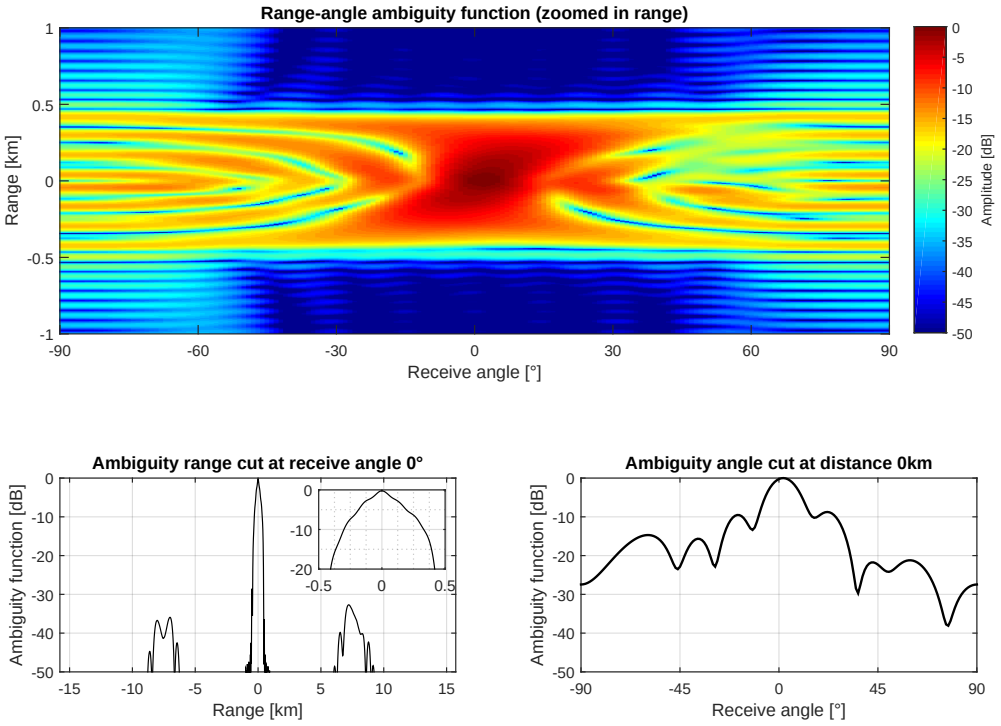

Figure B.3: Measurement results for one Circulating Codes pulse, without combiner. The parameters used in this simulation are the same as for the corresponding simulation and shown in table 4.2. Each channel was measured independently and then combined in Matlab. Top: two-dimensional ambiguity function in range and angle. Bottom left: range cut at angle $0°$. Bottom right: angle cut at range 0km.

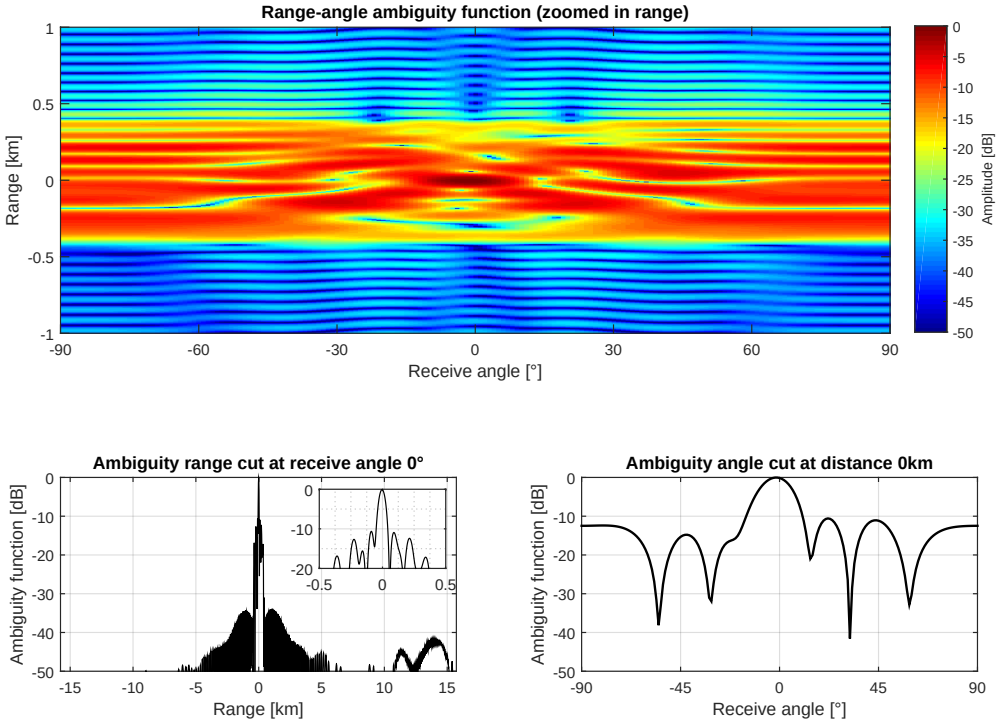

Figure B.4: Measurement results for one Hybrid Codes with Barker 7 code pulse, without combiner. The parameters used in this simulation are the same as for the corresponding simulation and shown in table 4.3. Each channel was measured independently and then combined in Matlab. Top: two-dimensional ambiguity function in range and angle. Bottom left: range cut at angle $0°$. Bottom right: angle cut at range 0km.

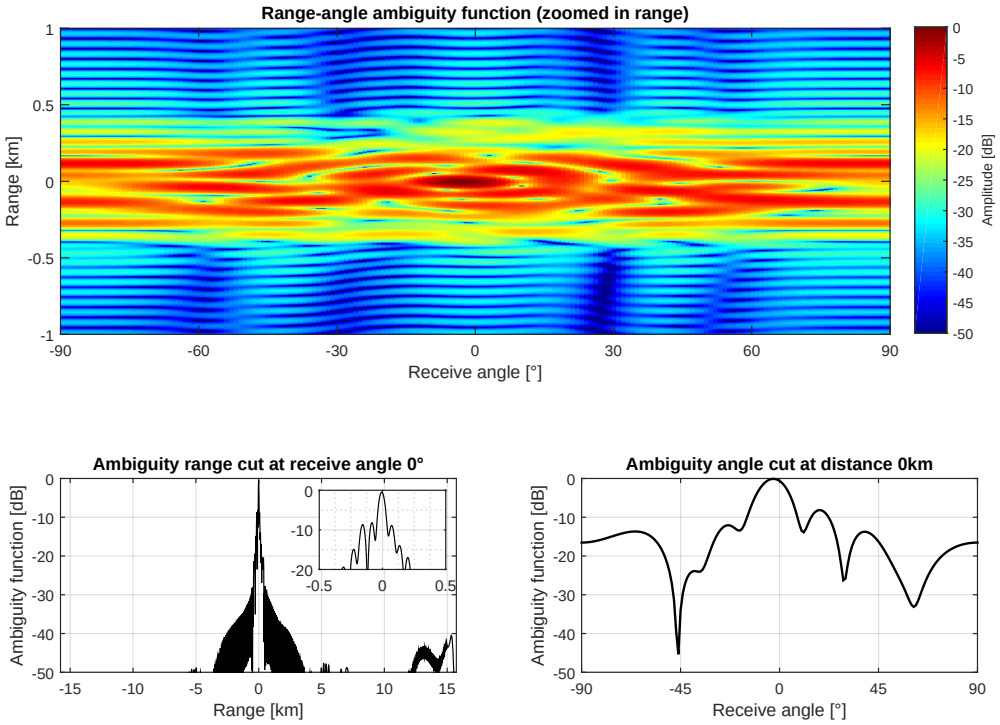

Figure B.5: Measurement results for individually processed Hybrid Codes pulses with Golay sequences, without combiner. The parameters used in this simulation are the same as for the corresponding simulation and shown in table 4.4. Each channel was measured independently and then combined in Matlab. Top: two-dimensional ambiguity function in range and angle. Bottom left: range cut at angle $0°$. Bottom right: angle cut at range 0km.

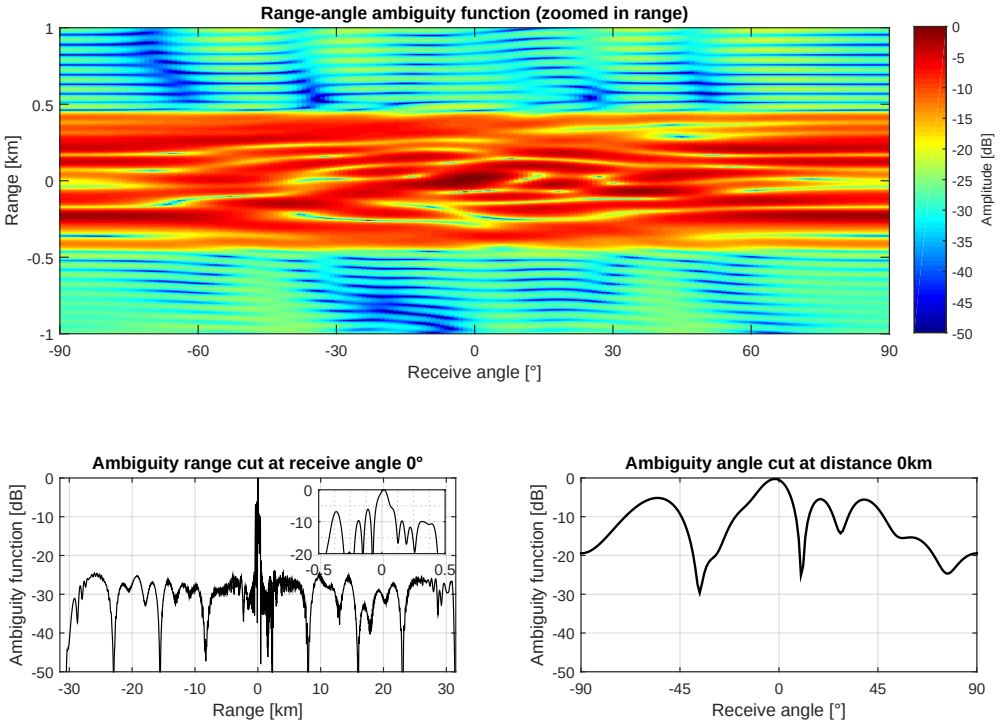

Figure B.6: Measurement results for Hybrid Codes pulses with Golay sequences transmitted very closely in time in Matlab with one LFM up- and one LFM down-chirp, without combiner. The parameters used in this simulation are shown in table 4.8. Each channel was measured independently and then combined in Matlab. Top: two-dimensional ambiguity function in range and angle. Bottom left: range cut at angle $0°$. Bottom right: angle cut at range 0km.

C

Matlab code

C.1. generate_lfm.m

```
% Generate LFM transmit signal

clear all
close all

% Input parameters
N = 8;          % Number of elements
Fs = 1.25e9;    % Sampling frequency
phi0 = 0;       % Extra phase shift
Fc = 10e9;      % Carrier frequency
B = 2.55e6;     % Bandwidth
dt = 1/B;       % Circular time shift (used to steer beam)
T = 100e-6;     % LFM sweep length in time

% Choice of spatial code
% code = [1 1 1 -1 1 -1 1 1]';      % Golay 8 (1)
% code = [1 1 1 -1 -1 1 -1 -1]';    % Golay 8 (2)
% code = [1 1 1 -1 1 -1 1 1 1 1 1 -1 -1 1 -1 -1]';  % Golay 8 (1+2)
% code = [1 1 1 -1 -1 1 -1]';       % Barker 7
code = ones(1,N)';                  % All ones

Ts = 1/Fs; % Sampling time
shift = round(dt/Ts);   % Circular time shift in number of samples

% Generate LFM sweep
t2 = linspace(-T/2,T/2,round(T/Ts));
signal = exp(1i*pi*(B/T).*t2.^2);

% Generate Circulating Codes
original_simout = gen_circ_sig(signal,N,shift); % Circulating signal
simout = diag(code)*original_simout;            % Apply spatial code

% New time vector according to new signal length
t = 0:Ts:(length(simout)-1)*Ts;

% Function to generate a Circulating Code signal according to section
% 2.2.1. in thesis
function y = gen_circ_sig(signal,N,shift)

    ref_signal = zeros(N,length(signal)+(N-1)*round(shift));
    for i=1:N
        ref_signal(i,:) =  circshift([signal zeros(1,(N-1)*round(shift))],[1 (i-1)*round(shift)]);
    end

    y = ref_signal;

end
```

C.2. af_normalized.m

```
% Plot ambiguity function of measurement

% Speed of light
c = 3e8;

% Range [km] and angle of target
r1 = 0;
ra1 = 0;

%%%% Input parameters for ambiguity function %%%%
theta_r = (-90:1:90)*pi/180;        % Observation direction on receive in radian
theta_t = theta_r;                  % Direction of transmitted signal in radian
angle_r1 = theta_r==deg2rad(ra1);   % Angular position of target in radian vector

%%%% Other parameters for waveforms %%%%
Nth_r = length(theta_r);        % Length of receive angle vector
Nth_t = length(theta_t);        % Length of transmit angle vector
lbd0 = c/Fc;                    % Wavelength at carrier frequency
k0 = 2*pi/lbd0;                 % Wavenumber at carrier frequency
d = lbd0/2;                     % Antenna separation in meter (lambda/2)
```

```
x_tx = (-(N-1)/2:(N-1)/2)*d;     % Tx antenna positions
x_rx = x_tx;                     % Rx antenna positions

% Weightings over antennas
a_win = ones(length(x_rx),1);
% a_win = taylorwin(length(x_rx));

% Received signal with phase shifts due to receive and transmit antenna
% element positions
received = [zeros(length(x_rx),2*round(((r1*1000)/c)/Ts)) diag(a_win)*(exp(1i*k0*x_rx'*(sin(theta_r(angle_r1))))*(exp(1i*k0*x_tx'*(sin(theta_r(
    angle_r1))))).'.*(ones(1,N)))*simout)];

% New time vector for received signal
t_r = 0:Ts:(length(received)-1)*Ts;

% Apply time weightings to reference signal
% window = hamming(length(simout)).';
window = ones(1,length(simout));

%%%% Ambiguity function for receiving angle %%%%
display('Calculating ambiguity function...');
w = waitbar(0,'Calculating ambiguity function...');
Chi = zeros(Nth_r,length(received)*2-1);     % Define size of Chi
ii = 0;
for th = 1:Nth_t
    ii = ii+1;
    DBF1 = exp(1i*k0*x_tx(1:end)*sin(theta_t(th)))*(simout(1:end,:));   % Beamforming part 1 (transmit signal in direction theta)
    DBF2 = exp(1i*k0*fliplr(x_rx)*sin(theta_t(th)))*(received);         % Beamforming part 2 (receive signal in direction theta)
    Chi(th,:) = xcorr(DBF2,DBF1.*window);                               % Apply matched filter
    waitbar(ii/Nth_t);
end
close(w)

[XCorLFMCirc,lags] = xcorr(DBF2,DBF1);  % Calculate lags for proper range vector

Range = (lags*1/Fs*c/2)/1000;           % Range vector [km]
[M,dist_r1] = min(abs(Range-r1));       % Range bin closest to the position of target

Chi_norm = abs(squeeze(Chi))/max(abs(squeeze(Chi(:,:)))); % Absolute value and normalize ambiguity function

%%%% Plot result %%%%
display('Plotting ambiguity function...');

figure
subplot(6,2,[1,2,3,4,5,6])
imagesc(rad2deg(theta_r),Range,20*log10(squeeze(Chi_norm(:,:))'))
colormap(jet)
c = colorbar;
title('Range-angle ambiguity function (zoomed in range)')
xlabel('Receive angle [°]')
ylabel('Range [km]')
ylabel(c,'Amplitude [dB]')
% ylim([min(Range) max(Range)])
xlim([-90 90])
ylim([-1 1])
caxis([-50 0])
axis xy

ax = gca;
ax.XTick = [-90 -60 -30 0 30 60 90];

subplot(6,2,[9,11])
plot(Range,20*log10(squeeze(Chi_norm(angle_r1,:)))','k','LineWidth',1.5)
xlabel('Range [km]')
ylabel('Ambiguity function [dB]')
xlim([min(Range) max(Range)])
% xlim([-15 15])
ylim([-50 0])
% xlim([-20 20])
str = sprintf('Ambiguity range cut at receive angle %i° ',ra1);
title(str)
grid on
grid minor

% ax = gca;
% ax.XTick = [-15 -10 -5 0 5 10 15];

subplot(6,2,[10,12])
plot(rad2deg(theta_r),20*log10(squeeze(Chi_norm(:,dist_r1)))','k','LineWidth',1.5)
xlabel('Receive angle [°]')
ylabel('Ambiguity function [dB]')
xlim([-90 90])
ylim([-50 0])
str = sprintf('Ambiguity angle cut at distance %ikm',r1);
title(str)
grid on
grid minor

ax = gca;
ax.XTick = [-90 -45 0 45 90];

set(gcf,'units','points','position',[50,50,750,500],'PaperOrientation','landscape','Renderer','painters')
```

C.3. af_normalized_golay.m

```
% Calculate ambiguity function with two complementary codes

clear all
close all

tic

%%%% Waveform parameters %%%%
N = 8;       % Number of elements
phi0 = 0;    % Extra phase shift
Fs = 10e6;   % Sampling frequency
Fc = 10e9;   % Carrier frequency
B = 2.55e6;  % Bandwidth
```

```
T = 100e-6; % LFM sweep length in time

%%%% Number of Golay pulses (must be a multiple of 2) %%%%
np_max = 2;

%%%% Target parameters %%%%
r = 0;                          % Range of target
ra = 0;                         % Angle of target
R0 = 0;                         % Range at start of measurement
PRT = 2e-4;                     % Pulse repetition time (within Golay pair)
GRT = 2e-4;                     % Golay pair repetition time
fD = 1e3;                       % Doppler frequency of target in direction of the radar
fD_assumed = -4e3:0.5e2:4e3;    % Assumed Doppler frequencies

%%%% Speed of light %%%%
c = 3e8;
Ts = 1/Fs;  % Sampling time

%%%% Input parameters for ambiguity function %%%%
theta_r = (-90:1:90)*pi/180;    % Observation direction on receive in radian
theta_t = theta_r;              % Direction of transmitted signal in radian
angle_r = theta_r==deg2rad(ra); % Angular position of target in radian vector
fD_target = fD_assumed == fD;   % Doppler frequency of target in assumed Doppler frequency vector

% Velocity vectors
v = (fD*(c/Fc))./2;                     % Velocity of target [m/s]
v_assumed = (fD_assumed.*(c/Fc))./2;    % Assumed velocities [m/s]

%%%% Other parameters for waveforms %%%%
Nth_r = length(theta_r);        % Length of receive angle vector
Nth_t = length(theta_t);        % Length of transmit angle vector
lbd0 = c/Fc;                    % Wavelength at carrier frequency
k0 = 2*pi/lbd0;                 % Wavenumber at carrier frequency
d = lbd0/2;                     % Antenna separation in meter (lambda/2)
x_tx = (-(N-1)/2:(N-1)/2)*d;    % Tx antenna positions
x_rx = x_tx;                    % Rx antenna positions

%%%% LFM signal generation %%%%
dt = 1/B;               % Circular time shift (used to steer beam)
shift = round(dt/Ts);   % Circular time shift in number of samples

% Generate LFM sweep
t2 = linspace(-T/2,T/2,round(T/Ts));
signal = exp(1i*pi*(B/T).*t2.^2);

%%%% Define length of received signal and size of ambiguity function %%%%
len_r = length(signal)+(N-1)*shift+2*round((((r+v*(np_max-1)*PRT*1e-3)*1000)/c)/Ts);
Chi = zeros(Nth_r,length(fD_assumed),2*len_r-1);

%%%% Start loop of pulses %%%%
for puls = 1:round(np_max/2);

    % Spatial code
    code = [1 1 1 -1 1 -1 1 1]'; % Golay 8 (1)

    % Circulating codes generation
    original_simout = gen_circ_sig(signal,N,shift); % Circulating signal
    simout = diag(code)*original_simout;            % Apply spatial code

    %%%%%%%%%%%%%%%%%%%%%%%%%%%%%%%%%%%%%%%%%%%%%%%%%%%%%%%%%%%%%%%%%%%%%%%%%%%%%%%

    % Pulse delay due to PRT and GRT
    delay1 = (puls-1)*(PRT+(puls-1)*0.01e-4) + (puls-1)*GRT;

    % Weightings over antennas
    a_win = ones(length(x_rx),1);
%     a_win = taylorwin(length(x_rx));

    % Reflected signals from both targets, involving phase shifts due to
    % transmit and receive antenna element positions
    received = [zeros(N,2*round((((r+v*delay1*1e-3)*1000)/c)/Ts)) diag(a_win)*(exp(1i*k0*x_rx'*(sin(theta_r(angle_r))))*(exp(1i*k0*x_tx'*(sin(theta_r
        (angle_r))))).'.*(ones(1,N)))*simout)];

    % Received signal time vector
    t_r = 0:Ts:(length(received)-1)*Ts;

    % Apply weightings in time to reference signal
%     window = hamming(length(simout)).';
    window = ones(1,length(simout));

    %%%% Ambiguity function for receiving angle %%%%
    display(['Calculating␣ambiguity␣function␣',num2str(1+(puls-1)*2),'...']);
    w = waitbar(0,['Calculating␣ambiguity␣function␣',num2str(1+(puls-1)*2),'...']);
    Chi1 = zeros(Nth_r,length(fD_assumed),length(received)*2-1);    % Define size of Chi1
    ii = 0;
    for th = 1:Nth_t
        ii = ii+1;
        for m = 1:length(fD_assumed)
            DBF1 = exp(1i*k0*x_tx(1:end)*sin(theta_t(th)))*(simout(1:end,:));   % Beamforming part 1 (transmit signal in direction theta)
            DBF2 = exp(-1i*2*pi*Fc*2*(R0+v*delay1)/c).*(exp(1i*2*pi*fD.*t_r).*(exp(1i*k0*fliplr(x_rx)*sin(theta_t(th)))*received));     % Beamforming
                part 2 (receive signal in direction theta, including phase shift due to displacement)
            Chi1(th,m,:) = xcorr(DBF2,DBF1.*window);    % Apply matched filter
        end
        waitbar(ii/Nth_t);
    end
    close(w)

    %%%%%%%%%%%%%%%%%%%%%%%%%%%%%%%%%%%%%%%%%%%%%%%%%%%%%%%%%%%%%%%%%%%%%%%%%%%%%%%

    % Spatial code
    code = [1 1 1 -1 -1 1 -1 -1]'; % Golay 8 (2)

    % Circulating codes generation
    original_simout = gen_circ_sig(signal,N,shift); % Circulating signal
    simout = diag(code)*original_simout;            % Apply spatial code

    %%%%%%%%%%%%%%%%%%%%%%%%%%%%%%%%%%%%%%%%%%%%%%%%%%%%%%%%%%%%%%%%%%%%%%%%%%%%%%%

    % Pulse delay due to PRT and GRT
    delay2 = puls*(PRT+(puls-1)*0.01e-4) + (puls-1)*GRT;

    % Weightings over antennas
```

```
    a_win = ones(length(x_rx),1);
%     a_win = taylorwin(length(x_rx));

    received = [zeros(N,2*round((((r+v*delay2*1e-3)*1000)/c)/Ts)) diag(a_win)*(exp(1i*k0*x_rx'*(sin(theta_r(angle_r))))*(exp(1i*k0*x_tx'*(sin(theta_r
        (angle_r))))).*(ones(1,N))*simout)];

    % Time vector
    t_r = 0:Ts:(length(received)-1)*Ts;

    % Apply window to reference signal
%     window = hamming(length(simout)).';
    window = ones(1,length(simout));

    %%%% Ambiguity function for receiving angle %%%%
    display(['Calculating ambiguity function ',num2str(2+(puls-1)*2),'...']);
    w = waitbar(0,['Calculating ambiguity function ',num2str(2+(puls-1)*2),'...']);
    Chi2 = zeros(Nth_r,length(fD_assumed),length(received)*2-1);     % Define size of Chi2
    ii = 0;
    for th = 1:Nth_t
        ii = ii+1;
        for m = 1:length(fD_assumed)
            DBF1 = exp(1i*k0*x_tx(1:end)*sin(theta_t(th)))*(simout(1:end,:));   % Beamforming part 1 (transmit signal in direction theta)
            DBF2 = exp(-1i*2*pi*Fc*2*(R0+v*delay2)/c).*(exp(1i*2*pi*fD.*t_r).*(exp(1i*k0*fliplr(x_rx)*sin(theta_t(th)))*received)); % Beamforming
                part 2 (receive signal in direction theta, including phase shift due to displacement)
            Chi2(th,m,:) = xcorr(DBF2,DBF1.*window);    %Apply matched filter
        end
        waitbar(ii/Nth_t);
    end
    close(w)

    %%%%%%%%%%%%%%%%%%%%%%%%%%%%%%%%%%%%%%%%%%%%%%%%%%%%%%%%%%%%%%%%%%%%%%%%%%%%

    [XCorLFMCirc,lags] = xcorr(DBF2,DBF1);  % Calculate lags for proper range vector

    Range = (lags*1/Fs*c/2)/1000;           % Range vector [km]
    [M,dist_r] = min(abs(Range-r));         % Range bin closest to the position of target


    %%%%%%%%%%%%%%%%%%%%%%%%%%%%%%%%%%%%%%%%%%%%%%%%%%%%%%%%%%%%%%%%%%%%%%%%%%%%

    % Remove phase shift effect due to target displacement for both pulses
    for m = 1:1:length(v_assumed)
        Chi1(:,m,:) = exp(1i*2*pi*Fc*2*(R0+(v_assumed(m))*delay1)/c).*Chi1(:,m,:);
        Chi2(:,m,:) = exp(1i*2*pi*Fc*2*(R0+(v_assumed(m))*delay2)/c).*Chi2(:,m,:);
    end

    % Coherently add up all ambiguity functions
    Chi = Chi + Chi1 + Chi2;

end

% Normalize ambiguity function result
Chi_norm = abs(squeeze(Chi))/max(abs(squeeze(Chi(:)))); % Absolute value and normalize ambiguity function

%%%% Plot result %%%%
display('Plotting ambiguity function...');

figure
subplot(6,2,[1,2,3,4,5,6])
imagesc(rad2deg(theta_r),Range,20*log10(squeeze(Chi_norm(:,fD_target,:))'))
colormap(jet)
c = colorbar;
title('Range-angle ambiguity function (zoomed in range)')
xlabel('Receive angle [°]')
ylabel('Range [km]')
ylabel(c,'Amplitude [dB]')
% ylim([min(Range) max(Range)])
xlim([-90 90])
ylim([-1 1])
caxis([-50 0])
axis xy

ax = gca;
ax.XTick = [-90 -60 -30 0 30 60 90];

subplot(6,2,[9,11])
plot(Range,20*log10(squeeze(Chi_norm(angle_r,fD_target,:)))','k','LineWidth',1.5)
xlabel('Range [km]')
ylabel('Ambiguity function [dB]')
xlim([min(Range) max(Range)])
xlim([-15 15])
ylim([-50 0])
% xlim([-20 20])
str = sprintf('Ambiguity range cut at receive angle %i',ra);
title(str)
grid on
grid minor

ax = gca;
ax.XTick = [-15 -10 -5 0 5 10 15];

subplot(6,2,[10,12])
plot(rad2deg(theta_r),20*log10(squeeze(Chi_norm(:,fD_target,dist_r)))','k','LineWidth',1.5)
xlabel('Receive angle [°]')
ylabel('Ambiguity function [dB]')
xlim([-90 90])
ylim([-50 0])
str = sprintf('Ambiguity angle cut at distance %ikm',r);
title(str)
grid on
grid minor

ax = gca;
ax.XTick = [-90 -45 0 45 90];

set(gcf,'units','points','position',[50,50,750,500],'PaperOrientation','landscape')

figure
imagesc(v_assumed,Range,20*log10(squeeze(Chi_norm(angle_r,:,:))'))
colormap(jet)
c = colorbar;
title('Range-Doppler ambiguity function at 0° (zoomed in range)')
```

```
xlabel('Assumed velocity [m/s]')
ylabel('Range [km]')
ylabel(c,'Amplitude [dB]')
xlim([v_assumed(1) v_assumed(end)])
caxis([-50 0])
axis xy

set(gcf,'units','points','position',[50,50,700,400],'PaperOrientation','landscape')

toc

% Function to generate a Circulating Code signal according to section
% 2.2.1. in thesis
function y = gen_circ_sig(signal,N,shift)

    ref_signal = zeros(N,length(signal)+(N-1)*round(shift));
    for i=1:N
        ref_signal(i,:) =  circshift([signal zeros(1,(N-1)*round(shift))],[1 (i-1)*round(shift)]);
    end

    y = ref_signal;

end
```

Bibliography

[1] Bassem R. Mahafza. *Radar Systems Analysis and Design using MATLAB*. CRC Press, Huntsville, Alabama, USA, 3rd edition, 2013. ISBN 9781439884959.

[2] Clive Alabaster. *Pulse Doppler Radar - Principles, Technology, Applications*. SciTech Publishing, Edison, NJ, USA, 1st edition, 2012. ISBN 978-1-891121-98-2.

[3] Mark A. Richards, James A. Scheer, and William A. Holm. *Principles of Modern Radar: Basic Principles*, volume 1. SciTech Publishing Inc., Raleigh, NC, USA, 2nd edition, 2010. ISBN 978-1-891121-52-4.

[4] Merrill I. Skolnik. *Radar Handbook*. McGraw-Hill, New York, NY, USA, 3rd edition, 2008. ISBN 978-0-07-148547-0.

[5] Neltronics Australia. "How does a speed camera or radar gun work?". URL `https://www.neltronics.com.au/how-does-a-speed-camera-or-radar-gun-work/`. Accessed: 14-09-2017.

[6] François Le Chevalier. "Wideband Wide Beam Motion Sensing". In J. Taylor, editor, *Advanced Ultrawideband Radar: Signals, Targets, and Applications*, book section 12, pages 417–458. CRC Press, London, UK, 1st edition, 2016. ISBN 9781466586574.

[7] Nadav Levanon and Eli Mozeson. *Radar Signals*. John Wiley & Sons, Inc., Hoboken, NJ, USA, 1st edition, 2004. ISBN 9780471663089. doi: 10.1002/0471663085.

[8] Constantine A. Balanis. *Antenna Theory - Analysis and Design*. John Wiley & Sons, Inc., Hoboken, NJ, USA, 3rd edition, 2005. ISBN 9780471667827.

[9] Jian Li and Petre Stoica. *MIMO Radar Signal Processing*. John Wiley & Sons, Inc., Hoboken, NJ, USA, 1st edition, 2009. ISBN 9780470391488. doi: 10.1002/9780470391488.

[10] Michael S. Davis, Gregory A. Showman, and Aaron D. Lanterman. "Coherent MIMO Radar: The Phased Array and Orthogonal Waveforms". *IEEE A&E Systems Maganzine*, 2014. doi: DOI.No. 10.1109/MAES.2014.130148.

[11] Michael S. Davis. "MIMO radar". In William L. Melvin and James A. Scheer, editors, *Principles of Modern Radar Vol. II: Advanced Techniques*, chapter 4, pages 119–145. SciTech Publishing, Edison, NJ, USA, 1st edition. ISBN 978-1-61353-024-5.

[12] Vincent Pereira, Eric Grivel, and Julien Petitjean. "Coloured transmission based on multicarrier phase coded signals in MIMO radar". Radar Conference (RADAR). IEEE, 23-27 May 2011. doi: 10.1109/RADAR.2011.5960574. Kansas City, MO, USA.

[13] Galina Babur, Pascal Aubry, and Francois Le Chevalier. "Space-Time Radar Waveforms: Circulating Codes". *Journal of Electrical and Computer Engineering (Hindawi)*, 2013. URL `https://www.hindawi.com/journals/jece/2013/809691/`. Article ID 809691.

[14] Galina Babur, Pascal Aubry, and Francois Le Chevalier. "Simple transmit diversity technique for phased array radar". *IET Radar, Sonar & Navigation*, Vol. 10 (Issue 6), pages 1046-1056, 2015. ISSN 1751-8784.

[15] François Le Chevalier. "Space-Time Coding for Active Antenna Systems". In William L. Melvin and James A. Scheer, editors, *Principles of Modern Radar Vol. II: Advanced Techniques*, chapter 11, pages 499–527. SciTech Publishing, Edison, NJ, USA, 1st edition. ISBN 978-1-61353-024-5.

[16] François Le Chevalier. ”Space-time transmission and coding for airborne radars”. *Radar Science and Technology*, Vol. 6 (Issue 6), 2008. CIE - Chinese Institute of Electronics.

[17] T. Faucon, G. Pinaud, and F. Le Chevalier. ”Mismatched filtering for circulating space-time codes”. Radar Conferece 2015. IET, 14-16 Oct. 2015. doi: 10.1049/cp.2015.1185. Hangzhou, China.

[18] Thomas Faucon. ”MIMO radar Mismatched filter design for circulating codes”. Report, ENSTA Bretagne / TU Delft, 2014.

[19] Gaëtan Pinaud. ”Angle Tolerant Mismatched Filtering for Circulating Space-Time Codes”. Report, ENSTA Bretagne / TU Delft, 2015.

[20] Oliver Rabaste and Laurent Savy. ”Mismatched Filter Optimization via Quadratic Convex Programming for Radar Applications”. Radar Conference (RADAR). IEEE, 13-17 Oct. 2014. doi: 10.1109/RADAR.2014.7060333. Lille, France.

[21] Marcel J. E. Golay. ”Complementary Series”. *IRE Transactions on Information Theory*, Vol. 7 (Issue 2), pages 82-87, 1961. ISSN 2168-2712. doi: 10.1109/TIT.1961.1057620.

[22] Pulsar Microwave Corporation. ”1-2 GHz 8-Way Power Divider. Model: PS8-03-454/1S”. URL https://www.pulsarmicrowave.com/product/power_divider/PS8-03-454-1S. Accessed: 21-09-2017.